MOLECULAR CHARACTERIZATION OF FNBPA-MEDIATED *STAPHYLOCOCCUS AUREUS* HOST INTERACTIONS

A Dissertation

by

XIAOWEN LIANG

Submitted to the Office of Graduate and Professional Studies of
Texas A&M University
in partial fulfillment of the requirements for the degree of

DOCTOR OF PHILOSOPHY

Chair of Committee,	Magnus Höök
Committee Members,	Peter J. A. Davies
	Arthur Laganowsky
	Jonathan T. Skare
	Yi Xu
Head of Program,	Warren E. Zimmer

December 2017

Major Subject: Medical Sciences

ABSTRACT

Fibronectin-binding protein A (FnBPA) plays a crucial role in the pathogenesis of *Staphylococcus aureus* by binding to the host proteins fibronectin (Fn) and fibrinogen (Fg) found in the extracellular matrix and blood plasma, initiating tissue adherence, host cell invasion, and attachment to implanted materials. Although the interactions between FnBPA and host ligands Fn and Fg have been studied extensively using domains or segments of the proteins, the combined regulation of multiple ligands binding to FnBPA is poorly understood, and the underlining molecular mechanism of invasion is still not clear. Here, structure–activity relationships and regulation of FnBPA-dependent host interaction were investigated using a set of biochemical and biophysical techniques. With surface plasmon resonance (SPR) as the primary approach, the binding studies were performed using purified recombinant and native full-length proteins as well as a non-purified system (blood plasma). By capturing full-length FnBPA on a biosensor in the same orientation as on the *S. aureus* cell wall, SPR binding analysis show that circulating plasma can bind tightly to FnBPA with stronger affinity than that of Fn- and Fg-binding, also Fn and Fg can bind to FnBPA simultaneously. The results demonstrate that Fg binds to full-length FnBPA with 100-fold stronger affinity than previously reported, presumably through unidentified binding sites in both Fg and FnBPA. Furthermore, the structure analysis and binding study indicate that Fg conformation and structural orientation of surface-associated FnBPA are critical for high-affinity interaction between Fg and FnBPA. The proteolytic cleavage of N1 domain and low pH

affect the folding of N1 domain and Fg-binding activity of FnBPA, suggesting N1 fold-back conformation is required for fully active Fg-binding. Moreover, the strong interaction between FnBPA and Fn induces conformational changes in Fn and exposes cryptic integrin binding sites, resulting in an enhanced Fn-$\alpha_5\beta_1$ interaction for host cell signaling. In addition, SPR binding analysis indicates that amino acid substitutions, which reflect disease-related polymorphisms found in FnBPA-9, alter the Fn-binding reaction and, in turn, impact the formation and function of the ligand complex within specific pathological contexts. The regulation and biological consequences of FnBPA ligand-binding activities revealed in this study are likely to have important implications for *S. aureus* interactions with the host in vivo. This study provides mechanistic insights into the FnBPA-dependent ligand binding, activation, and host cell signaling.

DEDICATION

To my family.

To my beloved mother.

&

In loving memory of my father.

ACKNOWLEDGEMENTS

I would like to offer my special thanks to Dr. Magnus Höök and Mrs. Agneta Höök for giving me the opportunity to pursue my doctoral degree and get exposure to the SPR technique. Thanks also go to my committee members, Dr. Laganowsky, Dr. Xu, Dr. Skare, and Dr. Davies, for their guidance and support during this dissertation study.

I am also grateful to the following institution staff: Olivia Cabrera, our center Administrative Associate: she is always ready to help even during her most busy time. Cindy Lewis, our Graduate Program Coordinator, for her unfailing support and assistance. Thanks to my fellow graduate students, the institute faculty and other staff members for making my learning and working at IBT of Texas A&M Health Science Center in TAMU a unique experience.

CONTRIBUTORS AND FUNDING SOURCES

Contributors

This work was supervised by a dissertation committee consisting of Professors Magnus Höök [advisor] and Yi Xu of the Center for Infectious and Inflammatory Diseases, Peter J. A. Davies of the Center for Translational Cancer Research and Institute of Biosciences and Technology [Home Department], and Professors Jonathan T. Skare of the Department of Microbial Pathogenesis and Immunology, Texas A & M University Health Science Center, and Arthur Laganowsky of the Department of Chemistry, Texas A&M University [Outside Department].

Part of the molecular cloning and mass spectrometry analyses for Chapter III was provided by the laboratory of Dr. Arthur Laganowsky. All other work conducted for the dissertation was independently completed by the student, and some results were published in 2016 and 2017.

Funding Sources

Graduate study was supported by NIH grants AR044415, HL119648 and AI20624, and by the staff tuition assistance program of Texas A&M University.

TABLE OF CONTENTS

Page

LIST OF FIGURES

Page

LIST OF TABLES

Page

CHAPTER I

INTRODUCTION AND LITERATURE REVIEW

1.1. Overview

The opportunistic pathogen *Staphylococcus aureus* is highly human adaptive and has evolved to exploit host proteins to establish infections and for survival. Many of these pathological processes are facilitated by MSCRAMM (microbial surface components recognizing adhesive matrix molecules) on the staphylococcal surface.[1-2] Through the MSCRAMM family of proteins, bacteria bind to the specific molecules fibronectin (Fn) and fibrinogen (Fg) in the extracellular matrix (insoluble form) and blood plasma (soluble form). There are two major biological consequences of such binding events: first, it can mediate bacterial adherence to host tissue or protein-coated device materials, and second, it can help accumulate plasma proteins onto the bacterial surface to invade host cells and avoid immune recognition.[3]

To date, over 100 bacterial Fn-binding proteins (FnBPs) have been reported.[4] The Fn-binding protein A (FnBPA) of *S. aureus* was the first MSCRAMM protein characterized that binds Fn,[5-6] a glycoprotein component of host extracellular matrix (ECM) and plasma. The multiple functions of FnBPA were later discovered by its ability to engage fibrinogen (Fg) in wounds and blood,[7] as well as elastin in connective tissue.[8] FnBPA is present in all clinical isolates and is upregulated during the transition from commensal state to invasive infections.[9] It plays a critical role in development of infectious diseases such as endocarditis and mastitis.[10-11] In an *S. aureus* experimental

endocarditis model, it was shown that the Fg- and Fn-binding abilities of FnBPA synergistically promote valve infection and endothelial invasion.[12-13] A substantial body of evidence suggests that FnBPA can also manipulate physiological functions of Fn to activate integrin signaling pathways for host cell invasion,[14-16] thus contributing to pathogenesis, beyond mediating bacterial adhesion.[17-20] A multi-country genomic study in Europe showed that a common methicillin-resistant *S. aureus* (MRSA) strain has become more transmissible and virulent, partially due to genetic recombination events in *fnbpA*.[21] Recently, several studies found that polymorphisms in FnBPA are associated with cardiac device-related infection in *S. aureus* bacteremia.[22-23]

Because of the clinical prevalence and virulent roles in adhesion, invasion, and evasion, FnBPA can potentially be targeted in approaches to prevent and treat *S. aureus* infection. However, FnBPA has the most sequence diversity among all *S. aureus* MSCRAMMs,[24] and the emergence of new clonal types has created polymorphic variations in the gene,[25] making it difficult to target as a vaccine.[26] Therefore, detailed studies of how FnBPA binds to ligands and how the binding of multiple ligands contributes to adhesion and invasion are critical for understanding *S. aureus* pathogenesis, and they would greatly facilitate the development of anti-adhesin strategies.

1.2. Structure and organization of FnBPA

FnBPA has structural features that are common to other MSCRAMMs: a signal sequence at the N-terminus is followed by a ligand-binding A domain, and at the C-terminus, there is a large repeat region that is followed by segments and an LPXTG motif

involving cell wall localization and anchoring (Fig. 1). However, unlike other MSCRAMM repeat regions, which function as structural support for the A domain, the repetitive sequences in FnBPA are intrinsically disordered and responsible for the Fn-binding function of *S. aureus*; therefore, it is termed a Fn-binding repeat (FnBR).

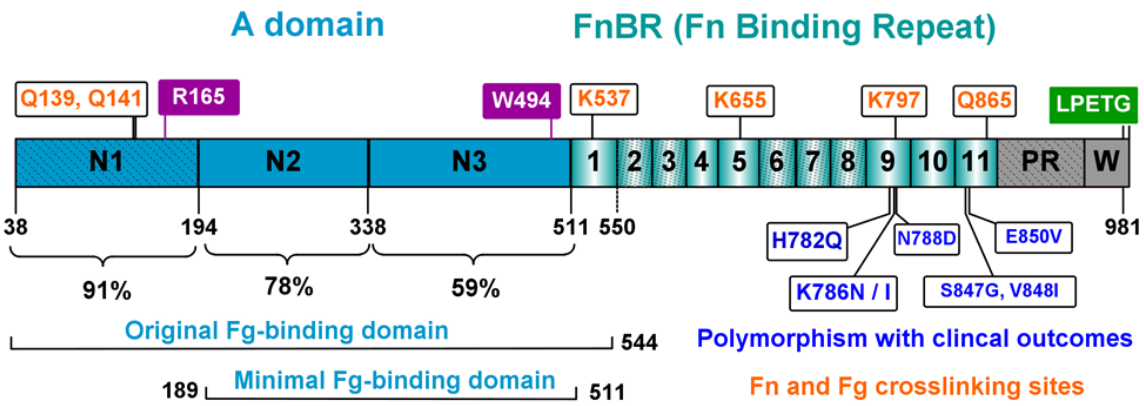

FnBPA-1	GPIIQNNKFEYKEDTIKETLTGQYDKNLVTTVEEEYDSS
FnBPA-4	IDF~EESTHENSKHHA~~~DVVEYEEDTNPG
FnBPA-5	GGQVTTESNLVEFDEESTKGIVTGAV~~~SDHTTVEDTK
FnBPA-9	KYEQGGNIVDIDFDSVPQIHGQNK~~~GNQSFEEDTEKDKP
FnBPA-10	KYEHGGNIIDIDFDSVPHIHGFNK~~~HTEIIEEDTNKDKP
FnBPA-11	SYQFGGHNSVDFEEDTLPKVSGQNE~~~GQQTIEEDTP

Figure 1. Domain organizations of FnBPA
Mature sequence corresponding to the extracellular region of FnBPA. Polypeptide contains an A domain that is divided into the N1, N2, and N3 subdomains (domain similarity among strains are indicated), followed by a sequential arrangement of 11 Fn binding repeat (FnBR), the proline-rich (PR) and cell wall (W) spanning regions, and a C-terminal sortase A recognition motif (LPETG). Thrombin cutting site (R165), single tryptophan residue (W494), and other functional sites, as well as disease-related sites, are shown. Function of the shaded regions has not been identified. Sequence alignment of the six high-affinity Fn-binding repeats is shown with major clinically related variant residues underlined. Highlighted in cyan are residues within each repeat that bind to or are presumed to engage Fn. Domains are drawn to scale using IBS (Illustrator for Biological Sequences, http://ibs.biocuckoo.org) based on UniProt ID: P14738.

The N-terminal A domain of FnBPA plays a multifunctional role and is capable of binding Fg and elastin.[7-8, 27] The A domain of FnBPA is predicted to contain three separately folded subdomains: N1, N2, and N3 (Fig. 1). The N2N3 subdomains were shown to be the minimal Fg-binding domain.[7] The structure of N2N3 ($FnBPA_{189–505}$) comprises two distinct domains dominated by β-strands connected by an eight-residue linker.[28] The main N2–N3 interdomain contacts involve strands and loops from each domain. To date, no structural or ligand-binding information regarding the N1 subdomain is available. However, it has been demonstrated that only a short sequence within the N1 subdomain is required for export and cell wall localization.[29] Within the A domain, there is a thrombin cleavage site close to the boundary between subdomains N1 and N2 of FnBPA.[30] The hemophilic interaction between the A domains on adjacent cells is important for biofilm formation by some strains of MRSA.[31-32]

FnBPA contains structured domains (N2N3 in A domain) that interact with Fg and intrinsically disordered regions that bind multiple Fn molecules. The synergy between disordered regions and structured domains increases the functional versatility of FnBPA.[12]

1.3. FnBPA binding to fibronectin

The binding of fibronectin (Fn) to *S. aureus* was first reported in 1978 by Pentti Kuusela from City of Hope National Medical Center in Duarte, California.[33] Ten years later, two Fn-binding MSCRAMMs were identified in *S. aureus*, FnBPA and FnBPB, and the corresponding genes, *fnbpA* and *fnbpB*, respectively, were cloned and expressed.[5, 34-36] During the past 30 years, the specific interaction between FnBPA and

Fn has been well characterized by a variety of biochemical, biophysical, and structural methods. The tandem β-zipper model[37] was proposed to describe the high-affinity interaction. More importantly, the physiological relevance and biological consequences of this specific interaction have been investigated both in vitro and in vivo.[38]

The Fn-binding activity of FnBPA was initially identified in repetitive sequences in the C-terminal region, termed Fn-binding repeats (FnBR). Subsequently, FnBR (Fig. 1) was considered the key binding domain, based on structural analysis of the complex of Fn and a bacterial peptide.[37, 39] The new boundary designation extended the number of potential Fn-binding repeats in FnBPA to 11, with six high-affinity binding repeats identified (~ 40 aa in length), including FnBPA-1 in the original A domain (Fig. 1).[40] Although not highly similar overall, the FnBRs contain several short conserved Fn-binding motifs (Fig. 1) that are arranged in the correct order to bind sequential modules in Fn.[37] In this tandem β-zipper interaction, the disordered FnBRs adopt a highly extended conformation upon binding to Fn with very high affinity, even though each motif weakly engages the corresponding Fn module.[40]

Fn is an essential multidomain protein that connects cells to the ECM via integrins, cell surface receptors. These glycoproteins play a significant role in cell adhesion, migration, growth, and differentiation, and they are essential for processes such as wound healing, angiogenesis, and oncogenesis.[41-42] Two types of Fn are present in vertebrates: insoluble cellular Fn, which is secreted by various cells and assembled into a fibrous matrix in tissue; and soluble plasma Fn expressed by hepatocytes and circulated in blood at a concentration of about 0.3 mg/mL. Despite distinct

conformations (plasma Fn is highly compact in shape) and independent functions from extended cellular Fn, the inert plasma Fn, upon activation, can be incorporated into the ECM and accounts for a significant fraction of Fn in tissue ECM.[43]

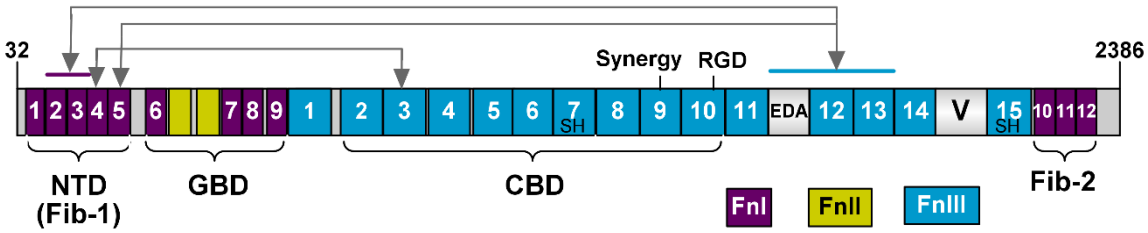

Figure 2. Domain organization of fibronectin
Fn is a C-terminal disulfide-linked heterodimer. Shown here is the larger monomer with the extra domain A (EDA) and variable region (V). The protease-stable Fn fragments include the N-terminal domain (FnNTD) or fibrinogen binding region 1 (Fib-1), the gelatin-binding domain (FnGBD), the cell-binding domain (FnCBD), and fibrinogen binding region 2 (Fib-2). The integrin $\alpha_5\beta_1$ "RGD" interaction motif and "synergy" site are shown. Two free cysteines (SH) were used to specifically label the FRET probes used in this study. Arrows indicate specific intramolecular interactions formed between domains of the FnNTD fragment and the distant FnCBD fragment.

Fn is secreted as a disulfide-linked heterodimer that is modular in nature. Alternative splicing results in Fn monomers that are similar, but not identical, with only one monomer carries a variable region (V). Each Fn module is composed of three structurally defined repeating units termed FnI, FnII, and FnIII (Fig. 2). Several functional protease-stable Fn fragments are known, including the N-terminal domain (NTD), the gelatin-binding domain (GBD), and the cell-binding domain (CBD). The CBD harbors the canonical integrin $\alpha_5\beta_1$, the "RGD" tripeptide interaction motif within the 10th FnIII module, and the "synergy site" in the 9th FnIII module. Fn serves as a

natural ligand for many other integrins, such as $\alpha_v\beta_3$, $\alpha_4\beta_1$, and $\alpha_{IIb}\beta_3$, and their binding sites are mainly located in the CBD. Through CBD and the highly reactive NTD, which interacts with many biological molecules, Fn carries out adhesive functions, linking cells to the substrates. For soluble plasma Fn, however, due to its compact structure, many important binding sites are somewhat cryptic, and they are only exposed after conformational changes during processes such as fibril assembly.[44]

1.4. FnBPA binding to fibrinogen

The A domain of FnBPA is predicted to be made of three separately folded subdomains of N1, N2, and N3 (Fig. 1), which are similar to the Fg binding ClfA of *S. aureus*.[45] Both FnBPA and ClfA use a minimal segment of the N2N3 subdomains to bind Fg at the C-terminus of γ-chain peptide (FgγC),[7] although the mechanisms are different.[28, 46] A recent structural analysis of the N2N3 domains of FnBPA (apo form and in complex with a Fg peptide) revealed that binding the FgγC peptide did not require a "latching" step,[28] one of the common steps in the "dock, lock and latch" ligand-binding mechanism proposed for MSCRAMM.[3] The FgγC peptide docks in a cleft between N2 and N3, forming an additional β-strand that is parallel to the G' strand in N3 in a β-zipper interaction.[28] Such an interaction triggers translocation of the G' strand in N3 to wrap around the FgγC peptide and interact with the N2 subdomain. This "locking" event only induces subtle conformation changes in the individual N2 and N3 subdomains.[28]

Fg, also called factor I, is a large glycoprotein produced in the liver and also found in blood plasma. The major function of Fg is to form fibrin clots that prevent the loss of blood upon vascular injury. Fg plays a role in physiological and pathological

processes related to wound healing, tumor growth, and metastasis, as well as defense mechanisms. These functions are highly regulated in specific ways through interactions with a variety of proteins such as enzymes, membrane receptors, ECM molecules, lipids, and other small molecules.[47] The 340-kDa Fg is composed of three polypeptide chains (α, β, and γ [Fig. 3]) that are arranged as a dimer with three domains: a central E domain and two peripheral D domains (FgD). Fg heterogeneity results from the glycosylation of β and γ chains, the phosphorylation of the α chain, polymorphisms in the α and β chains, and alternative splicing of the α and γ chains.[48] The "tail" of the γ chain extends from the globular domain, which includes the glutamine and lysine residues involved in factor XIIIa-catalyzed cross-linking (Fig. 3). The C-terminal γ-chain peptide is recognized by the platelet integrin $\alpha_{IIb}\beta_3$ during Fg-dependent platelet adherence and aggregation.[49] Fg is also targeted by *S. aureus*, causing Fg-dependent cell clumping and tissue adherence.[3] FnBPA binds to the C-terminal end of the γ chain (FgγC peptide $G^{397}QQ^{399}HHLGGAK^{406}QAGDV^{411}$)**[28]** overlapping with integrin $\alpha_{IIb}\beta_3$ binding sites. Within this region, there are γ chain cross-linking sites (Q^{399} and K^{406}) through which two fragment D moieties covalently link and form a FgD dimer (Fig. 3).

Approximately 75% of Fg is found at high concentration (~3 mg/mL) in blood plasma, and the remainder is distributed in interstitial fluid and lymph. The circulating plasma Fg can be deposited into the ECM with an altered conformation and then function as an ECM protein to facilitate cellular adhesion or the structural integrity of tissues. Recent studies have shown that Fg in cultured cell medium is incorporated into the ECM during the active secretion and assembly of Fn from fibroblasts. Functional

characterization of proteolytic Fn fragments have identified binding sites for Fg on the N-terminal domain of Fn (FnNTD) or fibrinogen binding region 1 (Fib1) and on fibrinogen binding region 2 (Fib2) (Fig. 2).[50-51] Therefore, similar to Fn, Fg also joins Fn that function as both plasma and matrix proteins to perform their diversified functions and also targeted by FnBPA of *S. aureus*.

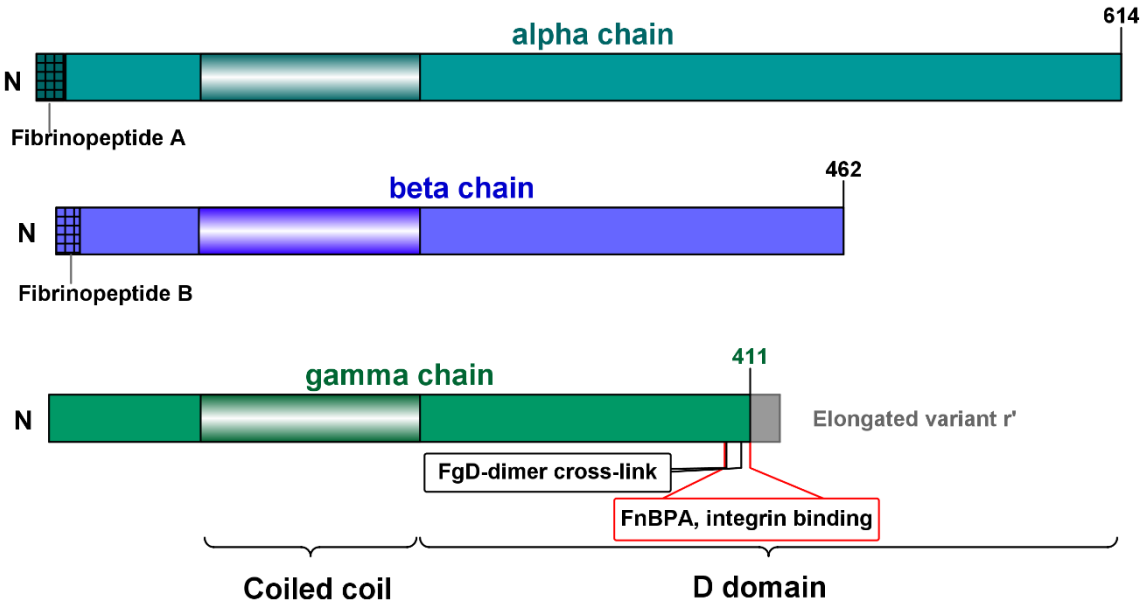

Figure 3. Domain organization of fibrinogen
Fg is formed by three pairs of α, β, and γ chains that are covalently linked to form a "dimer of trimers". The polypeptides are oriented such that N-terminal ends of each monomer meet, while the coiled coil regions stretch out and end in a globular D domain The D domain (FgD) is consist of C-terminal parts of all three chains. FnBPA binds to the C-terminal end of the γ chain (FgγC peptide GQ**Q**HHLGGA**K**QAGDV) overlapping with one of the integrin $\alpha_{IIb}\beta_3$ binding sites. Within this region, there are γ chain cross-linking sites (bolded residues, Q^{399} and K^{406}) through which two fragment D moieties are covalently linked to form a FgD dimer. The elongated variant has a 20 aa sequence insertion at the end ($\gamma'_{434–453}$). Amino acid numbers are based on UniProt sequences (P02671 for Aα, P02675 for Bβ, and P02679 for γ chain), from which the signal peptide sequence was deduced.

1.5. FnBPA-dependent host cell invasion

While *S. aureus* is typically considered an extracellular pathogen, intracellular *S. aureus* is associated with several chronic and reoccurring infections,[12, 52-53] and infection can be established, even in the presence of the vancomycin.[54] *S. aureus* can invade several types of host cells, and while this process requires FnBPA and integrins, it does not usually involve phagocytosis.[38] Thus, *S. aureus* internalized by non-professional phagocytes represents a bacterial reservoir that is protected from antibiotics and innate host defense systems. It has been suggested that tandemly arranged FnBR enables a single FnBPA molecule to interact with multiple Fn molecules to engage an array of $\alpha_5\beta_1$ integrins, triggering a bacterial uptake.[39] *S. aureus* only needs to express a low surface density of FnBPA to establish adhesion and initiate an invasion.[18]

Integrins are essential metazoan heterodimeric glycoproteins that mediate cell adhesion, establish transmembrane connections to the cytoskeleton, and play an integral role in cell signaling pathways.[55] Interestingly, integrins are common targets of pathogens, and they often participate in bacterial and viral adhesion to host cells.[56] Two modes of microbial integrin recognition have been described: direct binding by bacterial surface proteins,[57-59] or indirect binding via physiological ligands, such as Fn.[16, 56, 60] The latter mode is used by *S. aureus*; specifically, FnBPA manipulates Fn function as a natural ligand for $\alpha_5\beta_1$ integrin, activating endocytic pathways, ultimately resulting in the internalization of *S. aureus* by non-professional phagocytes.[14, 18-20, 61] A single high-affinity FnBR is sufficient for $\alpha_5\beta_1$ integrin-dependent in vitro invasion of endothelial cells by *S. aureus*.[18]

1.6. Disease-related polymorphisms in FnBPA

By comparing the *fnbpA* within the disordered FnBR region, several recent studies have found a correlation between cardiovascular infections caused by *S. aureus* and non-synonymous single nucleotide polymorphisms (SNPs) in FnBPA.[22-23, 25] All SNPs within this region are located in the high-affinity Fn-binding repeats 9 (FnBPA-9) and 11 (FnBPA-11), mainly in FnBPA-9 (Fig. 1). Single and double substitutions (H782Q and K786N) were identified in clinical isolates in patients from two continents with infected cardiac device implants[22-23] that exhibited a higher affinity for Fn, as measured by atomic force microscopy. Similar SNP variants (H782Q and K786I) were found in MRSA strains causing infective endocarditis.[25] Some strains had an additional FnBPA-9 inserted or a more immunogenic motif substitution in FnBPA-11. Interestingly, this polymorphism was not found in strains isolated from patients with infected arthroplasties where the abscess exists within a sanctuary space.[62] It seems that a certain "mutation" in FnBPA is selected during endovascular infections where the hemodynamic flow is a factor, and immobilized fibronectin molecules (on tissues or devices) are the dominant host ligand.

1.7. Goals of the study

Although the interaction between FnBPA and the host ligands Fn and Fg have been studied extensively using domains or segments of the proteins, the interplay, and regulation of multiple ligands binding to FnBPA at the same time is still poorly understood. Moreover, the underlining molecular events that lead to FnBPA-dependent invasion have remained elusive. With these in mind, the goals of this study were: first,

develop an expression and purification system to obtain full-length intact FnBPA; second, to carefully characterize the binding of FnBPA to host ligands, including human blood plasma; third, to understand the nature of structural changes induced by FnBPA and correlate these changes with quantitative and direct measurements of Fn–$\alpha_5\beta_1$ integrin interactions; and fourth, to understand how amino acid polymorphisms in Fn-binding repeats impact the strength and formation of the binding complex within specific pathological contexts.

1.8. Methods used in this study

In this study, purified recombinant and native full-length proteins, as well as non-purified blood plasma as materials, were utilized with surface plasmon resonance (SPR) and other biophysical and biochemical methods to investigate structure–activity relationships and regulation of FnBPA–host interactions. Circular dichroism (CD), steady-state fluorescence spectroscopy, dynamic light scattering (DLS), and fluorescence resonance energy transfer (FRET) were used to characterize and examine the conformational status of free or ligand-bound proteins in solution. For binding studies, isothermal titration calorimetry (ITC) and SPR were used to analyze thermodynamics and kinetics of the interactions, and monitor the complex formation in the presence of competing molecules.

1.9. SPR as the main approach

SPR occurs when surface plasmons (electromagnetic waves formed by electrons) propagate along the surface of a thin metal layer and give rise to the resonance.[63] Biacore is a microfluidic surface-based biosensor platform that exploits SPR phenomena to

monitor molecular interactions in real time. This approach requires the attachment of one interacting partner to the surface of a sensor chip and then passing a sample with another interaction partner over it. The binding of molecules to the sensor surface generates a response that is proportional to the bound mass, and the binding of molecules in the bulk sample solution on the sensor surface can be detected with picomolar resolution. The signal is shifted by a binding event or induced conformational changes.[64] The continuous registration of the signal makes it possible to characterize the binding mechanism and determine the association rate constant (k_{on} or k_a) and dissociation rate constant (k_{off} or k_d) as well as the binding affinity (K_D, $K_D = k_{off} / k_{on}$). Thermodynamic parameters can also be estimated by performing binding analyses at multiple temperatures. Aditional complex biological interactions can be investigated with sophisticated designs and comprehensive analyses.

The Biacore assay is performed by injecting the *analyte* (the interaction partner in solution phase) over the sensor chip to which the *ligand* is immobilized (the interaction partner in solid phase) under a continuous flow of *running buffer*. Then, the sensor chip will be regenerated, which is the process of removing bound analyte from the surface, without inactivating the ligand, so that a new cycle of analysis can be conducted on the same active ligand surface. The binding response is measured in *resonance units* (RU), which are proportional to the concentration of bound molecules on the surface. Real-time binding data is recorded as a *sensorgram*, which shows the response (RU) as a function of time (second).

SPR detects interactions that occur on the surface of a sensor chip. The specificity

of the interaction analysis is determined by the nature and properties of the molecule anchored to the sensor surface. There are three different approaches to attach a molecule onto the chip surface: (1) covalent immobilization, where the ligand is attached to a surface through a covalent chemical link, (e.g., the most commonly used amine coupling approach involves a chemical reaction between available primary amine group[s] on the ligand and reactive carboxylic group on the chip surface); (2) high-affinity capture, where the ligand is attached by non-covalent high-affinity interactions, with another molecule that is usually covalently immobilized; and (3) hydrophobic adsorption.

Among many available surface preparation techniques, amine immobilization is the most widely applied and accepted approach. However, amine coupling is a random process, and therefore, the orientation of the immobilized molecule cannot be determined. In addition, the chemical modification of the ligand can potentially affect binding activity. This is particularly true for proteins that have multiple domains and contain several available amine groups. Also, attachment to the surface can introduce heterogeneity in the ligand population. Capturing approaches are alternative strategies to avoid inactivation and achieve homogeneous orientations of the ligand, which is important for experimental design. Some common capturing approaches are streptavidin-biotin capture, antibody-based capture, and tagged-based capture. Interactions between the ligand and capturing molecule should be strong enough to hold the ligand in place so that it does not detach from the surface during an analysis cycle. Recombinant proteins used in the binding studies are often tagged for affinity purification and identification. Following the same principle, tagged recombinant proteins can be captured (or tethered)

onto the sensor chip with high-affinity antibodies for the specific tag, such as poly-histidine, glutathione S-transferase (GST), and Strep-tag II.

CHAPTER II

MATERIALS AND METHODS[*]

2.1. Plasmid construction

Genomic DNA of *S. aureus* USA300 TCH1516 was used as a template to amplify the DNA encoding full-length FnBPA, which corresponded to amino acids 38–981 and covered residues after the signal peptide to residues right before the LPXTG sortase cleavage motif. The initial construct was generated using a modified pET15b vector, which contains a C-terminal fusion to super-folder GFP (green fluorescent protein) that is cleavable by a TEV (Tobacco Etch Virus) protease, followed by a 6x His-tag.[65] This expression plasmid was further developed by adding a 2x StrepII-tag and a TEV protease cleavable site to the N-terminus of the FnBPA gene to generate a double-tagged FnBPA construct. The resulting N- and C-terminal fusion vectors were linearized with BamHI and NheI (New England Biolabs), purified using a QIAQuick Gel Extraction kit (Qiagen), and used in subsequent infusion cloning reactions (Clonetech). All truncated FnBPA proteins were constructed using the same template plasmid DNA, with primers designed for an infusion cloning reaction using the Clonetech online tool.

---

[*] Part of the material reported in this chapter is reprinted and adapted with permission from "Allosteric Regulation of Fibronectin/alpha5beta1 Interaction by Fibronectin-Binding MSCRAMMs" by Liang, X.; Garcia, B. L.; Visai, L.; Prabhakaran, S.; Meenan, N. A.; Potts, J. R.; Humphries, M. J.; Hook, M. *PLoS One* **2016,** *11* (7), e0159118. CC by PLoS. Copyright 2016.

All constructs were verified by sequencing plasmid DNA. The primer sequences are listed in Table 1.

Table 1. Oligonucleotides to generate tagged FnBPA constructs

Name	Designation	Vector with n/c tag	Primer sequence (5'-3')
ALC307	fnbpA38 forward	pET15b-GFPcHis	AAGGAGATATACATATGTCAGAA CAAAAGACAACTACA
ALC308	fnbpA981 reverse	pET15b-GFPcHis	GGTTTTCACCGCTAGCTTCAGATT TCTTAGATTGTGG
FnBPA38F	fnBPA38 forward	pET15b-nStrepII^GFPcHis	ATTTTCAGGGTGGATCCTCAGAA CAAAAGACAACTACAGTAG
FnBPA166F	fnBPA166 forward	pET15b-nStrepII^GFPcHis	ATTTTCAGGGTGGATCCACGGCA TCAGAAAGTAAGCCACGTG
FnBPA189F	fnBPA189 forward	pET15b-nStrepII^GFPcHis	ATTTTCAGGGTGGATCCGCGAAA GTGGAAACGGGTACAGATG
FnBPA511R	fnBPA511 reverse	pET15b-nStrepII^GFPcHis	GGTTTTCACCGCTAGCATTTTTCC CATTTCCGTTCG
FnBPA550R	fnBPA550 reverse	pET15b-nStrepII^GFPcHis	GGTTTTCACCGCTAGCTGATGAA TCATATTCCTCTTC
FnBPA672R	fnBPA672 reverse	pET15b-nStrepII^GFPcHis	GGTTTTCACCGCTAGCTTTCGTAT CTTCAACTGTTGT
FnBPA800R	fnBPA800 reverse	pET15b-nStrepII^GFPcHis	GGTTTTCACCGCTAGCAGGTTTG TCTTTTTCTGTATC

2.2. Recombinant FnBPA expression

The modified pET15b-GFPcHis plasmid was transformed into *Escherichia coli* BL21 (DE3) Gold cells, while the pET15b-nStrepII^GFPcHis plasmid was transformed into the *E. coli* Rosetta (DE3) pLysS strain. A starter culture was prepared by inoculating 50 mL of LB Miller medium with a frozen stock (~20 µl) of the expression strain, followed by growth overnight at 37 °C. The next day, 10 mL of starter culture was transferred into 1 L of growth media containing antibiotics and grown until the optical

density at 600 nm (OD600) reached 0.6–0.8. IPTG (isopropyl β-D-1-thiogalactopyranoside) was then added to the culture at a final concentration of 0.5 mM to induce target protein expression for 3 h at 37 °C or overnight at 20 °C. Then, *E. coli* cells were collected by centrifugation at 5,000*g* for 10 min at 4 °C, washed with TBS buffer, pelleted, and stored at -80 °C.

2.3. Protein purification

2.3.1. Purification of recombinant FnBPA proteins

The general purification strategy for recombinant FnBPA included nickel affinity chromatography, tag removal, "reverse" Nickel affinity, and, finally, gel filtration chromatography. For double-tagged FnBPA, an additional StrepTactin affinity chromatography step was included after the first nickel purification. The detailed steps are as follows: (1) thaw cell pellets and resuspend in Tris-buffered saline (TBS: 50 mM Tris, pH 7.5, and 300 mM NaCl) supplemented with cOmplete Protease Inhibitor Cocktail (Roche). (2) Lyse cells with 4–5 passes through an M-110P microfluidizer at 20,000 psi. (3) Spin down the homogenate at 20,000*g* for 25 min at 4 °C. (4) Collect and filter the supernatant, and then add concentrated imidazole to a final concentration of 20 mM. (5) Load the supernatant over the HisTrap-HP column (GE Healthcare) that was pre-equilibrated with HisTrap binding buffer (50 mM Tris, pH 7.5, 300 mM NaCl, and 20 mM imidazole). (6) Wash column with HisTrap binding buffer until a steady A280 baseline is reached. (7) Elute bound protein with two column volumes of HisTrap elution buffer (50 mM Tris, pH 7.5, 300 mM NaCl, and 200 mM imidazole). (8) Pool peak fractions and load them to a desalting column to exchange buffer to StrepTrap binding

buffer (100 mM Tris, pH 8.0, 150 mM NaCl, and 1 mM EDTA). (9) Load sample to the StrepTrap-HP column (GE Healthcare) and wash column with StrepTrap binding buffer until a steady A280 baseline is reached. (10) Elute bound protein with StrepTrap elution buffer (100 mM Tris, pH 8.0, 150 mM NaCl, 1 mM EDTA, and 2.5 mM desthiobiotin). (11) Add β-mercaptoethanol to a final concentration of 5 mM to the StrepTrap column eluent, add His-tagged TEV protease (10 units of TEV protease per mg of protein), and incubate for 2 h at room temperature and then overnight at 4 °C. (12) Filter the TEV-treated protein sample and load onto a pre-equilibrated HisTrap-HP column. (13) Collect the flow-through fraction, which contains the protein with the tag removed. (14) Concentrate and filter the sample using a 0.22 micron filter , and then pass it over a gel filtration column equilibrated with TBS (20 mM Tris, pH 7.5, and 100 mM NaCl). (15) Store the purified protein at -80 °C in the presence of 10% glycerol.

2.3.2. Thrombin treatment of FnBPA and isolation of fragment

Tag-free FnBPA was incubated with 60 U thrombin and incubated at 37 ˚C for 2 hours. Thrombin was removed from the mixture using a Benzamidine column (GE Healthcare). FnBPA fragments were further isolated using a gel filtration column. Tagged full-length $FnBPA_{38–981}$ was cut with thrombin, and then the mixture was diluted and injected onto the anti-His mAb sensor chip to capture His-tagged FnBPA fragments ($FnBPA_{166–981}$) for SPR analysis.

2.3.3. Purification of native Fn

Human Fn was purified from freshly drawn citrated plasma (Gulf Coast Regional Blood Center, Houston, TX) using gelatin affinity chromatography combined with

arginine affinity chromatography, as described previously.[66] Fn was stored at 4 °C in TBS (50 mM Tris-HCl, pH 7.4, and 150 mM NaCl), and used within one month. The Fn dimer concentration was calculated from the optical density at 280 nm with EC_{280} (1%) = 12.8 and a molecular weight of 500 kDa.

Table 2. Proteins and peptides used in this study

	Description	Source
$FnBPA_{38–981}$	Recombinant full-length FnBPA	This work
$FnBPA_{38–800}$	Recombinant of FnBPA (aa 38–800)	This work
$FnBPA_{38–672}$	Recombinant of FnBPA (aa 38–672)	This work
$FnBPA_{38–609}$	Recombinant of FnBPA (aa 38–609)	This work
$FnBPA_{38–550}$	Recombinant of FnBPA (aa 38–550)	This work
$FnBPA_{38–511}$	Recombinant of FnBPA (aa 38–511, A domain)	This work
$FnBPA_{166–550}$	Recombinant of FnBPA (aa 166–550, thrombin-cut)	This work
FnBPA-3 peptide	Synthetic peptide of FnBPA-3	This work
FnBPA-9 peptide	Synthetic peptide of FnBPA-9	This work
FnBPA-10 peptide	Synthetic peptide of FnBPA-10	This work
Fg	Native fibrinogen purified from human plasma	Enzyme Research
FgD	Proteolytic D-fragment of fibrinogen	Millipore
FgD dimer	Cross-linked fibrin degradation by plasmin	Hyphen BioMed
Fn	Native fibronectin purified from human plasma	This work
FnNTD	N-terminal domain of Fn	Sigma
FnGBD	GBD of Fn	Sigma
FnCBD	CBD of Fn	Millipore
Anti-Fn pAb	Polyclonal rabbit anti-human Fn	ICN Pharmaceuticals,
Anti-Fg pAb	Polyclonal rabbit anti-human Fg	Dako Cytomation
Thrombin	Protease purified from bovine plasma	GE Healthcare
Integrin $\alpha_5\beta_1$	Recombinant ecto domains	Coe[67]
Integrin $\alpha_{IIb}\beta_3$	Native receptor purified from human platelets	Enzyme Research

2.4. Other materials

The Fn-binding repeats of FnBPA (FnBPA-1, FnBPA-3, FnBPA-5, FnBP-9, FnBPA-10 and FnBPA-11) were expressed as GST fusion proteins and purified using the procedure described by Meenan et al.[40] The FnBPA-10 peptide was obtained from the laboratory of Prof. Jennifer R. Potts. BSA (bovine serum albumin) and heparin sodium

(from porcine intestinal mucosa, 17,000–19,000 Da) were obtained from Sigma. Other materials are listed in Table 2.

2.5. SPR-based binding assay

Surface plasmon resonance-based binding experiments were performed at 25 °C on a Biacore 3000 or T200 instrument (GE Healthcare/Biacore, Uppsala, Sweden). The sensorgrams are shown in a format of "analyte → ligand," in that various forms of soluble analyte (different concentration or mixtures with other molecules) were injected onto an immobilized ligand surface.

2.5.1. Sensor surface preparation

The protein ligands were covalently coupled to research-grade sensor chips (GE Healthcare) using an amine coupling kit containing *N*-(3-Dimethylaminopropyl)-*N′*-ethylcarbodimide hydrochloride (EDC), *N*-hydroxysuccinimide (NHS), and ethanolamine (pH 8.5) (GE Healthcare/Biacore AB). During immobilization, phosphate buffered saline (PBS: 137 mM NaCl, 2.7 mM KCl, 8.06 mM Na_2HPO_4 and 1.94 mM KH_2PO_4, pH 7.4) was used as running buffer, with a flow rate of 5 μL/min. The optimal immobilization condition for each protein was determined by a pH scouting experiment. Based on the scouting results and desired surface densities, various conditions (pH and concentration) were applied to each protein for the immobilization; they are listed in Table 3. The immobilization steps are: the flow cell surface was first activated by injecting EDC/NHS, followed by a protein amine reaction, and finally, the surface was deactivated with ethanolamine. A reference surface was made with activation and deactivation steps without coupled protein.

For the binding assay using the capture approach, approximately 10,000 RU of anti-His mAb (GE Healthcare/ Biacore) or StrepMAB-Immo (IBA GmbH) was immobilized on a CM5 chip to reversibly capture the fusion protein containing the His-

tag or Strep-tag. A surface with antibody immobilized and without captured ligand was used as a reference surface.

Table 3. Conditions for immobilization of proteins for Biacore binding experiments

Ligand	Concentration	buffer	Chip	Density
Anti-His mAb	10 μg/mL	10 mM sodium acetate, pH 5.0	CM5	11,000
StrepMAB-Immo	20 μg/mL	10 mM sodium acetate, pH 5.0	CM5	10,000
Fg	10 μg/mL	10 mM sodium acetate, pH 5.5	CM4	2700
FgD	5 μg/mL	10 mM sodium acetate, pH 5.0	CM4	900
FgD dimer	20 μg/mL	10 mM sodium acetate, pH 5.5	CM4	1000
FnNTD30k	20 μg/mL	10 mM sodium acetate, pH 5.5	CM3	2300
FnBPA	10 μg/mL	10 mM sodium acetate, pH 4.5	CM3	700
Integrin $\alpha_5\beta_1$	10 μg/mL	10 mM sodium acetate, pH 4.8	CM5	1400
BSA	25 μg/mL	10 mM sodium citrate, pH 5.0	CM5	5000

2.5.2. Binding studies

Frozen Fg stocks (about 10 mg/ml in 20 mM sodium citrate-HCl, pH 7.4) were thawed in a 37 °C water bath without any agitation and stored at room temperature before use. Other soluble proteins were prepared by dialysis using Slide-A-Lyzer MINI Dialysis Units or spin desalting columns with the proper molecular weight cutoff (Thermo Fisher Scientific). The peptide was dissolved in PBS, and the concentration was determined using the absorbance at 205 nm.[68]

To capture the tagged protein, a flow rate of 20 μL min^{-1} was used to inject the ligand until the desired density was reached, and then the surface was stabilized for 3 min before performing a binding experiment. A flow rate of 30 or 50 μL min^{-1} was used for all binding experiments. To regenerate the ligand surface, the captured protein was

removed by a 15-s injection of 10 mM glycine (pH 1.7). For the Fn–integrin interaction, the integrin surface was regenerated to remove bound Fn by injecting 1 M NaCl for 1 min.

2.5.3. Data analyses

All SPR responses were baseline corrected by subtracting the systematic noise from the corresponding reference surface. Double-referenced SPR response curves (with the buffer blank run also subtracted) were used for affinity determination.

For steady-state interactions, the equilibrium response of each injection was collected and plotted as a function of the concentration of injected protein. A one-site binding (hyperbola) model was fit to the data (GraphPad Prism 4, GraphPad Software, Inc.) to obtain the equilibrium dissociation constant K_D. Non-equilibrium data were globally fit to a 1:1 Langmuir binding model using BIAevaluation software (Version 4.1). Association and dissociation rate constants, k_a and k_d, were obtained from the fits, and the dissociation constant, K_D, was derived ($K_D = k_d / k_a$).

Kinetic constants were obtained from fitting the curve to a predefined bivalent analyte model using BIAevaluation software (Version 4.1). Heterodimeric Fn has two identical binding sites for integrin $\alpha_5\beta_1$. The reaction between soluble Fn analyte (A) and immobilized integrin ligand (L) can be described by

$$\mathrm{A} + \mathrm{L} \underset{k_{d1}}{\overset{k_{a1}}{\longleftrightarrow}} \mathrm{AL} + \mathrm{L} \underset{k_{d2}}{\overset{k_{a2}}{\longleftrightarrow}} \mathrm{AL_2}$$

Binding to the first ligand is described by a single set of rate constants (k_{a1}, k_{d1}), so that the two sites on the analyte are equivalent in the first binding step. Binding of the

second ligand is described by the second set of rate constants (k_{a2}, k_{d2}), which are reported in the unconventional units of $RU^{-1}s^{-1}$. The first set of rate constants was used to calculate the dissociation constant K_D ($K_D = k_{d1}/k_{a1}$).

2.6. ELISA-type binding assays

Enzyme-linked immunosorbent assay (ELISA) experiments were conducted at room temperature, and each sample was assayed in triplicate. The immunoassay microplate Immulon 2HB (Thermo Scientific, Waltham, MA) was coated with 2 µg integrins dissolved in TBS for 1 hour. The plate was then blocked for 1 h with 1% (w/v) BSA in a buffer "A" (TBS with 1 mM $MnCl_2$). Citrated plasma (stored at -20°C for less than 6 months) was quickly thawed at 37 ˚C and centrifuged to remove aggregates. The supernatant was diluted 10-fold in buffer "A" and then mixed with varying concentrations of the FnBPA-10 peptide to a final concentration of 5% plasma. The sample mixtures were added to the plate and incubated for 1 h. The plate was washed three times with buffer "B" (TBS with 1 mM $MnCl_2$, and 0.05% Tween-20) before the addition of the rabbit anti-Fn antibody. Following the wash with buffer "B," AP-conjugated goat-anti-rabbit IgG (BioRad, Hercules, CA) was added to the plate and incubated for 1 h. All antibodies were diluted 2000-fold in buffer "B" containing 1% BSA. Alkaline phosphatase substrate pNPP (para-Nitrophenylphosphate, Pierce) was added after washing, and the absorbance was measured at 405 nm using a Thermo Max plate reader (Molecular Devices, Sunnyvale, CA).

2.7. Isothermal titration calorimetry

Experiments were performed at 25 ˚C with a MicroCal PEAQ-ITC instrument

(Malvern) in PBS (137 mM NaCl, 2.7 mM KCl, 8.06 mM Na_2HPO_4 and 1.94 mM KH_2PO_4, pH 7.4). The protein concentration was determined using the absorbance at 280 nm and the calculated extinction coefficient. For Fg and Fn, dimer concentrations were used. Each titration began with a 0.4-µl injection followed by 4 µl injections. Each injection (at a speed of 0.5 µl/s) was spaced at 150-s intervals at a stirring speed of 600 rpm. Binding isotherms were fit to a One Set of Sites binding model using MicroCal PEAQ-ITC Analysis Software (version 1.1.0).

2.8. Circular dichroism spectroscopy

CD measurements were carried out at ambient temperature on a Jasco J-720 spectropolarimeter (Easton, MD) in the near-UV region (250–350 nm) with a 1-cm cell, and in the far UV region (190–250 nm) with a 0.2-mm cell. Ten scans were collected and averaged at a scan speed of 200 nm min^{-1}, with a time constant of 1 s and bandwidth of 1 nm. The data were reported as an original CD signal (mdeg) or mean residue ellipticity, which was calculated based on the measured CD signal and the mean residue molecular weight of the protein sample (for Fn, it is 110). The spectra of the protein solution were background-corrected with the CD signal obtained from the buffer.

2.9. Steady-state fluorescence spectroscopy

Fluorescence spectra were measured using spectrofluorimeter LS 50B (Perkin-Elmer). Two excitation wavelengths were used to excite intrinsic fluorescence: 280 nm (excite both Tyr and Trp) and 295 nm (excite only Trp). Fluorescence emission was measured in the 300–420 nm wavelength region, with bandwidths of both slits set to 5 nm. Each fluorescence spectrum was the average of three measurements, with a scan

speed of 300 nm/min. All spectra were corrected for background fluorescence by subtracting the appropriate blanks.

2.10. Dynamic light scattering

DLS measurements were performed using the DynaPro Titan Ambient laser unit (Wyatt Technology Corporation) with a wavelength at 828.5 nm and 10% to 12% laser power. Samples were dissolved in TBS and filtered through a 0.22-μm filter to eliminate any particles. Fn concentration was maintained at 0.8 mg ml^{-1} (1.6 μM as dimer) in TBS (50 mM Tris-HCl, pH 7.4, 150 mM NaCl) for the conditions tested. After equilibration at room temperature for 15 to 30 min, the samples were measured three times, with each measurement lasting 100 seconds (10 acquisitions, 10 seconds each). Data analyses were performed using Dynamics V6 software.

2.11. Fluorescence resonance energy transfer

Fluorescent labeling of human plasma Fn was performed at room temperature as described previously.[69] The fluorescent probes used in this study were purchased from Molecular Probes. Briefly, fresh purified human plasma Fn at 1.2 mg ml^{-1} in TBS was partially denatured in 4 M GdnHCl (Sigma) for 15 min to expose free cysteines in the Fn dimer. The denatured Fn was mixed with thiol-reactive Alexa Fluo 546 C5-maleimide (AF546, ~15-fold molar excess over Fn monomer concentration) and incubated for 2 h with gentle rocking. The acceptor fluorophore, AF546-conjugated Fn (~0.9 mg ml^{-1}), was labeled with a second probe, the amine-reactive Alexa Fluor 488 carboxylic acid-succinimidyl ester-mixed isomers (AF488, ~20-fold molar excess). After each labeling reaction, the unbound dye was removed using a PD-10 desalting column (GE

Healthcare). The labeling ratios were ~8 AF488 donors and ~4 AF546 acceptors in each Fn dimer.

FRET between the donor- and acceptor-labeled Fn was measured using spectrofluorimeter LS 50B (Perkin-Elmer) at room temperature with an excitation wavelength at 493 nm. The sensitivity of the FRET response to Fn unfolding was evaluated under a mild denaturant (up to 2 M GdnHCl). Measurements of MSCRAMM-induced FRET within Fn were performed by titrating 0.5, 2 or 5 µl of 50 µM FnBPA-10 into 500 µl of labeled Fn. Subsequently, the emission spectra collected for each titration were recorded and normalized to the donor emission peak so that changes were only reflected by changes in the acceptor peak. Control experiments were conducted using an equimolar solution of donor-labeled Fn with acceptor-labeled Fn in the presence and absence of 2 M GdnHCl to confirm the absence of energy transfer between adjacent Fn molecules in solution.

CHAPTER III

RESULTS*

3.1. Double-tagged full-length FnBPA shows Fg- and Fn-binding activities

Initially, I constructed a C-terminal tagged full-length FnBPA using a modified pET15b vector that contains a TEV protease cleavable C-terminal fusion to GFP, followed by a 6×His-tag. The gel filtration chromatography showed two partially overlapping peaks after tag removal (data not shown). As shown in Figure 4A and C, there are two bands on the SDS-PAGE gel, and both were able to bind Fn (Fig. 4D); however, only the higher MW band exhibited Fg-binding activity (Fig. 4B) in the ligand blot analysis. The larger band migrated as an apparent molecular mass around 180 kDa (Fig. 4A), which was much greater than the calculated MW (105 kDa) for full-length FnBPA. This is expected, because FnBPA is composed of 11 repetitive disordered segments, and slower SDS-PAGE migration is a hallmark of an intrinsically disordered protein.

* Part of the data reported in this chapter is reprinted and modified with permission from "Allosteric Regulation of Fibronectin/alpha5beta1 Interaction by Fibronectin-Binding MSCRAMMs" by Liang, X.; Garcia, B. L.; Visai, L.; Prabhakaran, S.; Meenan, N. A.; Potts, J. R.; Humphries, M. J.; Hook, M. *PLoS One* **2016,** *11* (7), e0159118. CC by PloS, copyright 2016; and from "Amino acid polymorphisms in the fibronectin-binding repeats of fibronectin-binding protein A affect bond strength and fibronectin conformation" by Casillas-Ituarte NN, Cruz CHB, Lins RD, DiBartola AC, Howard J, Liang X, Höök M, Viana IFT, Sierra-Hernández MR, Lower SK. *J Biol Chem*. 2017, 292(21):8797-8810. doi: 10.1074/jbc. M117. 786012. Copyright 2017.

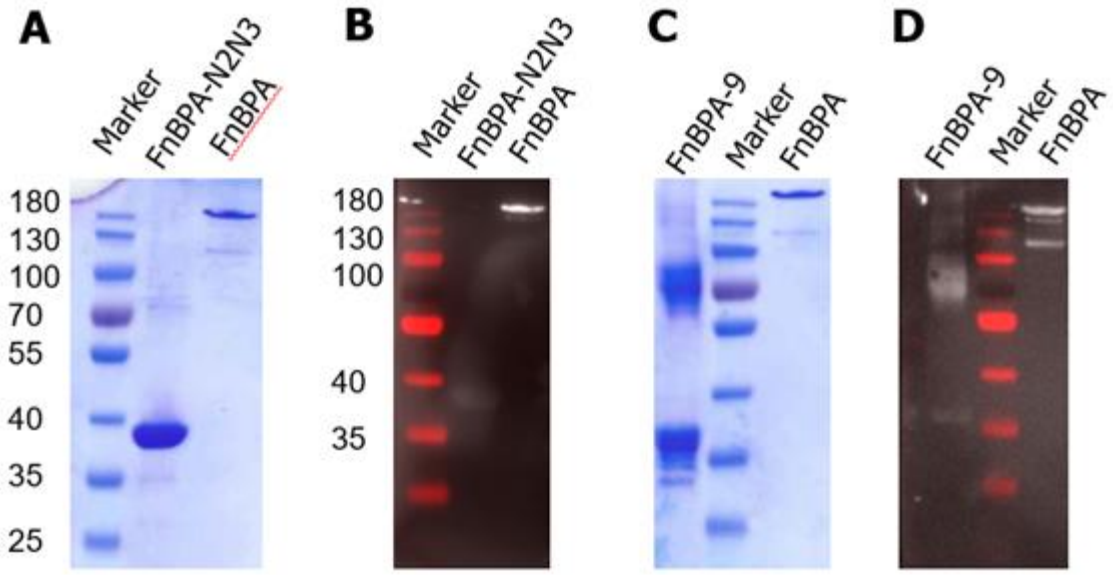

Figure 4. Far-Western ligand blot of recombinant FnBPA with Fg and Fn
(A and C) Purified and tag-removed recombinant FnBPA are separated and visualized on an SDS-PAGE gel with Coomassie staining. Calculated MW of full-length FnBPA protein is 105 kDa. (B) Fg ligand blot was probed with anti-Fg pAb. FnBPA-N2N3 (Fg-binding domain) was included as a positive control. (D) Fn ligand blot was probed with anti-Fn pAb. One high-affinity Fn-binding repeat FnBPA-9 (GST-tagged) was used as a positive control.

This initial characterization indicates that the full-length FnBPA is prone to degradation, resulting in reduced Fg binding. The degradation of FnBPA must occur from the N-terminus since the purification happens through the C-terminal His-tag. To generate intact, full-length, and stable truncations of FnBPA, I improved the initial expression and purification strategy by adding a 2xStrepII-tag and a TEV protease cleavable site to the N-terminus of the FnBPA gene to generate a double-tagged FnBPA construct (Fig. 5) for purification and characterization of full-length FnBPA ($FnBPA_{38–981}$ or $FnBPA_{fl}$) and different truncations.

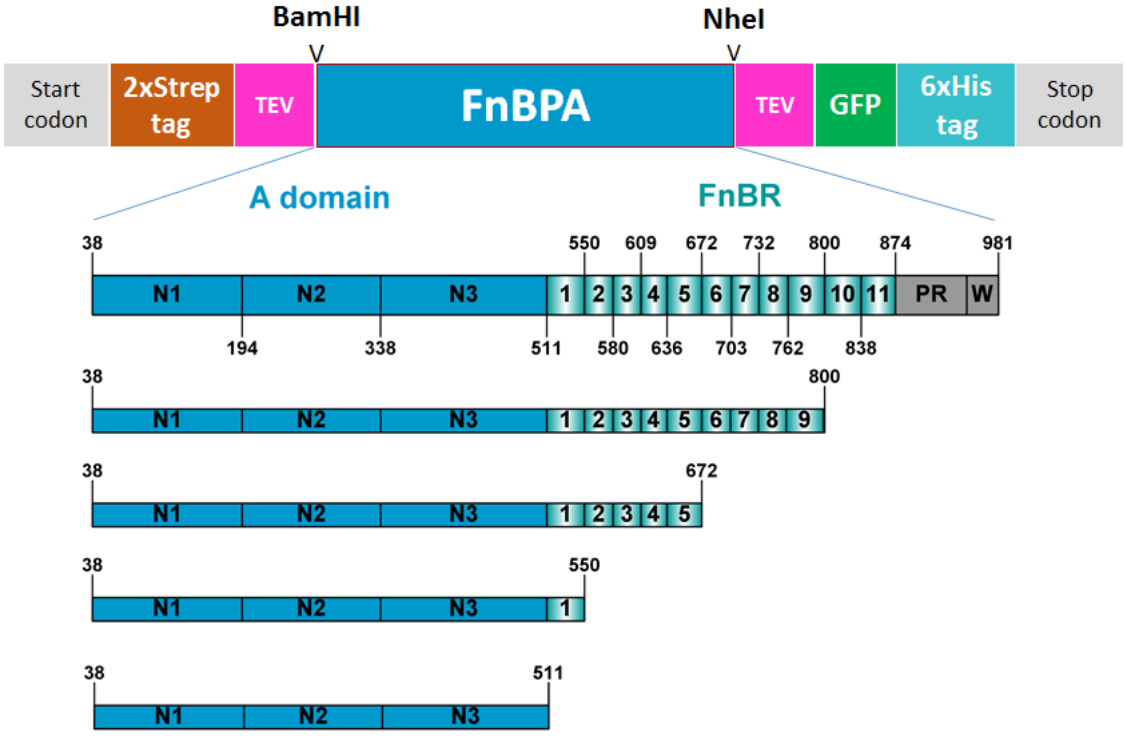

Figure 5. Construct designed for double-tagged FnBPA expression and purification Sequence encoding FnBPA was cloned into the BamHI/NheI multiple cloning sites of the modified pET15b vector. Construct utilizes N-terminal twin Strep-tag II and an expression tag at the C-terminus that encodes for GFP, followed by the 6xHis tag. The tags at both ends can be removed with TEV protease cleavage sites. Five constructs used for this study are shown.

3.2. Generation of FnBPA biosensor for SPR-binding study

Adhesion reactions depend on the conformation of the surface molecule and whether a system is static or dynamic.[70-72] To characterize the interaction that is more relevant to physiological conditions, I used the SPR-based Biacore platform to create sensor surfaces that mimic the surface orientations of the molecules studied, for example, FnBPA on the bacterial surface and the integrin receptor on host cell surface.

Figure 6 shows the schematic of the SPR sensor chips and capture strategies. This approach generates a directed structural orientation of FnBPA that is tethered to the surface, potentially offering optimal site exposure and flexibility. Taking advantage of the double tags, N-terminal capturing can provide additional binding information and validation of the assay system.

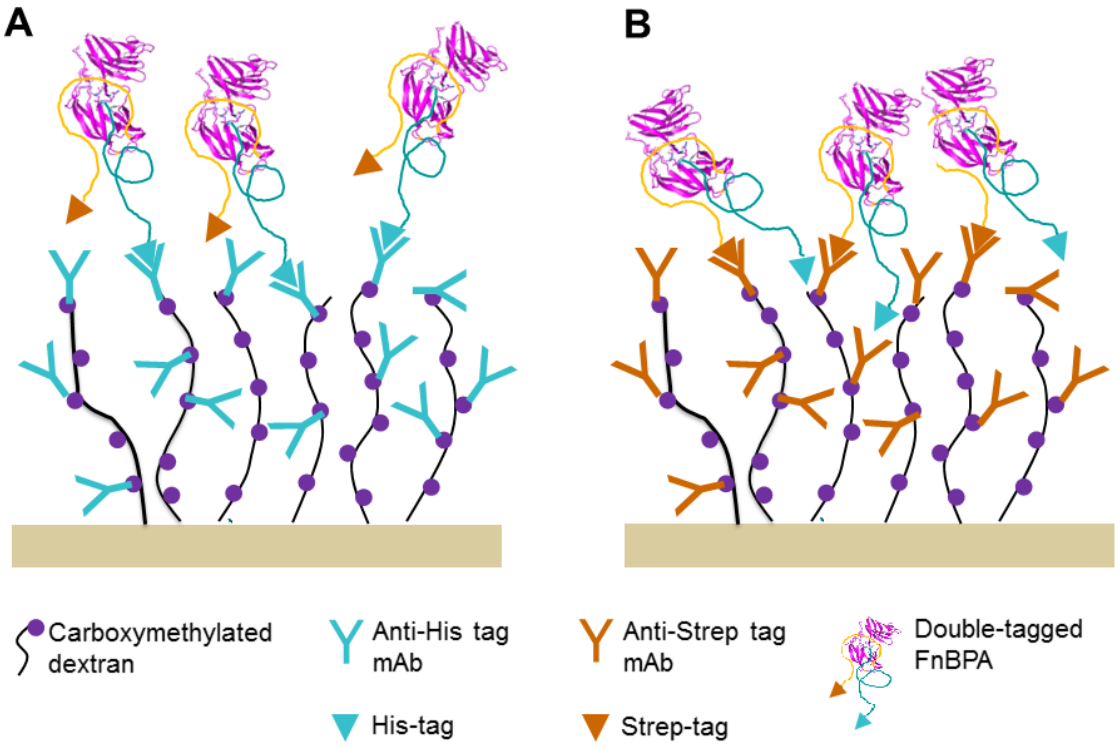

Figure 6. Schematic of the SPR sensor chips and capture strategies
Biacore sensor chip CM5 was used to capture antibodies. All chips have a gold layer coated with a carboxymethylated dextran matrix and use amine coupling to covalently link (A) an anti-histidine tag antibody that can capture a C-terminal His-tagged FnBPA protein, or (B) an anti-Strep-tag II antibody that can capture an N-terminal Strep-tag II-linked FnBPA protein to the chip surface. This approach generates a directed structural orientation of FnBPA that is tethered to the surface, offering optimal site exposure and flexibility.

3.3. Strong binding of Fg, Fn, and plasma to surface-anchored FnBPA

The interaction between Fg and FnBPA has been studied by different groups using such techniques as ELISA, fluorescence polarization, ITC, and SPR.[7, 28] The reported affinities between FnBPA truncates and FgγC peptide or immobilized Fg were from 1 to 10 μM. In this study, when full-length FnBPA was tethered to sensor chip surface, it reacted rapidly and tightly with the host ligands. As shown in Fig. 7, Fg binds to FnBPA with a K_D value of 10 nM (Fig. 7A), which is more than 100-fold stronger than previous values, while K_D value for Fn binding of 0.4 nM (Fig. 7B) was similar to the previously determined K_D using ITC and SPR methods. Interestingly, when the FnBPA surface was exposed to human blood plasma, the plasma–FnBPA interaction (Fig. 7C) was tighter, based on the slower observed off-rate (smaller k_d value). Although the k_a and K_D values for plasma binding could not be determined because the concentration of the binding component was unknown, comparing the dissociation phase (k_d or complex halftime, which is concentration independent) after complexation (Fig. 7D) indicates that plasma strongly reacts with FnBPA surface and forms much more stable complex than Fn or Fg alone. It is unclear why there is such a huge difference in the complex halftime values measured for plasma with Fn and Fg (5095 s, 577 s, and 164 s, respectively) in Fig. 7D. While Fg dissociates rapidly, the plasma component did not dissociate from FnBPA surface.

On the same FnBPA surface, the occupancy of plasma binding is ~ 800 RU (Fig. 7C), which is much higher than the combined occupancy from Fg (~ 50 RU, Fig. 7A) and Fn (~ 180 RU, Fig. 7B). This is expected because, within a single FnBPA molecule,

there are more than six Fn binding sites and one Fg binding site. Multivalent Fn binding is clear with the intact and compact Fn in the plasma compared to the purified Fn with an extended conformation (multiple steps and harsh conditions partially unfolded the Fn tertiary structure). Such an effect of Fn binding may also contribute to the observed stable plasma–FnBPA complex.

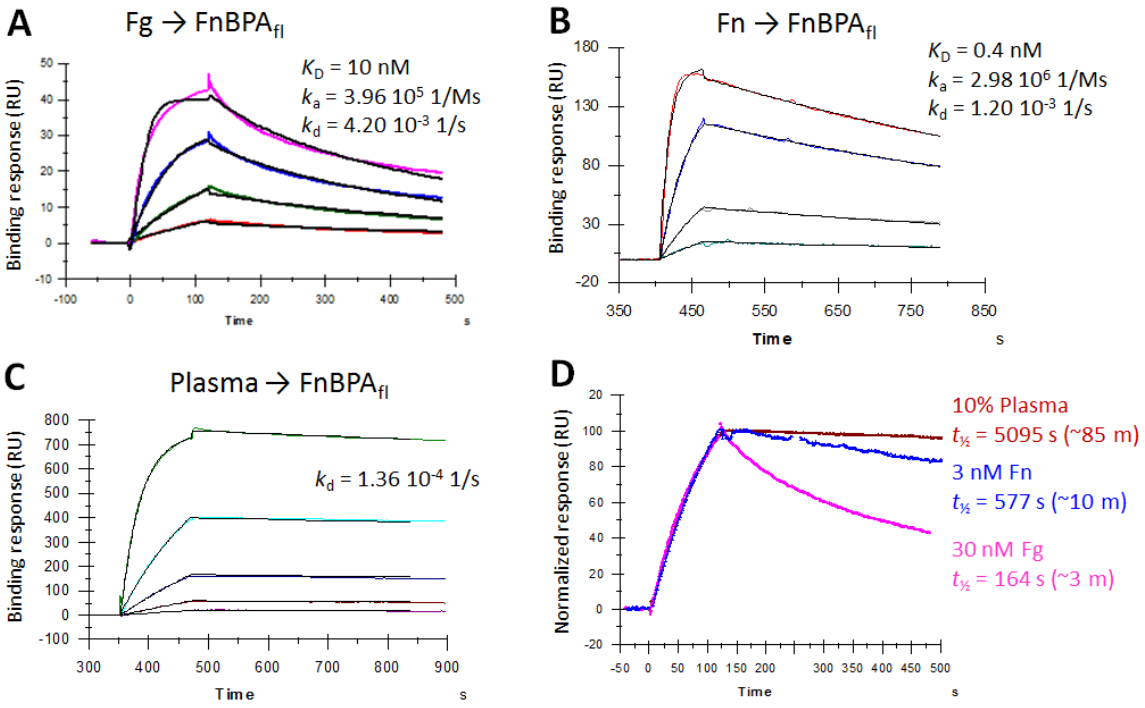

Figure 7. SPR binding analyses of Fg, Fn, and plasma binding to FnBPA surface $FnBPA_{fl}$ was captured by the SPR sensor chip which had immobilized anti-His mAb. (A) Fg at 10, 30, 90, and 270 nM; (B) Fn at 1, 3, 9, and 27 nM; and (C) human blood plasma at 0.37%, 1.1%, 3.3%, 10%, and 50% was injected onto the $FnBPA_{fl}$ surface. SPR response curves are shown with colored lines: lowest curve corresponds to the lowest concentration of sample injected. Kinetic analyses were performed by fitting SPR response curves to a 1:1 Langmuir binding model (fit lines are shown in black). k_a and K_D values for plasma binding could not be determined due to unknown ligand concentration. (D) Complex halftime ($t_{½} = \ln 2/k_d$) was determined based on the dissociation constant of the complex and used as a signature of FnBPA:ligand(s) complex for comparison.

3.4. Fg and Fn in plasma simultaneously bind FnBPA

The previous study of Fg binding to a FnBPA construct ($FnBPA_{189–550}$) containing adjacent Fg- and Fn-binding sites revealed that Fg binding is negatively regulated by the binding of Fn. To evaluate whether such regulation also occurs in full-length FnBPA, the plasma–FnBPA interaction was characterized in more detail. As shown in Fig 8, when the FnBPA sensor surface was exposed to the plasma, both Fg and Fn can bind simultaneously. The half maximum binding of plasma to $FnBPA_{fl}$ was estimated to be 15% (Fig 8A). The expected Rmax for the 1:1 interaction of Fn: $FnBPA_{fl}$ was 150 RU, while that for Fg: $FnBPA_{fl}$ was 100 RU. Based on the experimental Rmax value of 980 RU, if Fn and Fg were the only components that bound to FnBPA, the stoichiometry calculated as Fg:$FnBPA_{fl}$ = 6:1 and Fg:$FnBPA_{fl}$ = 1:1. This suggests that all six high-affinity Fn-binding sites in $FnBPA_{fl}$ can be saturated with Fn, and Fg can still bind to $FnBPA_{fl.}$ Figure 8B shows that molecules in the blood plasma binding to $FnBPA_{fl}$ resulted in a total response of ~ 780 RU. This plasma component could be recognized by anti-Fg (~300 RU) and anti-Fn (~1800 RU) at a recognition ratio of 6:1 (anti-Fn:anti-Fg). This reveals that six times more Fn than Fg can be recognized in the plasma by $FnBPA_{fl}$, implying that all the six high-affinity Fn-binding sites are occupied by the compact Fn molecule, without steric hindrance effects and with such high Fn occupancy Fg can still bind.

3.5. Fg binds tightly to the FnBPA surface at additional contact sites

There is a large discrepancy in FnBPA–Fg binding affinity measurements between those previously reported (micromolar range) and the SPR results from this

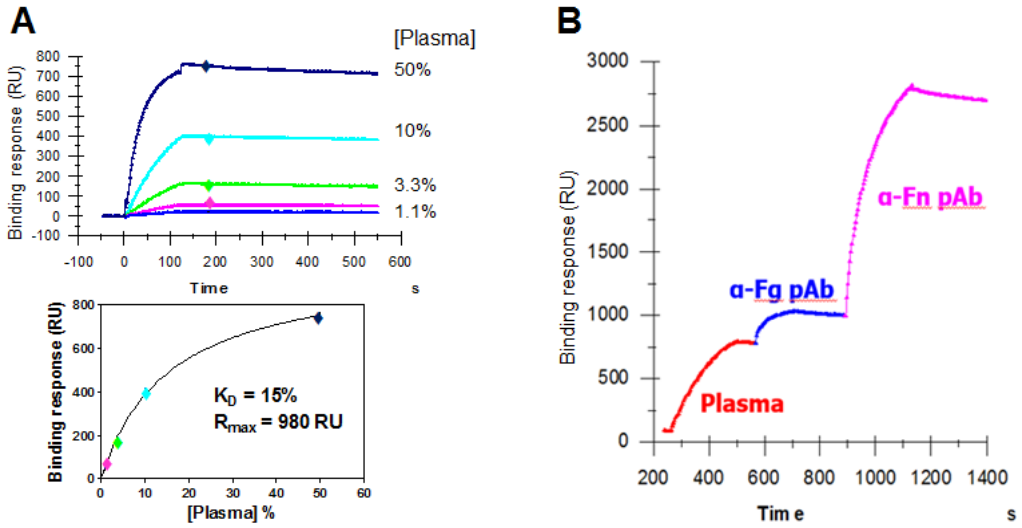

Figure 8. Characterization of plasma–FnBPA interaction
$FnBPA_{fl}$ was captured by the anti-His antibody on the Biacore chip and (A) serially diluted plasma was injected onto the $FnBPA_{fl}$ surface (~30 RU). (B) Plasma (10%) was injected onto $FnBPA_{fl}$, followed by anti-Fg and anti-Fn polyclonal antibodies.

study (~ 10 nM). Some possible explanations are: (1) the amine coupling of Fg or FgD in the previous studies[7, 28] could potentially destroy the conformation of the Fg or FgD molecules. (2) The slower off-rate observed in Figure 7A, compared to the previously shown very fast off-rate (too fast to detect any kinetics, based on the sensorgrams shown in the papers[28]), indicates that complex formation may involve another region of Fg in addition to the γ-chain peptide. To address these questions, FgD-dimers, whose FnBPA binding site is blocked or inactivated by γ chain cross-linking (Fig. 3) and directly immobilized Fg and FgD, were used for the SPR assay. As shown in Figure 8, amine coupled Fg molecules (Fig. 9A to C) bind weaker (micromolar affinities) compared to soluble Fg molecules (Fig. 9D to F), with low nano-molar affinities. FgD and FgD dimer (FgγC inactive form) show similar binding strength to FnBPA, indicating that there is an

alternative FnBPA binding site in FgD, in addition to that on the γ-chain. When the FnBPAfl surface was exposed to Fg (Fig. 9D), stronger binding was observed (K_D = 10 nM) compared to FgD (K_D = 86 nM), suggesting that there may be alternative binding site or conformation in Fg that is not present in FgD. Data from these SPR binding analyses are summarized in Table 4.

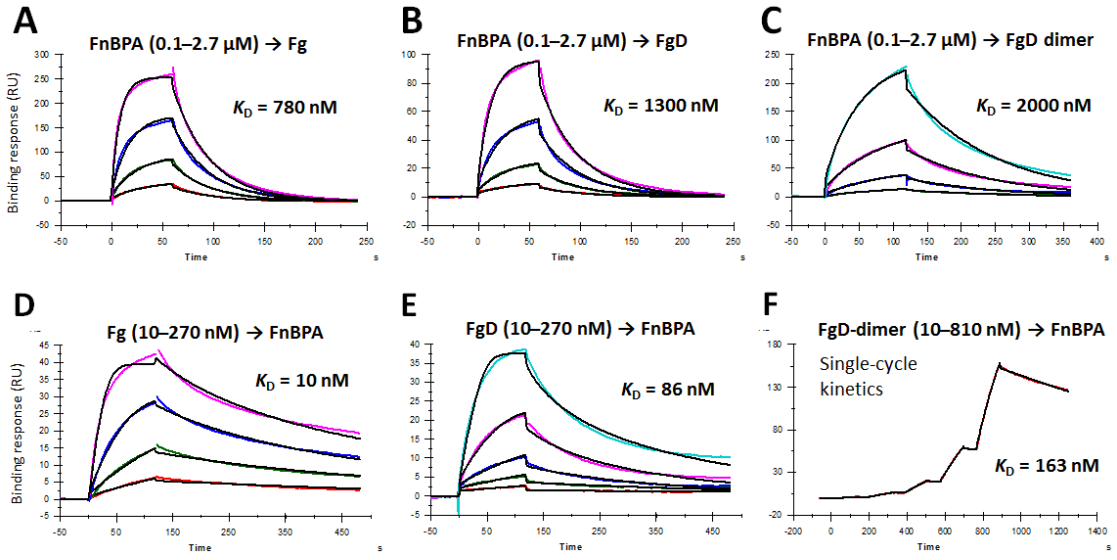

Figure 9. SPR analyses of the interaction between Fg and FnBPA
Analyte solution at indicated concentration was injected onto the ligand surface. (A–C) Host ligand was directly immobilized on the sensor chip. (D–F) $FnBPA_{fl}$ was captured on the SPR sensor chip with immobilized anti-His mAb. SPR response curves are shown with colored lines; lower curve corresponds to the lower sample. Kinetic analyses were performed by fitting SPR response curves to a 1:1 Langmuir binding model (fitted lines are shown in black). SPR experiments for other FnBPA proteins were done in the same way. K_D and kinetic values are summarized in Table 4. FgD dimer binding was analyzed using the single-cycle kinetics method.

3.6. Thrombin cleaves FnBPA and alters Fg-binding activity

It was previously shown that proteolytic removal of N1 subdomain by thrombin

Table 4. Summary of the kinetic parameters for interactions from SPR

Analyte solution	Ligand surface	K_D	k_a	k_d	$t_{1/2}$ (s)	Reference
	Amine coupled	**(nM)**	**($\times 10^6$ $M^{-1}s^{-1}$)**	**($\times 10^{-3}$ s^{-1})**		
Fn	$FnBPA_{189–550}$	0.359 ± 0.001	ND	ND		Stemberk[28]
FnNTD	$FnBPA_{189–550}$	0.393 ± 0.002	ND	ND		Stemberk[28]
	His-tag Captured	**(nM)**	**($\times 10^6$ $M^{-1}s^{-1}$)**	**($\times 10^{-3}$ s^{-1})**		
Plasma	$FnBPA_{fl}$	ND	ND	0.136	5095	This work
Fn	$FnBPA_{fl}$	0.321 ± 0.066	3.00 ± 0.20	1.08 ± 0.18	642	This work
FnNTD	$FnBPA_{fl}$	0.263 ± 0.027	3.03 ± 0.42	0.80 ± 0.14	866	This work
Fn	$FnBPA_{38–800}$	0.714 ± 0.146	1.70 ± 0.41	1.18 ± 0.06	587	This work
Fn	$FnBPA_{38–672}$	0.639 ± 0.057	2.66 ± 0.46	1.58 ± 0.05	439	This work
Fn	$FnBPA_{38–550}$	0.277 ± 0.042	4.04 ± 0.04	1.12 ± 0.01	619	This work
FnNTD	$FnBPA_{38–550}$	0.260 ± 0.054	7.73 ± 1.64	1.95 ± 0.04	355	This work
Fn	$FnBPA_{38–511}$	NB				This work
	Amine coupled	**(nM)**	**($\times 10^4$ $M^{-1}s^{-1}$)**	**($\times 10^{-3}$ s^{-1})**		
$FnBPA_{37–605}$	Fg	11,000 ±1200	ND	ND		Wann[7]
$FnBPA_{189–511}$	FgD	1500 ± 100	ND	ND		Stemberk[28]
$FnBPA_{189–550}$	FgD	1500 ± 100	ND	ND		Stemberk[28]
$FnBPA_{fl}$	Fg	725 ± 74	3.81 ± 0.39	27.5 ± 0.02	25	This work
$FnBPA_{fl}$	FgD	1180 ± 165	2.32 ± 0.21	27.2 ± 1.32	25	This work
$FnBPA_{fl}$	FgD dimer	1610 ± 511	0.52 ± 0.20	7.78 ± 0.02	89	This work
$FnBPA_{38–550}$	Fg	605 ± 29	3.89 ± 0.19	23.5 ± 0.00	29	This work
$FnBPA_{38–550}$	FgD	939 ± 40	2.21 ± 0.09	20.7 ± 0.00	33	This work
$FnBPA_{38–511}$	Fg	1420 ± 207	1.21 ± 0.55	17.1 ± 1.68	41	This work
	His-tag Captured	**(nM)**	**($\times 10^6$ $M^{-1}s^{-1}$)**	**($\times 10^{-3}$ s^{-1})**		
Fg	$FnBPA_{fl}$	15.7 ± 5.6	24.2 ± 13.3	3.45 ± 0.75	201	This work
FgD	$FnBPA_{fl}$	71.6 ± 20.0	23.7 ± 12.6	15.7 ± 4.26	44	This work
FgD dimer	$FnBPA_{fl}$	163	0.339	0.553	1253	This work
Fg	$FnBPA_{38–800}$	27.3 ± 1.8	10.4 ± 3.6	2.58 ± 1.47	269	This work
Fg	$FnBPA_{38–672}$	22.3 ± 8.1	13.0 ± 3.7	2.70 ± 0.19	257	This work
Fg	$FnBPA_{38–550}$	20.2 ± 7.6	18.6 ± 2.0	3.67 ± 1.13	189	This work
FgD	$FnBPA_{38–550}$	375 ± 151	2.16 ± 0.6	7.63 ± 0.86	91	This work
Fg	$FnBPA_{38–511}$	1030 ± 20	ND	ND		This work

$FnBPA_{fl}$: full-length FnBPA or $FnBPA_{38–981}$; ND: not determined; NB: no binding detected

did not affect fibrinogen binding or biofilm formation.[30] However, this study used an engineered *S. aureus* strain that harbored multiple copies of a shuttle plasmid carrying the *fnbpA* gene, and bacteria were grown in broth supplemented with thrombin. The size

of the cleaved product was estimated by SDS-PAGE of the surface-extracted FnBPA. In such an assay system, thrombin cleavage could be incomplete, and high expression of FnBPA within the strain and surface avidity could still allow bacteria to attach to the Fg-coated plate. In this study, I used analytic methods with purified recombinant proteins as the substrate and re-purified the thrombin cut product for functional characterization. As shown in Fig. 10, thrombin digested full-length FnBPA into two fragments (Fig. 10A), and each appeared to have a higher than expected molecular mass (90,842 and 13,938 Da), suggesting the presence of a disordered segment in the fragments. The thrombin treated full-length FnBPA, after gel filtration separation, the large protein peak was subjected to electrospray native mass spectrometry analysis (Fig. 10B). The mass of 104,900 correlates to the full-length FnBPA, and the mass of 90,880 corresponds to $FnBPA_{166–981}$ after thrombin cuts at Arg165.

The activity of the thrombin-treated FnBPA surface was analyzed using SPR. The double-tagged FnBPA was first treated with thrombin and then captured on an anti-His sensor chip (the capturing step is actually a purification step). As shown in Fig. 10C and D, Fg binding was significantly reduced for FnBPA cut with thrombin, while Fn binding was unchanged.

3.7. $FnBPA_{38–550}$ is the minimal fully active Fg-binding domain

The additional contact in Fg and strong Fg–FnBPA interaction raised the possibility that FnBPA may also require a specific conformation other than the previously identified N2N3 cleft region. Following this line of investigation, I isolated and characterized a series of FnBPA truncates to identify the minimal structure or

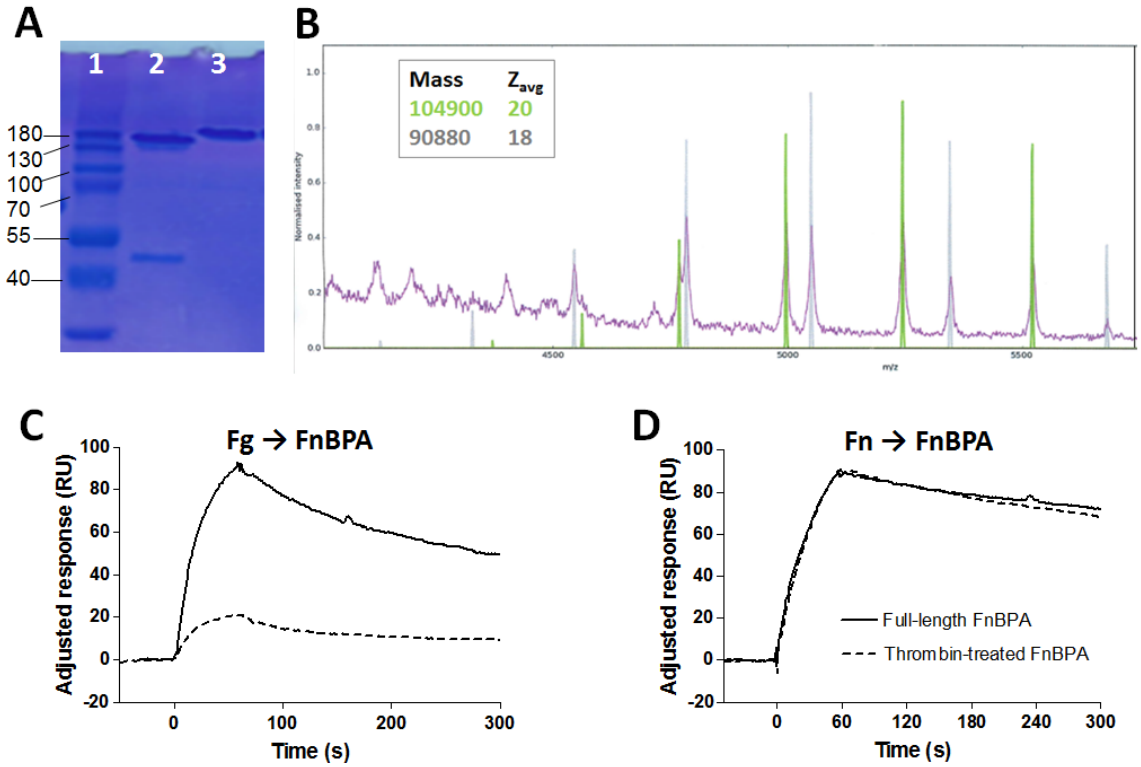

Figure 10. Thrombin cuts full-length FnBPA and alters Fg binding
(A) SDS-PAGE gel indicates FnBPA can be processed by human thrombin proteinase. 1, Marker, 2, thrombin-treated FnBPA, and 3, untreated FnBPA. (B) Electrospray native mass spectrometry of purified FnBPA. Mass of 104,900 correlates to full-length FnBPA, and mass of 90,880 corresponds to $FnBPA_{166–981}$ after thrombin cuts at Arg165. (C) Fg at 270 nm and (D) Fn at 9 nm were injected onto the FnBPA surface (full-length FnBPA or $FnBPA_{166–981}$ captured with anti-His mAb). The binding response was adjusted to represent the same amount of FnBPA captured.

domain required for Fg binding, using the same SPR His-tag capturing approach. The binding data are listed in Table 4 and show that the C-terminal truncations $FnBPA_{38–800}$, $FnBPA_{38–672}$, and $FnBPA_{38–550}$ bind to Fg with similar affinity (K_D values of 27, 22 and 20 nM, respectively) values as the full-length FnBPA ($K_D \approx 16$ nM). Further truncation ($FnBPA_{38–511}$) resulted in dramatically reduced affinity ($K_D \approx 1030$ nM), about a 50-fold reduction. When the N1 region was removed by thrombin, the N-terminal truncated

FnBPA ($FnBPA_{166–981}$) showed impaired Fg binding (Fig. 10). Together, these data suggest that $FnBPA_{38–550}$ is the minimal fully active Fg-binding domain. It also confirms the original assignment of the Fg-binding domain (Fig. 1).

3.8. Characterization of FnBPA conformation in solution

Figure 11 shows the CD spectra of FnBPA proteins after tag removal. The CD spectrum indicates that $FnBPA_{189–511}$, which includes the N2N3 domain of FnBPA, mainly consists of β-sheets. Comparing the CD spectra of all proteins containing the A domain ($FnBPA_{38–981}$, $_{38–800, 38–672, 38–550, and 38–511}$) (Fig. 11A), a slightly stronger negative peak at 220 nm for $FnBPA_{38–550}$ suggests that it contains more β-strands than $FnBPA_{38–511}$ and other constructs. The deduced spectral regions for FnBR all exhibit a random coil structure, except the deducted 511–550 (or FnBPA-1) region. FnBPA-1 is the first Fn-binding repeat and predicted to be disordered by itself, but the deduced structure (Fig. 11B) indicated that it is partially a β-strand when it is connected with the structured A domain as a single protein. The negative peak near 200 nm is characteristic of random coils and can be seen in proteins that harbor disordered FnBR ($FnBPA_{38–981}$, $_{38–800}$, $_{and 38–672}$), with more disordered repeats showing a stronger negative signal.

Conformational changes of proteins under various external influences (pH, ionic strength, temperature, etc.) can be investigated using intrinsic fluorescence, which is generated by aromatic amino acid residues (tryptophan [Trp], tyrosine [Tyr] and phenylalanine [Phe]).[73] Among them, Trp is most ideal fluorophore because of its high quantum yield in proteins and the sensitivity of fluorescence to the local environment. For instance, when a ligand binds to a protein in the vicinity of a Trp residue, changes in

fluorescence intensity may occur. Moreover, the maximum wavelength of the fluorescence spectrum of Trp strongly depends on the polarity of its microenvironment.

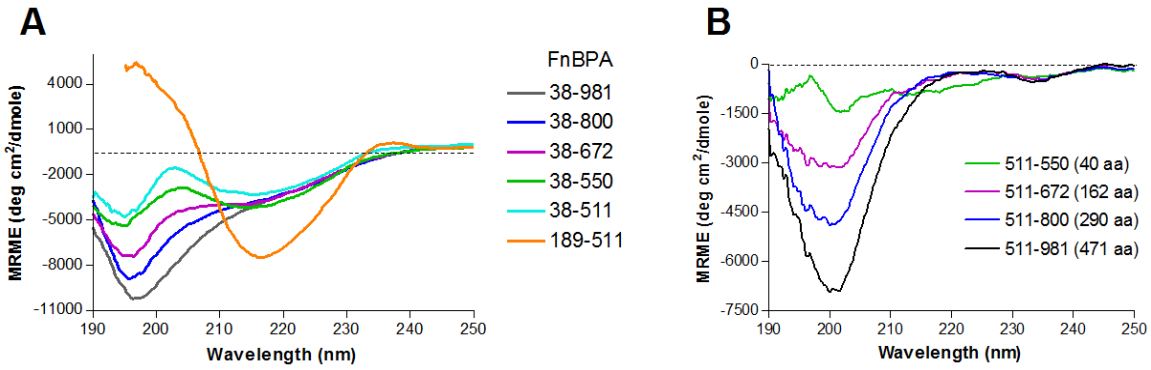

Figure 11. CD spectra of FnBPA proteins
(A) Secondary structure of recombinant FnBPA proteins (tag-free) in 10% PBS examined using CD spectroscopy. (B) Spectrum of the A domain (38–511) was subtracted from those of proteins containing FnBR (FnBPA$_{38–550}$, $_{38–672}$, $_{38–800}$, and $_{38–981}$), and the deduced spectra reflect the secondary structure of the FnBR region (511–550, 511–672, 511–800, and 511–981) in each protein.

FnBPA contains only one Trp residue, at position 494 (Fig. 1) in the G' strand in the N3 subdomain; there are 34 Tyr residues distributed throughout the protein (Table 5). G' strand is directly involved in the β-zipper interaction with the FgγC peptide, as shown in the crystal structure of the complex.[28] Figure 12 shows the fluorescence emission spectra of different FnBPA proteins (each containing the N1N2N3 domain) when excited at 280 nm (targeting Tyr) or 295 nm (targeting Trp). When the protein solution was excited at 295 nm, the maximum Trp fluorescence emission wavelength did not change (~340 nm, Figure 12B), indicating that Trp was partially buried in all proteins examined. Since there is only 1 Trp residue in the entire protein, when the protein concentration was

kept at 1 µM, the Trp concentration was also at 1 µM concentration. Comparing the emission spectra indicated a significantly higher quantum yield for longer constructs $FnBPA_{38–981}$ and $FnBPA_{38–550}$ than for $FnBPA_{38–511}$ (Fig. 12 A and B). This difference is not due to structural changes because the maximum wavelength remained the same; it is due to the contribution of the excitation energy being transferred from additional Tyr residues (in FnBR region) nearby (Table 5). It is possible that a non-linear structure

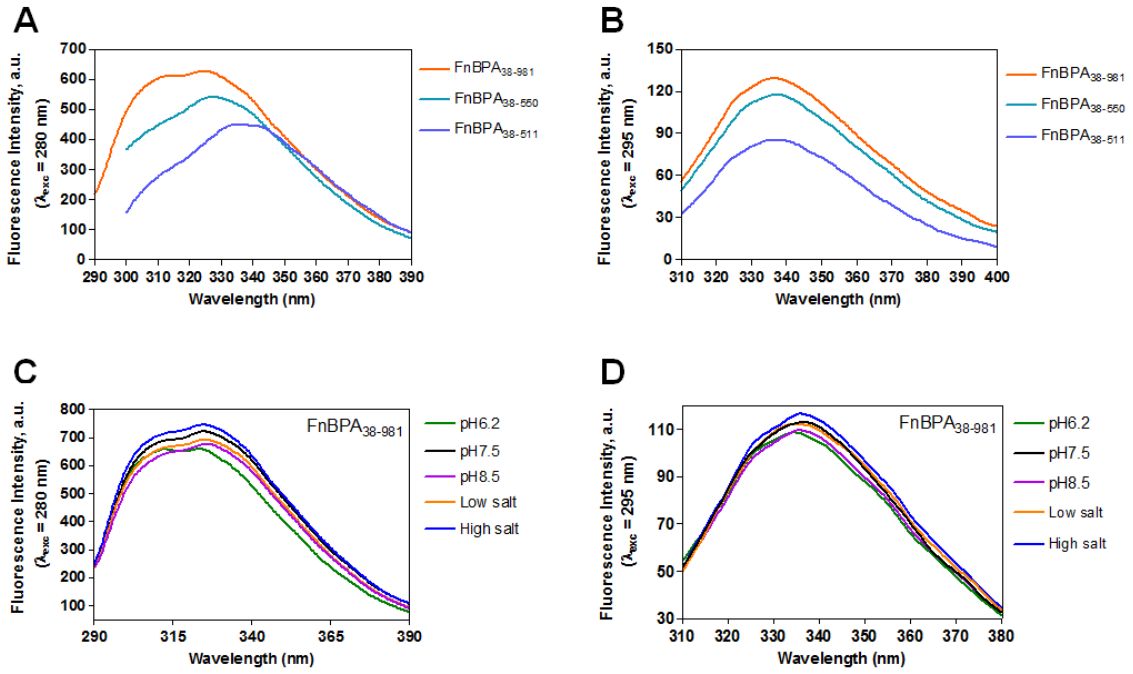

Figure 12. Intrinsic fluorescence spectra of FnBPA proteins
(A and B) Comparison of intrinsic fluorescence spectra of $FnBPA_{38–981}$, $FnBPA_{38–550}$, and $FnBPA_{38–511}$ (1 µM protein in 50 mM Tris and 150 mM NaCl, pH 7.5) excited at 280 or 295 nm. (C and D) Intrinsic fluorescence spectra of 1 µM FnBPA and emission ratio comparison of Trp (335 nm) and Tyr (310 nm) under 5 conditions: 1) 50 mM sodium phosphate (pH 6.2), 2) 50 mM Tris (pH 7.5), and 3) 50 mM sodium borate (pH 8.5), all contain 150 mM NaCl, and 4) 50 mM Tris pH 7.5, 50 mM NaCl (low salt) and 5) 50 mM Tris pH 7.5, 500 mM NaCl (high salt).

existed in the full-length FnBPA, in which the C-terminal disordered region was close to the structured A domain at the N-terminus. The larger fluorescence difference between $FnBPA_{38–550}$ and $FnBPA_{38–511}$ (Figure 12B) indicates that FnBPA-1 may closely associate with the N3 domain to form a compact structure. It also suggests that the original A domain assignment, which included FnBPA-1 as a subdomain, is more relevant. Furthermore, the conformational fluctuation of full-length FnBPA was observed in different pH and ionic strength solutions (Figure 12C and D); low pH (pH 6.2) had a more dramatic effect on the tertiary structure of FnBPA (Figure 12C).

Table 5. FnBPA amino acid composition and properties

Region	Residues	# of aa	pI	# of Tyr	Tyr % (Tyr total=34)
N1	38–194	157	4.66	1	2.9 %
N2	195–338	144	5.36	4	11.7 %
N3	339–511	173	6.34	14	41.1 %
FnBPA-1	512–550	39	4.25	3	8.8 %
FnBPA-2	551–580	30	3.54	3	8.8 %
FnBPA-3	581–609	29	3.94	2	5.9 %
FnBPA-4	610–636	27	4.24	1	2.9 %
FnBPA-5	637–672	36	4.12	0	0
FnBPA-6	673–703	31	3.63	1	2.9 %
FnBPA-7	704–732	29	4.66	1	2.9 %
FnBPA-8	733–762	30	4.05	1	2.9 %
FnBPA-9	763–800	38	4.35	1	2.9 %
FnBPA-10	801–838	38	5.01	1	2.9 %
FnBPA-11	839–874	36	3.89	1	2.9 %
PR	875–951	107	4.84	0	0
$FnBPA_{38–511}$	*38–511*	*474*	*5.13*	*19*	*55 %*
$FnBPA_{38–550}$	*38–550*	*513*	*4.98*	*22*	*65 %*
$FnBPA_{551–981}$	*551–981*	*454*	*4.23*	*12*	*35 %*

3.9. Fg-binding activity of FnBPA is affected by ionic strength and pH

The interaction between Fg and FnBPA is presumably driven by electrostatic interactions. As shown in Figure 13A and B, the K_D values are 15, 22, 125, and 197 nM for binding under 50, 150, 300, and 600 nM NaCl, respectively. This suggests that Fg-FnBPA interaction is weaker when ionic strength increases. The difference in binding affinity is primarily due to a faster on-rate in lower salt concentrations (Fig. 13C). The pH difference (ranged from 7.0 to 8.5) did not seem to affect binding affinity (Fig. 13F).

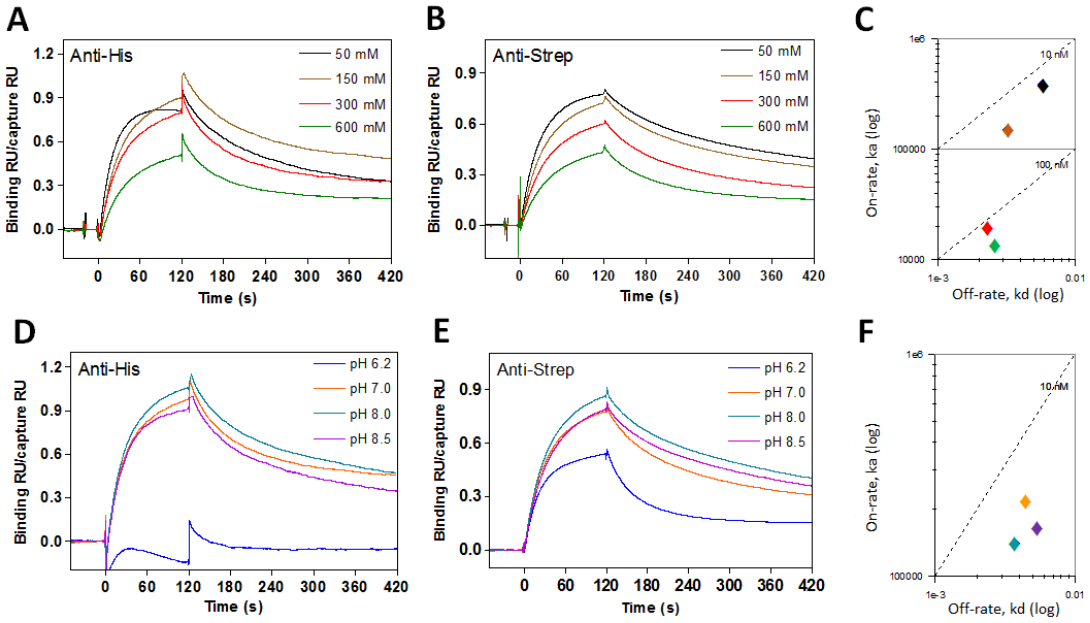

Figure 13. Binding of Fg to FnBPA under different conditions with SPR
Fg in 50 mM Tris (pH 7.5) and different concentrations of NaCl (50, 150, 300, or 600 mM) was injected (250 nM Fg was shown) onto (A) anti-His or (B) anti-Strep captured $FnBPA_{fl}$. (C) Binding kinetics were measured for each condition and compared in on-off rate map. Fg in four different pH buffer systems containing 150 mM NaCl (50 mM $KHPO_4$ pH 6.2, 50 mM Tris pH 7.0, 50 mM Tris pH 8.0, and 50 mM borate pH 8.5) was injected (250 nM Fg shown) onto $FnBPA_{fl}$ captured by (D) anti-His or (E) anti-Strep. (E) Binding kinetics were measured for each condition and compared in on-off rate map. All buffers contained 0.02% Tween-20.

However, at pH 6.2, Fg was not able to bind C-terminally captured FnBPA (Fig. 13D), while the N-terminally captured FnBPA was still able to bind Fg (Fig. 13E).

Table 6. Thermodynamic parameters for the interactions (25 °C) by ITC and SPR

Interaction	K_D	ΔG (kJ/mol)	ΔH (kJ/mol)	$-T\Delta S$ (kJ/mol)	n	Method	Reference
	(μM)						
$FnBPA_{189–550}$:Fg	1.1 ± 0.1	-33.8	-25.5 ±0.0	-8.3	2.11	ITC	Stemberk[28]
$FnBPA_{38–550}$:Fg	0.23 ± 0.08	-37.9	-28.3 ±0.4	-9.5	1.91	ITC	This work
$FnBPA_{38–550}$:Fg	0.66 ± 0.19	-35	-37 ± 1.7	2.0		SPR	This work
$FnBPA_{fl}$: Fg	1.23 ± 0.16	-34	-19 ± 1.3	-15		SPR	This work
$FnBPA_{38–550}$:FgD	0.86 ± 0.17	-35	-24 ± 1.2	-11		SPR	This work
$FnBPA_{fl}$:FgD	1.04 ± 0.15	-34	-22 ± 1.6	-12		SPR	This work
	(nM)						
$FnBPA_{189–550}$:FnNTD	0.7 ± 0.2	-52.4	-150 ±1.2	97.3	0.89	ITC	Stemberk[28]
$FnBPA_{fl}$:Fn	0.9 ± 0.7	-51.5	-986 ± 49	935	0.15	ITC	This work
FnBPA-1:FnNTD	4.8 ± 0.6		-108	61	0.84	ITC	Meenan[40]
FnBPA-4:FnNTD	10.5 ± 0.9		-120	75	0.37	ITC	Meenan[40]
FnBPA-5:FnNTD	44.2 ± 9.7		-71	29	0.91	ITC	Meenan[40]
FnBPA-8:FnNTD	~ 3000		-81	50	0.76	ITC	Meenan[40]
FnBPA-9:FnNTD	7.9 ± 0.4		-117	71	0.99	ITC	Meenan[40]
FnBPA-10:FnNTD	19.5 ± 1.1		-102	58	0.98	ITC	Meenan[40]
FnBPA-11:FnNTD	<1.0		-118	-	1.01	ITC	Meenan[40]

The observation suggested that the folding of the FnBPA C-terminus affects Fg binding at the N-terminus, providing experimental evidence to support the folded-back conformation of active FnBPA. Since ionic strength does not change the local N2N3 conformation, as indicated by the intrinsic tryptophan fluorescence of FnBPA (Fig. 12C and D), the change in the binding activity might be caused by the region outside the N2N3 domain. Furthermore, the pH effect on FnBPA conformation is most obvious at pH 6.2, as demonstrated by the fluorescence (Fig. 12C) when Tyr residues outside the N2N3 region were excited. These results further support a model where the N1 and C-

terminus of FnBPA form the folded-back structure. The conditions tested did not affect Fn binding to FnBPA (data not shown).

3.10. Thermodynamics of FnBPA binding to Fg and Fn

The binding energies of FnBPA interactions with Fg and Fn were directly measured by ITC (Fig. 14) or determined using SPR with van ‘t Hoff analyses (Fig. 15). By comparing the ITC data (Table 6) for the interaction of Fg and $FnBPA_{38–550}$ and Fg and $FnBPA_{189–550}$, a 5-fold stronger affinity (0.23 µM vs. 1.1 µM, respectively) for the longer construct was driven by a favorable extra enthalpy contribution of ~2.8 kJ/mol

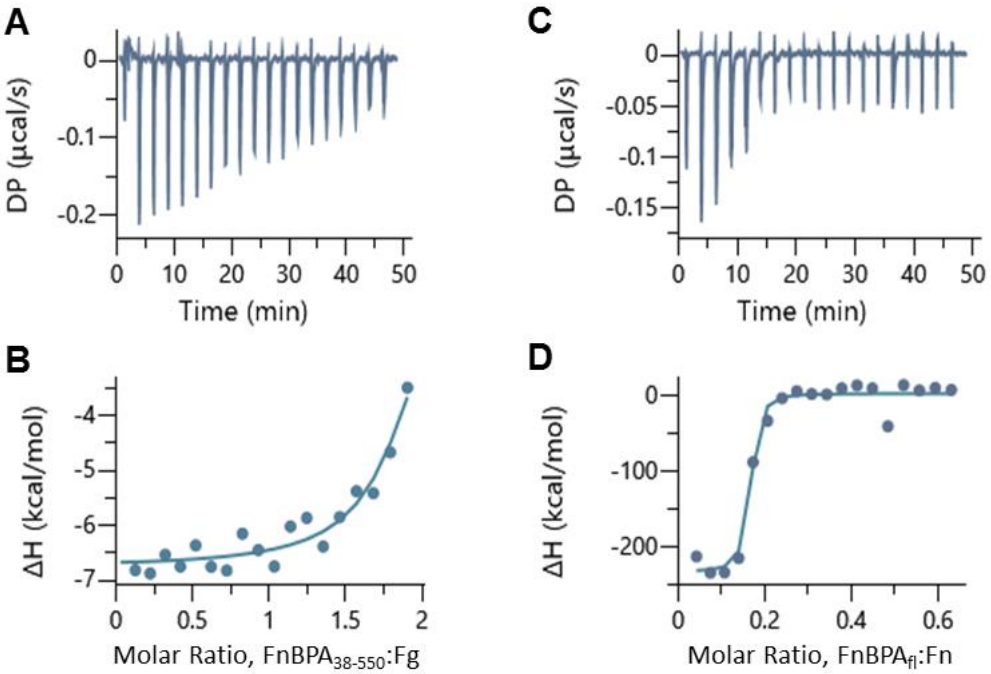

Figure 14. ITC experiment for FnBPA and host ligand interaction
(A and C) Curves for each injection heat. (B and D) The estimated heat of binding (ΔH) as a function of molar ratio, and fitted curve calculated from integrated raw data using the One Set of Sites fitting model. Measured and deduced parameters are listed in Table 6 and converted to kJ/mol.

(Δ*H* = -25.5 vs. -28.3 kJ/mol), as well as an extra entropy contribution of ~ 1.2 kJ/mol (-TΔ*S* = -8.3 vs. -9.5 kJ/mol), suggesting that the N1 region (aa 38–189) is involved in direct binding driven by both enthalpic and entropic interactions. The stoichiometry of 1.91:1 for the Fg:FnBPA$_{38–550}$ interaction was consistent with the presence of two identical binding sites on intact dimeric Fg.

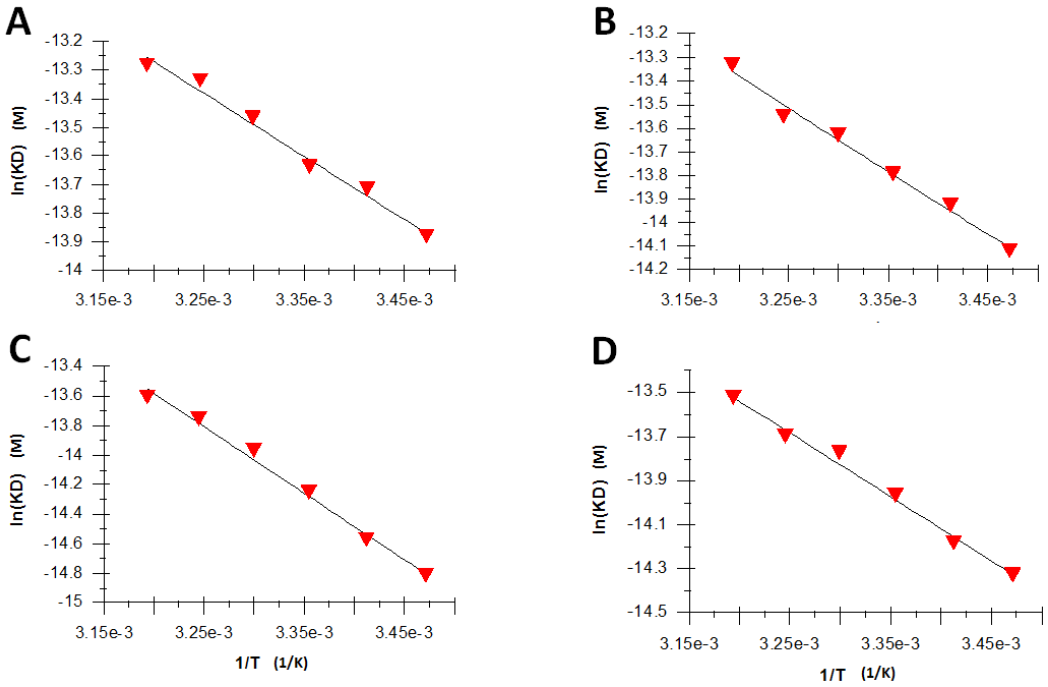

Figure 15. SPR determination of binding thermodynamics
Van ‘t Hoff plots generated for the binding of FnBPA$_{fl}$ to immobilized Fg and FgD, and FnBPA$_{550}$ to Fg and FgD. K_D values were obtained by SPR kinetic analysis at a series of temperatures (15, 20, 25, 30, 35, and 40 ˚C). The resulting plot of ln K_D against 1/T is linear, with a slope of Δ*H*/R and an intercept on the y-axis of Δ*S*/R at standard 25 °C (R is the universal gas constant). Thermodynamics parameters derived from van ‘t Hoff analysis are listed in Table 6.

Thermodynamics data derived from SPR measurements demonstrated a reduced enthalpy of binding (except for Fg and FnBPA$_{38–550}$), but binding was still enthalpy

dominated. By comparing the same Fg-FnBPA$_{38–550}$ interaction with ITC and SPR, the 3-fold weaker affinity (K_D = 0.23 vs. 0.66 μM) obtained from the SPR method was mainly due to an unfavorable entropic penalty (-TΔS = 0.8 kJ/mol), presumably arising from immobilization of Fg, which blocks the hydrophobic region from binding and restricts conformational freedom. This steric hindrance and lack of conformational flexibility for immobilized Fg and FgD is also a limiting factor for FnBPA$_{fl}$ binding, which might require an extended interface, evidenced by smaller binding enthalpy (ΔH = -19 and -22 kJ/mol) and non-dominated entropy.

ITC measurements upon the binding of FnBPA to Fn indicated that binding is completely driven by favorable enthalpic contributions and an unfavorable entropy signature that is expected, given that the disordered repeat region becomes structured upon binding (β-zipper mechanism). Full-length FnBPA is composed of seven measurable Fn-binding sites (FnBPA-1, 4, 5, 8, 9, 10, and 11) and six exhibits high affinity.[40] FnBPA$_{189–550}$ has only one Fn-binding site, FnBPA-1 (FnBPA$_{511–550}$), in the protein. The K_D values for FnNTD binding, determined with ITC measurements, were 0.7 nM for FnBPA$_{189–550}$ and 4.8 nM for FnBPA-1 peptide. These different K_D values indicate that the presence of the N2N3 domain in FnBPA$_{189–550}$ can stabilize the FnBPA–Fn interaction by ~6-fold. This is supported by more favorable enthalpy (ΔH = -150 vs. -108 kJ/mol), which could potentially strengthen the interaction. The greater entropic cost (ΔS = 97 vs. 61 kJ/mol) suggests that conformational rearrangement could extend to other regions of the protein. Applying an additional enthalpy contribution of -42 kJ/mol and an entropic penalty of 36 kJ/mol to the other five high-affinity Fn-binding repeats

(Table 6), the total ΔH will become -972 kJ/mol, and total ΔS will be 621 kJ/mol for FnNTD binding to longer a FnBPA protein that contains N2N3 and all repeats. Interestingly, the experimentally determined parameters for the $FnBPA_{fl}$–Fn interaction are consistent with overall tight binding (K_D value of 0.9 nM) and a dominant enthalpy contribution (ΔH = -986 kJ/mol), as well as stoichiometry of ~6:1 (n=0.15). The larger entropic term ($-T\Delta S$ = 935 kJ/mol) indicates that other regions of the full-length proteins might be affected, for example, the N1 region in FnBPA of GBD region in Fn.

3.11. Specificity of FnBPA ligand bindings

To confirm the binding specificity between FnBPA and host ligands Fg/Fn, several inhibition assays were performed using SPR to exam the ability, efficacy, and interplay of soluble ligands inhibiting FnBPA binding to immobilized ligands.

3.11.1. Inhibition of FnBPA binding to Fn surface

Fn can interact with Fg at two binding sites on Fn. The primary high-affinity site is located at the FnNTD30k region (F4-F5 domains, the same region that FnBPA binds) ,and the second binding site is cryptically located at the C-terminal Fib-2 region (Fig. 2).[51] For this reason and the possibility of Fn self-association, the ability of soluble Fg or Fn to inhibit FnBPA binding to Fn or the FnNTD30k surface could not be determined.

3.11.2. Inhibition of FnBPA binding to Fg surface

Figure 16 shows that Fn did not inhibit or interfere with full-length FnBPA binding to immobilized Fg (Fig. 16A), demonstrating that Fn binding to FnBPA is independent of Fg binding. Both soluble Fg and FgD could inhibit FnBPA binding to immobilized Fg (Fig. 16B and C); the IC_{50} for inhibiting $FnBPA_{fl}$ binding to Fg was 0.21

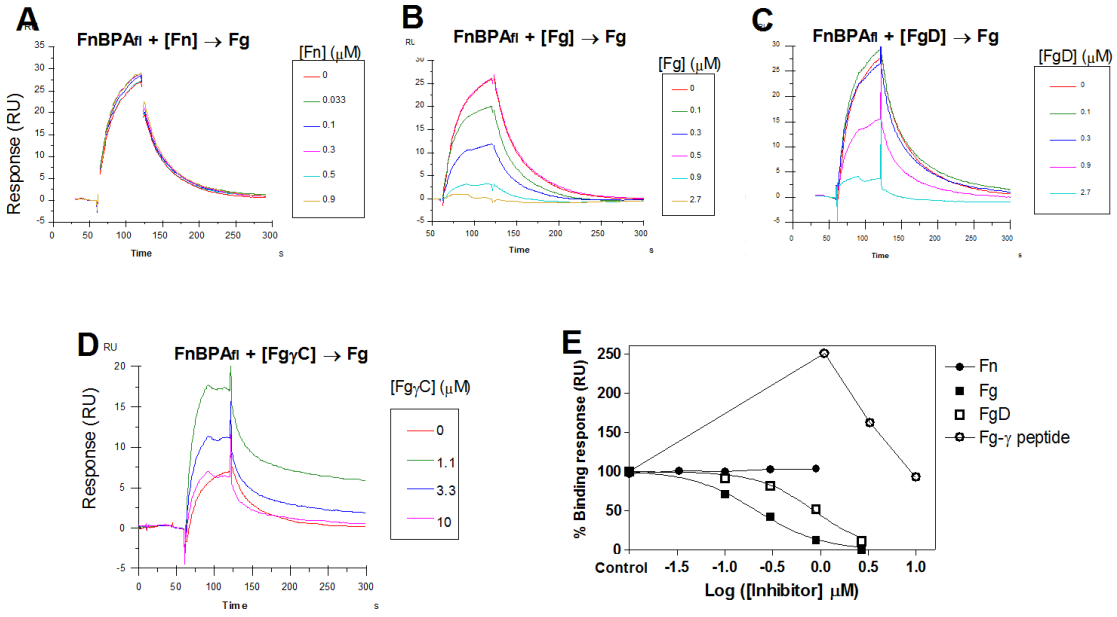

Figure 16. Inhibition of FnBPA binding to Fg surface
Dose-response for inhibition by different concentrations of (A) Fn, (B) Fg, (C) FgD, or (D) Fgγ peptide of 0.5 μM $FnBPA_{fl}$ binding to immobilized Fg. The maximum (100%) response was $FnBPA_{fl}$ binding without any inhibitors (control). (E) $FnBPA_{fl}$ binding responses from A–D were plotted against inhibitor concentrations (dimer Fg and Fn concentrations were used) and fit to a four-parameter logistic function. Fg IC_{50} for inhibiting $FnBPA_{fl}$ binding to Fg was 0.21 μM, and the FgD IC_{50} was 0.85 μM.

μM, and the FgD IC_{50} was 0.85 μM (Fig. 16E). The 4-fold less efficacy in inhibition suggests possible contact sites outside the FgD fragment in Fg. Interestingly, the FgγC peptide could not inhibit the Fg–FnBPA interaction under the tested conditions; instead, it enhanced FnBPA binding to the Fg surface (Fig. 16D and E). A possible explanation is that amine coupled Fg is a modified Fg surface that exposes another specific binding site for FnBPA. These data indicate that the Fg–FnBPA interaction is more complex than previously considered.

3.11.3. Specific engagement of FgγC requires FnBPA N1 domain

To address the unexpected effect observed in the inhibition assay on FnBPA, a protein fluorescence quenching experiment was used to study FnBPA–FgγC peptide binding in solution. Static quenching of tryptophan fluorescence of FnBPA after the addition of the FgγC peptide, which does not contain any aromatic residues, was analyzed according to the Ster–Volmer plot and modified Stern–Volmer plot.[74] The data displayed in Figure 17 show that the quenching of FnBPA fluorescence by the addition of FgγC was only seen in N1 containing FnBPA proteins (A, B, D, and E) but not in $FnBPA_{189–511}$, which only has the N2N3 domains (C and F). The Stern–Volmer curves exhibit linearity (Fig. 17G), suggesting that the quenching process arises from binding between the tryptophan fluorophore and the quencher peptide. The linearity of the modified Stern–Volmer plots indicates static quenching (or binding) in the presence of an inaccessible population of fluorophores. The K_D values are almost the same for both full-length FnBPA (K_D =1.83 μM) and $FnBPA_{38–511}$(K_D =1.82 μM), which is consistent with a solution affinity of ~1.1 μM for the Fg–$FnBPA_{189–550}$ interaction measured by ITC[28] (Table 4). The lower accessibility of Trp in full-length FnBPA (48%) than $FnBPA_{38–511}$ (68%) indicates that FnBR may be involved in the dynamic folding of the A domain. Since FnBPA has only one Trp residue in the protein, the end-point measured accessibility of 48–68% suggests possible equilibrium between cleft-occupied and cleft-unoccupied conformations. The N1-dependent quenching events also suggest that N1 is involved in regulating cleft occupancy. No quenching in $FnBPA_{189–511}$ does not mean that there is not binding between the protein and FgγC peptide (pair shown in the

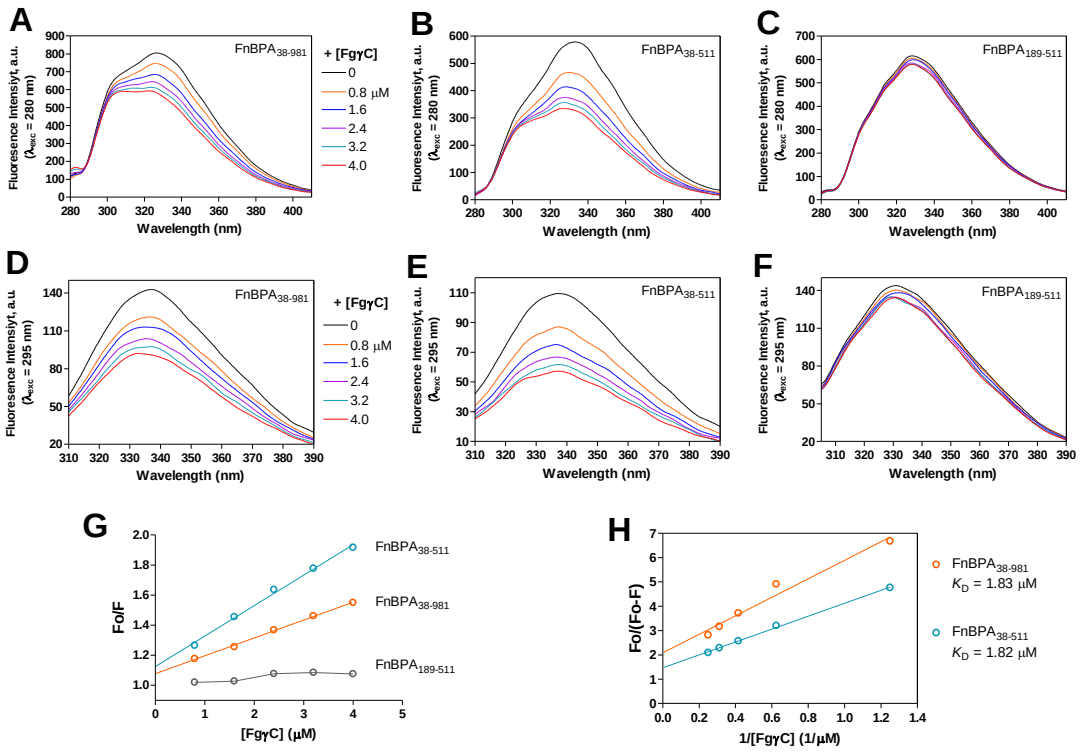

Figure 17. Static quenching of tryptophan fluorescence in FnBPA by FgγC peptide (A–F) Fluorescence emission spectra of FnBPA proteins (1 μM), and quenching of the fluorescence when the FgγC peptide was titrated into protein solutions. Quenching of FnBPA tryptophan fluorescence by addition of FgγC peptide (which does not contain any aromatic residues) are only seen in N1 containing FnBPA proteins (A, B, D, and E), not in $FnBPA_{189–511}$, which has only N2N3 domains (C and F). (G) Stern–Volmer curves (data from 295 nm excitation), where F_0 and F are the fluorescence intensities at 335 nm in the absence and presence of FgγC peptide, respectively, exhibit linearity, suggesting that the quenching process arises from binding between the tryptophan fluorophore and the quencher peptide. (H) The linearity of the modified Stern–Volmer plots indicates static quenching (or binding) in the presence of an inaccessible population of fluorophores. Plots allow calculation of K_D (slope/intercept) and percentage of tryptophan accessibility (100/intercept) for quenching: 48% for $FnBPA_{38–981}$, and 68% for $FnBPA_{38–511}$.

complex structure[28]), rather it indicates that the binding did not result in a change of Trp fluorescence due to a lack of conformational change.

3.11.4. Inhibition of Fg and Fn binding to FnBPA surface

FnBPA contains multiple binding sites for Fn interaction. To avoid complexity, the Fn inhibition assay was performed using an individual peptide of FnBR region. As shown in Figure 17, soluble FnBPA can inhibit Fg binding to the full-length FnBPA surface (Fig. 18A). The IC_{50} value of 424 nM (Fig. 18C) is not very compatible with the Fg–FnBPA affinity value (10 nM) determined in Figure 7A, suggesting that Fg prefers binding surface-anchored FnBPA, which has an optimal structural orientation. In contrast, soluble FnBPA could completely inhibit Fn binding to the full-length FnBPA surface (Fig. 18B). The IC_{50} value of 0.86 nM (Fig. 18C) was compatible with the affinity values measured for surface-anchored FnBPA (0.4 nM, Fig. 7B and Table 4), because FnBPA has multiple Fn-binding sites, and each site is unstructured for binding.

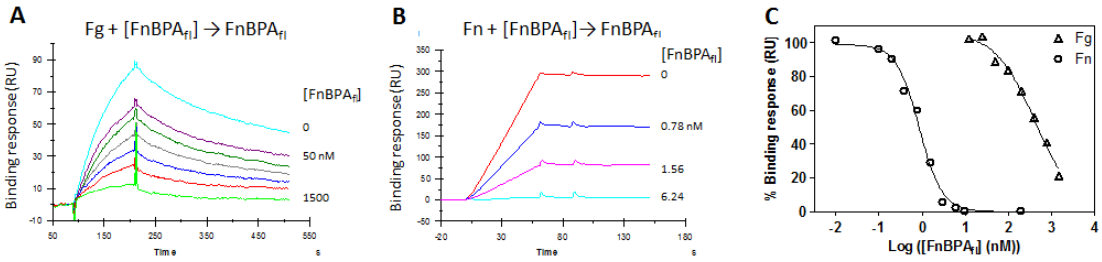

Figure 18. Inhibition of Fg and Fn binding to FnBPA surface by soluble FnBPA
Various concentrations of $FnBPA_{fl}$ were mixed with (A) 100 nM Fg and (B) 10 nM Fn and then injected onto the $FnBPA_{fl}$ sensor surface. (C) Fg and Fn binding responses from A and B were plotted against inhibitor $FnBPA_{fl}$ concentrations and fitted to a four-parameter logistic function. $FnBPA_{fl}$ IC_{50} for inhibiting Fg binding to $FnBPA_{fl}$ was 424 nM, and the IC_{50} for inhibition of Fn binding was 0.86 nM.

Although a FnBPA–Fn interaction is mediated by several high-affinity repeats in FnBPA, binding of Fn to full-length FnBPA was completely inhibited by the single

repeat FnBPA-9 (Fig. 19), suggesting that this repeat plays a major role in Fn binding. This result is consistent with previously reported results that FnBPA-9 is a hot spot for infection related polymorphisms;[22-23] also, an epitope in FnBPA-9 is exposed on the surface of *S. aureus*, and it is an effective target for murine mAb (15E11), which can inhibit the attachment of *S. aureus* to surface-coated Fn.[75]

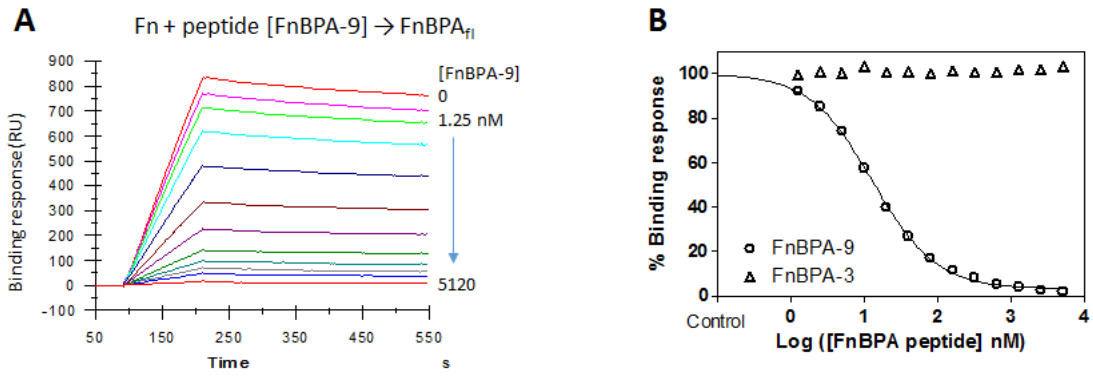

Figure 19. Inhibition of Fn binding to FnBPA surface by synthetic FnBR peptide (A) Various concentrations of FnBPA-9 were mixed with 10 nM Fn and injected onto the high-density $FnBPA_{fl}$ sensor surface. (B) Fn binding responses plotted against inhibitor FnBPA-9 concentrations and fit to four-parameter logistic function. FnBPA-9 IC_{50} for inhibiting Fn binding to $FnBPA_{fl}$ was 13 nM. Synthetic peptide FnBPA-3 (repeat that binds weakly to Fn) was used as a negative control that did not interact with Fn.

3.11.5. Inhibition of plasma adsorption to FnBPA surface

To investigate whether the inhibition observed in the purified system is still applicable to the more biologically relevant system, human blood plasma was used for the SPR binding assay. In these assays, the co-injection command was used to inject two samples in direct succession, with no dissociation time or wash procedures after the first injection, enabling the blocking of the ligand surface to be monitored.

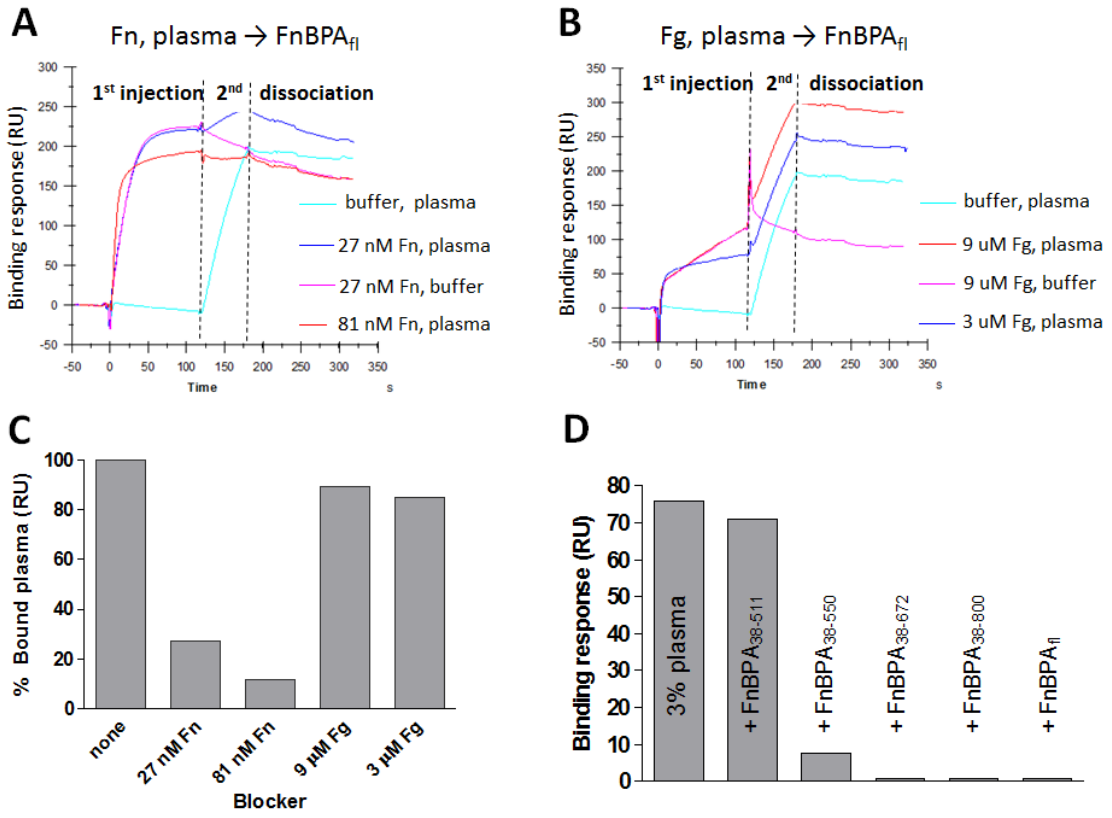

Figure 20. Blockage and inhibition of plasma adsorption to FnBPA surface
(A and B) Using the co-injection command, inhibitor (Fn, Fg or buffer) was first injected over the FnBPA$_{fl}$ surface, immediately followed by injection of 10% blood plasma, with no dissociation time after the first injection. (C) Data in A and B (adsorbed plasma response at the dissociation) are plotted to show the effect of blockage. (D) Each recombinant FnBPA fragment at 10 nM was mixed with 3% plasma (final concentration) and injected onto the FnBPA$_{fl}$ surface.

The results indicated that as the concentration of Fn increased to 81 nM, the FnBPA surface became saturated with Fn and could almost completely block plasma adsorption to FnBPA (Fig. 20A and C). Fg could weakly and partially block plasma adsorption to FnBPA (Fig. 20B and C), even at 9 μM (equivalent to Fg concentration in plasma). These data suggest that Fn is the major (~ 90%) component in plasma that adsorbs to the FnBPA surface, while Fg only counts for ~10%. These results are

consistent with the ratio of FnBPA-bound Fn vs. FnBPA-bound Fg from plasma using antibody detection (Fig. 8A). Premix plasma with truncated FnBPA that contained FnBR (FnBPA$_{38–511}$ does not contain FnBR) could also effectively inhibit plasma binding to full-length FnBPA (Fig. 20D). This further supports that FnBPA$_{38–550}$ is likely minimal fully functional ligand binding domain.

3.12. Allosteric regulation of Fg and Fn binding to FnBPA

The Fn and Fg binding sites on FnBPA do not overlap, and the data presented in Section 3.4 demonstrates that Fn and Fg can simultaneously bind to surface-anchored FnBPA. To investigate how these two ligands influence the binding of the other to FnBPA to form a ternary complex, an SPR assay was developed in which the α-His and α-Strep antibodies were immobilized on the same sensor chip to detect complex formation when double-tagged FnBPA$_{fl}$ (His-tag at the C-terminus and Strep-tag II at the N-terminus) was mixed with Fg and Fn.

Figure 21 shows that Fn-bound FnBPA had more Fg bound than the un-liganded FnBPA; thus a bigger complex could be detected by α-His (Fig. 21A and C). However, this enhanced Fn-FnBPA–Fg complex could not be detected by α-Strep, which recognizes the N-terminus of FnBPA (Fig. 21B and C). This suggests that Fn binding may involve the N-terminal region by stabilizing the fold-back conformation for optimal Fg binding, thus, sterically blocking the N-terminal tag from recognized by the antibody. In contrast, Fg-bound FnBPA showed less Fn binding than Fg-free FnBPA (Fig. 21D and F), but when a threshold concentration of Fn (100 nM) was reached, Fg– FnBPA-Fn complex formation was enhanced. However, α-Strep could not detect this enhancement,

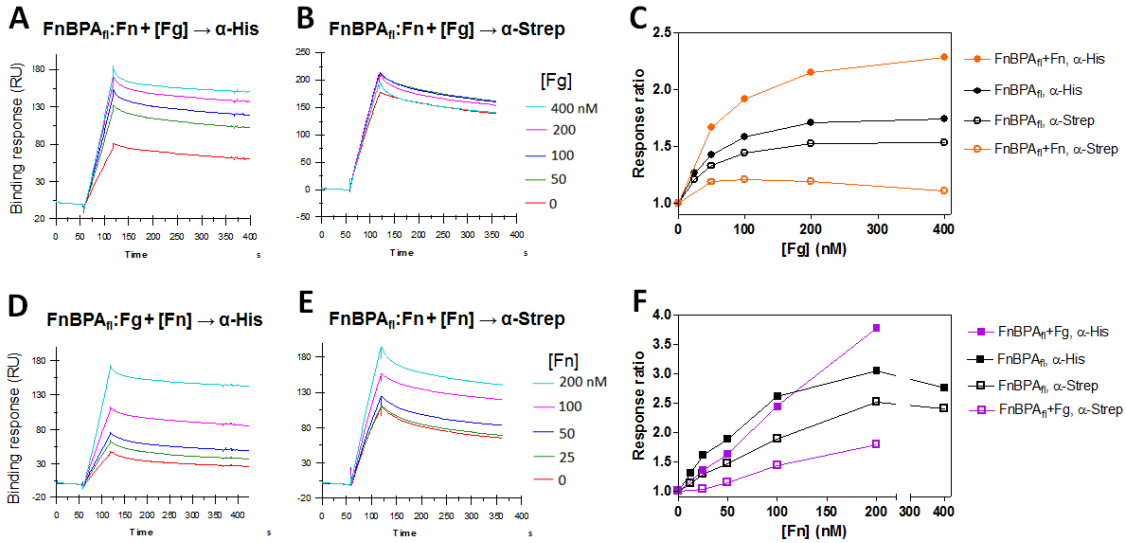

Figure 21. Complexation of FnBPA with Fg and Fn in solution detected by SPR
In an SPR assay, immobilized α-His and α-Strep antibodies were used as a sensor surface to detect double-tagged $FnBPA_{fl}$ under different complex formation conditions. (A–C) 100 nM of $FnBPA_{fl}$ was mixed with increasing concentrations of Fg in the absence (data not shown) or presence of a saturating amount of 200 nM Fn; the mixture was then injected onto antibodies immobilized on the same sensor chip. (D–F) 100 nM of $FnBPA_{fl}$ was mixed with increasing concentrations of Fn in the absence (data not shown) or presence of saturating Fg (400 nM).

which further confirmed that the N-terminal region of FnBPA is involved in ligand binding.

These findings demonstrated that Fn is a positive allosteric effector of FnBPA binding to Fg, and Fg binding negatively influenced FnBPA binding to Fn when Fn concentration was low. However, this negative effect could be overcome with a greater available concentration of Fn. This positive cooperativity of ligand binding can explain the more stable interaction of FnBPA with plasma than the individual Fg or Fn ligand alone (Fig. 7).

3.13. Tertiary structure of Fn is altered by FnBPA

Although high-resolution crystal structures have been solved for some smaller Fn fragments, a complete structure for full-length Fn remains to be determined. To understand whether conformational changes are induced by individual FnBR of FnBPA, DLS, CD, and fluorescence spectroscopy were used to analyze the native Fn conformation in solution.

3.13.1. DLS detection of extended conformation of Fn altered by FnBPA

The hydrodynamic radii (R_h) of Fn in the presence or absence of the FnBPA Fn-binding repeat FnBPA-10 was measured using DLS (Table 7). Fn adopted an extended conformation in the presence of high salt or heparin (R_h = 13.27 ± 0.15; 12.50 ± 0.29, respectively) compared to a more compact structure found in physiological buffer (R_h =10.20 ± 0.12). An addition of FnBPA-10 resulted in a significantly increased R_h (R_h = 12.73 ± 0.69), suggesting that Fn adopts an extended structure upon binding to FnBPA.

Table 7. Comparison of hydrodynamic radii of Fn under various conditions

Fn treatments	R_h (nm)
TBS	10.20 ± 0.12
High salt	13.27 ± 0.15
Heparin	12.50 ± 0.29
FnBPA-10	12.73 ± 0.69

Fn was maintained in TBS at a final concentration of 0.8 mg ml^{-1} (1.6 μM). Different treatments included an additional 350 mM NaCl (high salt), 15 μM of heparin, or FnBPA-10 peptide. Values are mean ± SE.

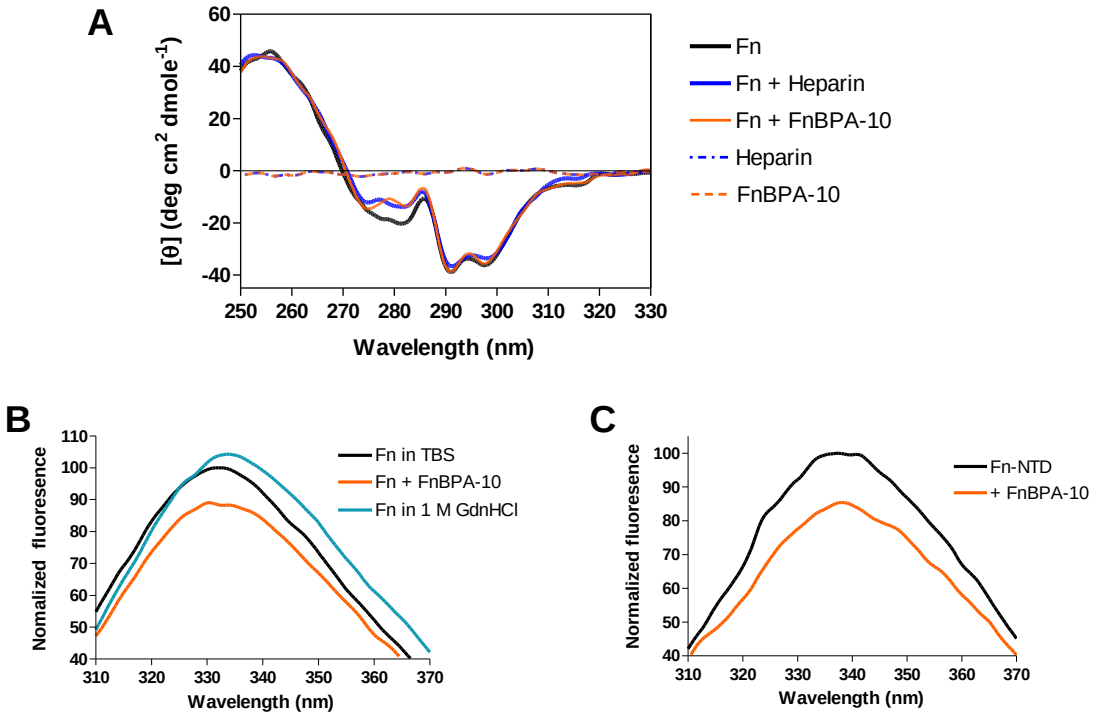

Figure 22. Near-UV CD and steady-state fluorescence spectra of Fn
(A) CD spectra in the range 250–350 nm are shown for individual molecules or mixtures: Fn dimer (0.82 mg ml^{-1}, 1.6 µM), FnBPA-10 (0.07 mg ml^{-1}, 15 µM), and heparin (0.27 mg ml^{-1}, 15 µM). TBS (50 mM Tris, pH 7.4, and 150 mM NaCl) was used for all experiments. (B and C) When excited at 295 nm, intrinsic tryptophan fluorescence spectra were recorded for Fn (0.1 µM) in TBS, TBS with 1 M GdnHCl or 2 µM of FnBPA-10, and FnNTD (1.6 µM) with and without 16 µM of FnBPA-10. All concentrations are final. Spectra were corrected by subtracting buffer blanks.

3.13.2. CD detection of partial unfolding of Fn by FnBPA

Native Fn contains large numbers of aromatic residues in the type I and III domains, which exist in common hydrophobic environments and give rise to a signature near-UV CD spectrum that is characterized by two strong negative peaks centered at 291 and 299 nm, and a weaker negative peak at 282 nm (Fig. 22A).[76-77] The binding of Fn by the glycosaminoglycan heparin has been shown to alter the tertiary structure of Fn, which can be

monitored by shifts in this signature spectrum.[78] When Fn was incubated in the presence of FnBPA-10, the complex produces different spectra relative to native Fn (Fig. 22A). Interestingly, the similarity in the near-UV spectra for heparin-bound Fn when compared to FnBPA-10 bound Fn (Fig. 22A) was noted. Importantly, heparin and the FnBPA-10 peptide used in these experiments are intrinsically disordered polymers that do not contain a Trp residue and, therefore, lack near-UV optical activity. However, since FnNTD is engaged by FnBPA-10, such an interaction could potentially cause near-UV CD optical activity changes within the NTD domain. FnBPA-10 caused intrinsic Trp fluorescence quenching in Fn (Fig. 22B) and FnNTD (Fig. 22C), suggesting that Trp environments in the NTD are affected by binding and may partially contribute to the near-UV CD changes in Fn.

3.13.3. FRET detection of partially unfolded Fn by FnBPA

To learn whether FnBPA causes allosteric changes in Fn upon binding and to confirm apparent conformational changes in solution Fn indicated by CD, a FRET-based approach was employed. To this end, Fn was site-specifically labeled by conjugating an acceptor fluorophore to free cysteine residues using a technique previously described.[69] Native Fn contains only two free cysteines (four per dimer molecule), and these are found in the C-terminally positioned ^{7}FnIII and ^{15}FnIII modules[79] (denoted in Fig. 2). When Fn is denatured by introducing increasing amounts of GdnHCl (Fig. 23A and B) or increasing the ionic strength (Fig. 23C), the distance between the amine coupled donor fluorophores and cysteine coupled acceptor fluorophores increased, and the acceptor fluorescence peak was diminished. There was no FRET observed between adjacent or denatured Fn molecules (Fig. 23D). To determine whether the FnBPA-induced structural

changes measured by CD and DLS involve Fn domains outside of the FnBPA binding site, spectra were then collected in the presence of various concentrations of FnBPA-10 (Fig. 23F) GST fusion proteins. These experiments showed a clear dose-dependent loss of the acceptor peak signal for FnBPA-bound Fn. Importantly, an identical effect was observed when a 36-amino-acid peptide lacking the GST fusion and corresponding to the high-affinity FnBPA repeat FnBPA-5 was used (Fig. 23G). GST alone or a GST fusion

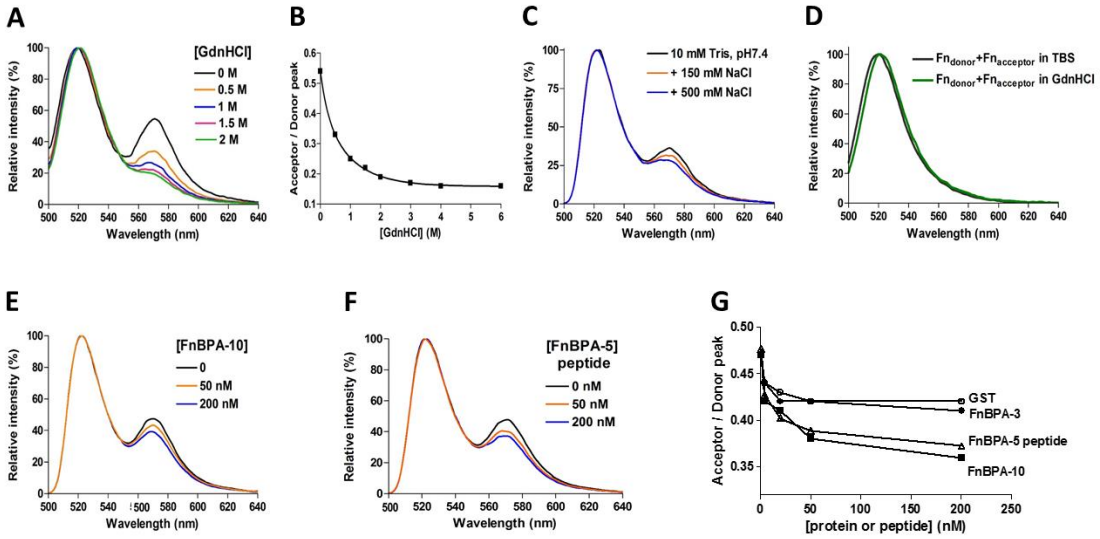

Figure 23. FRET of Fn
Fluorescence emission spectra of Fn-donor or Fn-acceptor (50 nM in 10 mM Tris, pH 7.4, 150 mM NaCl) were collected with excitation at 493 nm (A) in the presence or absence of denaturant (GdnHCl). (B) Accompanying acceptor/donor peak ratio as a function of denaturant concentration. Fn-donor or Fn-acceptor fluorescence changes (C) under different ionic strengths and (E and F) in the presence of different concentrations of GST-FnBPA-10 or FnBPA-5 peptide, respectively. (G) Acceptor/donor peak ratio vs. concentration (0, 1, 5, 20, 50, or 200 nM) of protein or peptide added. Spectra were normalized to the donor emission peak at 522 nm such that changes in energy transfer were reflected only by changes in the acceptor peak at 570 nm. (D) Control experiments were conducted by mixing 50 nM of donor-labeled Fn (Fn_{donor}) with 50 nM of acceptor-labeled Fn ($Fn_{acceptor}$) in TBS or 2 M GdnHCl.

to the low-affinity FnBPA repeat FnBPA-3 exhibited no effect in this assay system (Fig. 23H). Taken together, the DLS, CD, and fluorescence-based assays indicated that FnBPA profoundly modifies the native solution structure of Fn by promoting an extended Fn conformation that results in the large-scale rearrangement of Fn domains at sites distant from the FnBPA binding site.

3.14. Fn recognition of the $\alpha_5\beta_1$ integrin enhanced by FnBPA

Fn serves as a primary ECM substrate for several adhesion molecules, including the major Fn cell surface receptor, $\alpha_5\beta_1$ integrin.[42] Whether conformational changes induced by binding FnBPA, as shown in Fig. 22–23 and Table 7, resulting in modified Fn–integrin interactions were investigated. To more directly test this, an SPR-based system was developed to study the effects of FnBPA on recognition of the $\alpha_5\beta_1$ integrin by Fn.

3.14.1. Validation of SPR-based assay for integrin binding analysis

In this assay system, a recombinant $\alpha_5\beta_1$-Fc fusion protein representing the minimal functional unit of the integrin[67] was immobilized on the surface of a Biacore CM5 chip. Fn interacts with the $\alpha_5\beta_1$ biosensor, and binding is enhanced by Mn^{2+} (Fig. 24A), as previously reported.[67] Further validation of this experimental approach was performed using Fn fragments, including the cell-binding domain (FnCBD) possessing the canonical $\alpha_5\beta_1$-binding "RGD" and synergy sites[80-81] (Fig. 2). As expected, the FnCBD fragment exhibited a dose-dependent interaction with $\alpha_5\beta_1$, while the FnNTD fragment lacking the integrin interaction domains failed to bind the integrin (Fig. 24B and C).

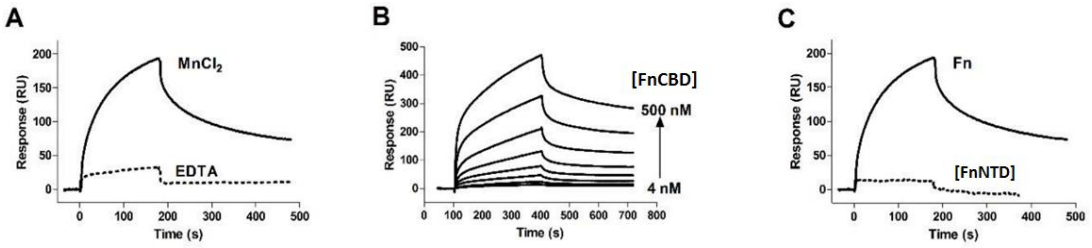

Figure 24. SPR analyses of Fn–α5β1 interaction
The α5β1 biosensor was validated by demonstrating metal ion dependence and domain specificity: (A) Fn (250 nM) was injected over the immobilized α5β1 surface in the presence of 1 mM $MnCl_2$ (solid line) or 3 mM EDTA (dashed line). (B) Response curves for a two-fold linear dilution series of FnCBD over immobilized α5β1 are shown. (C) Comparison of Fn (250 nM, solid line) and FnNTD fragment lacking the canonical integrin-binding RGD-motif (500 nM, dashed line).

3.14.2. SPR analysis revealed enhanced Fn-$\alpha_5\beta_1$ interaction by FnBPA

Using this SPR approach, a moderate affinity of ~1 μM for Fn-$\alpha_5\beta_1$ (Fig. 25A and C) was measured, which is in good agreement with affinities reported for fibroblast cell interactions with plasma Fn.[82] To understand whether FnBPA binding to Fn affects the Fn–$\alpha_5\beta_1$ interaction, mixtures of FnBPA-10/Fn (fixed FnBPA + varied Fn concentrations) were injected over the immobilized $\alpha_5\beta_1$ integrin. A remarkable enhancement of the binding response was observed for FnBPA-bound Fn relative to native Fn (Fig. 25 B). To obtain a quantitative measure of the increase in affinity, kinetic parameters were obtained by fitting SPR response curves to a bivalent analyte binding model. This model was selected based on closeness of fit ($\chi^2 \approx 1$, Table 1) and the assumption that dimeric Fn contributes one identical $\alpha_5\beta_1$ binding site per subunit. The analysis for each interaction revealed that the approximately four-fold increase in apparent affinity ($K_D^{Fn/\alpha5\beta1}$=1000 nM vs. $K_D^{FnBPA\text{-}10/Fn/\alpha5\beta1}$ = 260 nM) was due to an

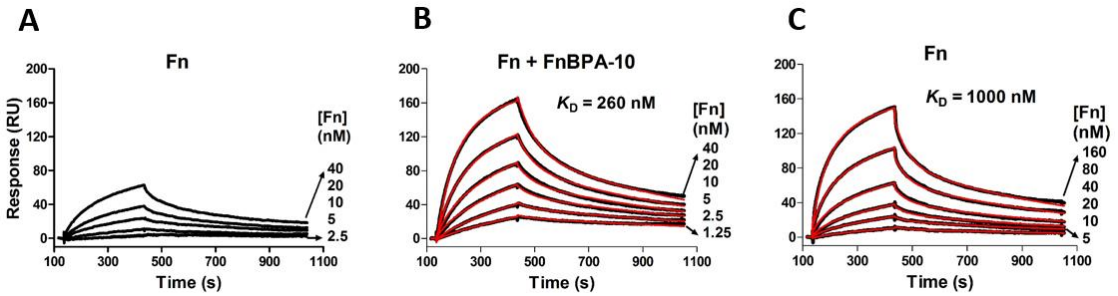

Figure 25. SPR analysis of direct Fn-$\alpha_5\beta_1$ interaction in the presence of FnBPA
(A) Two-fold linear dilution series of Fn in HBS-T containing 1 mM $MnCl_2$, and in the presence of (B) 1 µM of FnBPA-10, was injected over the $\alpha_5\beta_1$ biosensor. (C) Higher Fn concentration series was used to measure Fn-$\alpha_5\beta_1$ binding kinetics in the absence of MSCRAMMs. SPR response curves generated from Fn binding to $\alpha_5\beta_1$ are shown in black, with a lower curve corresponding to a lower concentration of Fn injected. K_D values for the Fn–$\alpha_5\beta_1$ interaction (B and C) were obtained by fitting SPR response curves to a bivalent analyte binding model (fitted lines are shown in red), and kinetic parameters are listed in Table 2. No detectable binding when FnBPA-10 (1 µM) was injected over the same $\alpha_5\beta_1$ surface (data not shown).

increase in the initial association rate (k_{a1}= 1.5 vs. 6.1 x10^4 $M^{-1}s^{-1}$). Interestingly, all other rate constants (k_{d1}, k_{a2}, and k_{d2}) (Table 8) were similar across experiments, indicating that the $\alpha_5\beta_1$ binding site in native Fn is the same as that for FnBPA-bound Fn. Because there is always a mix of conformers in the native Fn solution, the apparent association constant is the population-weighted average of association constants. The key point here is the binding affinity difference, not the absolute values of the binding affinities.

3.14.3. Specificity of FnBPA-induced enhancement of Fn-$\alpha_5\beta_1$ interaction

To address the specificity of enhanced Fn-$\alpha_5\beta_1$ activity and to further dissect the kinetic observations presented above, mixtures with varied FnBPA and fixed Fn concentrations were injected onto integrin (Fig. 26A and C). Again, a dose-dependent and saturable increase in the response was observed, similar to the results obtained in

Table 8. Kinetic parameters for Fn-$\alpha_5\beta_1$ interactions

Analyte injected	k_{a1} ($\times 10^4$ $M^{-1}s^{-1}$)	k_{d1} ($\times 10^{-2}$ s^{-1})	k_{a2} ($\times 10^{-5}$ $RU^{-1}s^{-1}$)	k_{d2} ($\times 10^{-3}$ s^{-1})	K_D (nM)	χ^2
Fn alone	1.5 ± 0.0	1.5 ± 0.0	1.1 ± 0.1	0.9 ± 0.0	1000 ± 130	1.15 ± 0.26
Fn + FnBPA-10	6.1 ± 0.6	1.5 ± 0.2	1.3 ± 0.3	1.0 ± 0.1	260 ± 90	1.10 ± 0.29

Association (k_{a1}, k_{a2}) and dissociation rate (k_{d1}, k_{d2}) constants obtained from fitting SPR response curves (Fig. 25 B–D) to a bivalent analyte binding model. Statistical value χ^2 is also listed to show the closeness of each fit. Values are mean values (with standard error in parentheses) obtained from at least three experiments.

Figure 25B. Likewise, only the initial association rate k_{a1} was changed, while the stability of the complex (k_{d1}), second-rate step (k_{a2} and k_{d2}), and maximum response when all binding sites on active $\alpha_5\beta_1$ were saturated (R_{max}) were unaffected by the presence of FnBPA-10 (Fig. 26B). The initial association rate, k_{a1}, was the only kinetic parameter directly affected by analyte concentration (units = $M^{-1}s^{-1}$). As the concentrations of Fn used in all experiments were the same, the observed increase in k_{a1} for Fn bound by increasing concentrations of FnBPA-10 likely represents an increase in the apparent concentration of the active integrin binding site (or active conformer) in native Fn.

3.15. High-affinity FnBPA–FnNTD interaction is required for Fn activation

Of the 11 Fn-binding repeats found in FnBPA, six were characterized as high-affinity binders (FnBPA-1, -4, -5, -9, -10, -11). The higher affinity of these repeats has been attributed to their ability to interact with four sequential FnI modules of the FnNTD fragment.[40] For example, while FnBPA-10 contains correctly spaced motifs to interact with $^{2-5}$FnI in a β-tandem zipper model of binding, the low-affinity repeat FnBPA-3

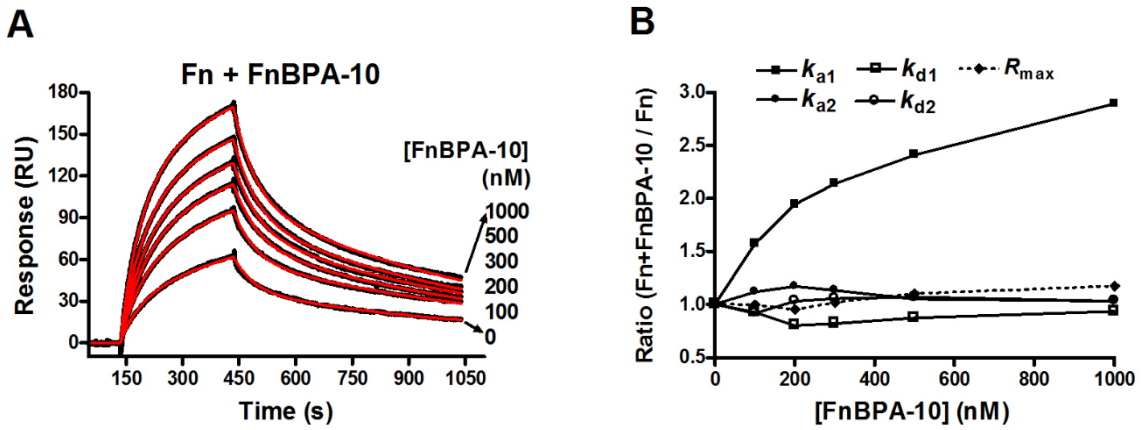

Figure 26. **Kinetic components of the Fn-$\alpha_5\beta_1$ interaction affected by FnBPA**
(A) Fn (50 nM) in the presence of an indicated concentration of FnBPA-10 was injected over a $\alpha_5\beta_1$ surface on a Biacore sensor chip. (B) Kinetic components (k_{a1}, k_{d1}, k_{a2}, and k_{d2}) and R_{max} obtained from local fitting were normalized to those of Fn alone and plotted as a function of FnBPA-10 concentrations.

appears to lack the ^{5}FnI interaction motif. Intriguingly, these particular Fn modules have been implicated in mediating long-range intramolecular contacts within native Fn dimers (Fig. 2).[83-85] To understand whether the high-affinity interaction is required for the FnBPA-induced increase in Fn-$\alpha_5\beta_1$ recognition, a panel of high and low-affinity FnBPA repeats was tested (Fig. 27). All studied high-affinity repeats (FnBPA-1, -5, -9, -10, and -11) increased the Fn-$\alpha_5\beta_1$ binding response, while the low-affinity repeat FnBPA-3 exhibited a control-level signal.

3.16. FnBPA enhances Fn–$\alpha_5\beta_1$ integrin interactions in human plasma

The SPR-based activity assay utilizing purified native and recombinant reagents enabled a quantitative kinetic assessment of the FnBPA-induced enhancement of Fn-$\alpha_5\beta_1$ binding. Next, whether this effect could be recapitulated using human plasma as a source of native Fn was investigated. Indeed, a FnBPA-dependent increase in plasma Fn-$\alpha_5\beta_1$

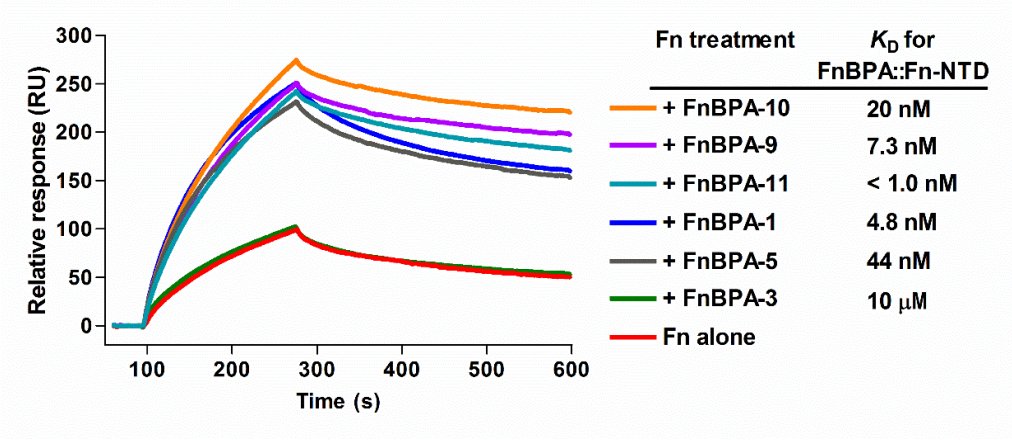

Figure 27. Relationship of FnNTD interaction and $\alpha_5\beta_1$ integrin activation
SPR sensorgrams were generated by injecting 50 nM Fn in the presence of GST-fused FnBPA repeats (0.5 μM for high-affinity repeats FnBPA-1, -5, -9, -10, -11 and 15 μM for low-affinity repeat FnBPA-3) over immobilized $\alpha_5\beta_1$. K_D values reported for direct binding of FnNTD by high-affinity FnBPA repeats are provided for reference and were obtained from previously published ITC experiments.[40] Weak affinity between FnBPA-3 and FnNTD was measured by SPR (data not shown). None of the repeats bound directly to $\alpha_5\beta_1$ (data not shown).

binding was observed with FnBPA-10, when purified native Fn (Fig. 28A) and unpurified intact Fn in 5% human plasma (Fig. 28B) were used in an ELISA-type binding assay. Interestingly, the activation of integrin $\alpha_{IIb}\beta_3$ was less specific for intact Fn in plasma compared to $\alpha_5\beta_1$, although they both recognized the = RGD site, suggesting possible involvement and fine tuning of the synergistic site on Fn by $\alpha_5\beta_1$ binding.

3.17. Disease-related polymorphisms in FnBPA affect Fn-binding activity

SPR was also used to investigate the direct interactions between Fn and peptide variants synthesized to mimic FnBPA-9 of FnBPA from clinical isolates of *S. aureus*: H782A+K786A, H782Q+K786N, H782Q+K786I, H782A, H782Q, K786I, and a wild-type peptide (H782+K786).

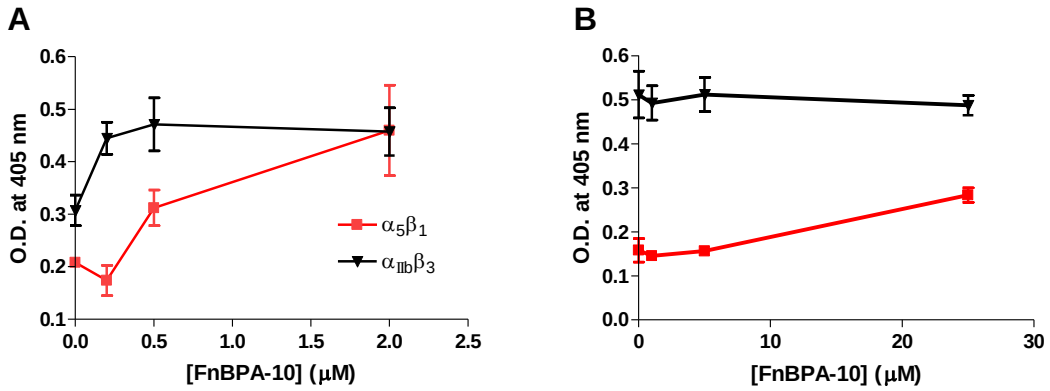

Figure 28. Effect of FnBPA on intact Fn in plasma for integrin binding
In an ELISA type assay, FnBPA-10 peptide was pre-incubated with (A) 0.2 μM purified Fn, and (B) 5% human blood plasma, and then added to integrin-coated wells. Bound Fn was probed with anti-Fn pAb.

Figure 29 shows the sensorgrams of the binding of FnBPA-9 peptides to FnNTD, and the curves were fit with a two-state binding model to calculate the kinetic parameters (Table 3). This model was chosen based on the zipper type of binding that involves the conformational transition of the peptide from disordered to ordered.[37] The two-step binding model includes (i) the initial binding of the peptide to the FnNTD (A + B ↔ AB) followed by (ii) a conformational change to form a more stable complex (AB ↔ AB*). This model reproduced the experimental SPR sensorgrams better than the 1:1 Langmuir model and also described the interaction between FnBR9 and FnNTD. The binding affinity for the interaction between FnBR9 wild-type peptide and FnNTD (K_D = 0.66 μM) is similar to the K_D value of 0.5 μM for the interaction between the 19-mer FnBR1 peptide and ^{2}FI^{3}FI detected by NMR chemical shifts [37]. All peptides contained the same recognition motifs (G_{783} and EDT_{795}) to interact with ^{2}FI^{3}FI, which was indicated by the

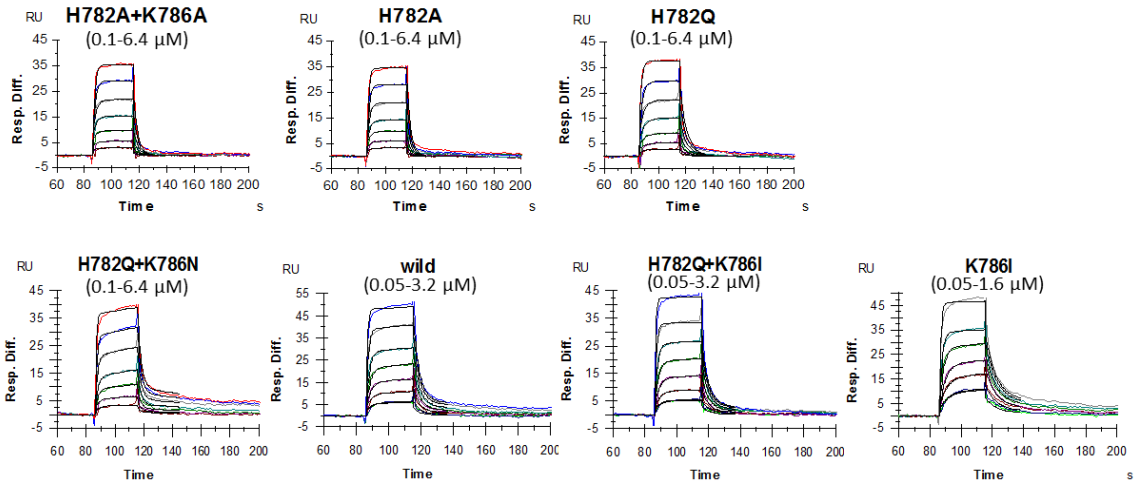

Figure 29. SPR analysis of interactions between FnBPA-9 peptides and FnNTD
Two-fold linear dilution series of the peptide, at the indicated concentration range, were injected over the immobilized FnNTD. SPR response curves generated from peptide binding are shown as colored lines, with a lower curve corresponding to a lower concentration of peptide injected. Sensorgrams were globally fit to a 1:1 Langmuir model to obtain K_D or to a two-state reaction model to obtain apparent dissociation constants (K_D^{app}) for the interaction (fit lines are shown in black). Kinetic parameters are listed in Table 9.

overall similar responses for peptides binding to FnNTD. Upon binding, FnBPA-9 underwent a conformational transition from disordered to a β-strand, complementing the β-sheet structure in FnNTD. As a result, bound FnBPA-9 formed a large intermolecular surface and stable complex with FnNTD.[40]

Table 9 lists the kinetic and affinity constants obtained from fitting (Fig. 29). Within the two-step processes, the progression of the second step is more than 18-fold slower than the first dissociation step (k_{a2} vs. k_{d1}), suggesting that the conformational change step is rate-limiting for the generation of a stable complex. The mutations at positions H782 and K786 with disease-associated SNPs result in ~20-fold stronger

Table 9. Kinetic parameters for FnBPA-9 peptides binding to FnNTD

Peptide	$k_{a(1)}$ (x10^5 $M^{-1}s^{-1}$)	$K_{d(1)}$ (x10^{-1} s^{-1})	k_{a2} (x10^{-3} s^{-1})	k_{d2} (x10^{-2} s^{-1})	K_D or K_D^{app} (μM)	K_{D1} (μM)	k_{d1}/k_{a2}
H782A+K786A	0.54 ± 0.07	3.20 ± 0.04			6.04 ± 0.81		
H782A	0.73 ± 0.19	3.22 ± 0.29			4.52 ± 0.81		
H782Q	0.62 ± 0.07	2.05 ± 0.21			3.35 ± 0.71		
H782Q+K786N	1.74 ± 0.11	4.02 ± 0.24	11.5 ± 1.13	1.03 ± 0.04	1.10 ± 0.04	2.31 ± 0.0	35 ± 4
Wild type	2.23 ± 0.44	2.70 ± 0.52	10.3 ± 0.42	1.23 ± 0.18	0.66 ± 0.06	1.21 ± 0.1	26 ± 4
H782Q+K786I	4.87 ± 1.30	3.07 ± 0.86	6.55 ± 0.40	2.47 ± 0.38	0.50 ± 0.10	0.64 ± 0.1	46 ± 11
K786I	5.05 ± 1.31	1.57 ± 0.17	8.70 ± 0.64	1.07 ± 0.10	0.18 ± 0.05	0.32 ± 0.0	18 ± 2

binding affinity than the alanine substitutions (K_D^{app} value = 0.18 μM for K786I, compared to 6.04 μM for H782A+K786A). The enhanced affinity of K786I for FnNTD is due to the increased affinity of initial binding step (K_{D1}), with a higher on-rate and slower off-rate and a favorable conformational change indicated by the smaller value of ratio k_{d1}/k_{a2}. The intrinsic disorder FnBR forms a fuzzy complex when it binds to Fn,[86] where some of the disordered region is maintained upon interaction with Fn, directly impacting biological function.[86] Even though the ligand-binding motifs of FnBPA-9 are intact, the changes in the regions flanking the motifs can influence ligand binding by fine-tuning the kinetics of the reaction. This provides a mechanistic explanation for the association of H782Q+K786I SNPs in *S. aureus* FnBPA in patients with persistent bacteremia,[25] where fast adherence to and invasion of host cells may be enhanced by fast association and conformational changes that expose cryptic integrin sites in Fn,[87] while H782Q+K786N is associated with patients with infected cardiac device implants in which invading host cell and rapid attachment are not critical for pathogenesis.

CHAPTER IV

DISCUSSION

Many studies have shown that the virulent properties of FnBPA depend on tight and multivalent binding to Fn,[88-90] and in some cases, cooperative binding to Fg.[12-13] Structural and mechanistic characterizations have been carefully conducted for interactions of FnBPA and Fn,[39-40] and a structure of FnBPA bound to the previously identified single target site in Fg was recently reported.[28] However, most in vitro studies were completed with domains or segments of the proteins. The host protein interactions with the full-length FnBPA presented on the surface has not been characterized to date. The mechanism by which multifunctional FnBPA unifies the Fg- and Fn-binding capacities are still unclear. One challenge is that FnBPA contains a large portion of repetitive disordered segments, making it difficult to clone and express. The large size and multiple domains of Fn and Fg molecules also create complexity for bioanalytical binding measurements. In this study, I utilize SPR technology to explore the FnBPA interaction in a non-pure system (blood plasma) and then use native purified proteins and domains to investigate complex binding. Using both solid phase and solution phase analyses, this work studied, in molecular detail, how surface-anchored full-length FnBPA binds to Fn and Fg, as well as the interplay and regulation of these interactions.

The biochemical characterization of FnBPA binding with Fn and Fg indicates that both interactions are strong with quick recognition (fast on-rate) and stable bonding (slow off-rate). These measurements confirm biological functions, as FnBPA is

expressed at a low density (log phase during growth), and the highly adhesive and invasive properties will become necessary for bacteria to establish colonies. FnBPA on *S. aureus* infecting different positions in the human body is exposed to very different external forces, ranging from the dynamic shear force (blood flow) associated with endovascular environments to more static conditions in the anterior nares. Different conditions may select for FnBPA adhesin with rapid and strong binding attributes.

Strong binding of FnBPA to Fn mediates the attachment of *S. aureus* to the endothelium under dynamic conditions. This also leads to allosteric activation of integrin binding sites in Fn, which, in turn, are recognized by $\alpha_5\beta_1$ integrin on the endothelial surface, triggering bacterial uptake. Many earlier studies showed that FnBPA binds weakly to Fg via a linear sequence (about 15 aa) in the C-terminus of the Fg γ-chain (FgγC peptide), but this study provides evidence suggesting that this primary site has to engage with additional sites in Fg to achieve a strong interaction. Multiple contacts between FnBPA and Fg are possible, and they presumably involve molecular rearrangements within each protein. As a result, it is possible that residue changes in critical areas of FnBPA could influence ligand binding.

The work accomplished in this dissertation is significant. It provides critical insights into the interactions between MSCRAMM and host proteins regarding overall affinity, active conformation, and effects on host protein structure/function. It correlates a molecular interaction study with clinical outcomes, and it also improves scientific knowledge and technical capability in the field of adhesin-mediated host-pathogen interactions.

4.1. SPR for studying binding of surface-associated protein

SPR is a unique technique for studying binding interactions because of the determination of the binding affinity and kinetics, and for direct observing the binding dynamics in real time. Capture of tagged recombinant proteins is an attractive approach for protein attachment in the SPR-based Biacore systems since physiological conditions can be used during the whole procedure. Also, the capture of tags generates a directed structural orientation of the protein on the surface, potentially offering optimal site exposure. In the present study, a receptor sensor was created to mimic the same surface orientations of the molecules studied, for example, FnBPA on the bacterial surface and integrin receptor on host cell surface. This approach enables the assay condition for binding kinetics and affinity measurement that is more relevant to the physiological condition.

Previous in vivo study of Fn and Fg binding to *Lactococcus lactis* expressed FnBPA suggested the functional versatility may be partly related to the location of the protein, in which the in vivo conformation of surface-bound FnBPA may be different from that of unbound recombinant proteins.[13] The results of the present study provide experimental evidence to support this hypothesis. On the surface of the staphylococci, FnBPA is anchored to the cell wall at its C-terminus, with the Fg binding domain extended from the surface. To mimic FnBPA surface orientation, a Biacore method was developed to capture FnBPA through its C-terminal His-tag onto α-his mAb surface. Host ligands in solution (purified proteins or non-purified plasma) was injected onto the functionalized FnBPA sensor. The results from the binding analysis indicate that binding

of soluble Fg to surface-anchored FnBPA is ~50-fold stronger than soluble FnBPA binding to immobilized Fg (K_D values of 15.7 ± 5.6 nM and 725 ± 74 nM, respectively. Fig. 9A and D, and Table 4). Even when both FnBPA and Fg are in solution, the affinity detected by ITC is 230 ± 80 nM, still 15-fold weaker than surface-bound FnBPA.

Furthermore, when physiological materials and conditions are applied, SPR with functionalized sensor approach can provide valuable kinetic insights into what or how the pathogen and host see each other. Sometimes, the individual ligand-binding events in isolation cannot explain the measured outcome from the non-purified system. For example, the results in Fig. 7, 8 and 20 demonstrate that blood plasma is far more potent reactant than purified Fg/Fn alone or combined, and likely Fg alone in plasma does not react with FnBPA but only when it is complexed with Fn. A new hypothesis will have to be tested.

4.2. New binding sites in Fg and FnBPA

In this study, the binding analysis and structural characterization of FnBPA indicate that Fg conformation and structural orientation of FnBPA are critical for Fg–FnBPA interaction. By comparing FnBPA binding activity of different forms of Fg molecule, such as plasma (extremely tight binding and not dissociated molecule observed), soluble Fg (K_D = 10 nM, Fig. 7), amine immobilized Fg (K_D = 780 nM, Fig. 9), FgD (K_D = 86 nM, Fig. 9), FgD dimer (FgγC inactive form, K_D = 163 nM, Fig. 9), and FgγC peptide (K_D = 1.82 μM, Fig. 17), it is clear that other binding sites in Fg may participate in the observed strong FnBPA recognition. Both Fg and minimal binding domain $FnBPA_{38–550}$ are negatively charged at physiological pH, with pI values of 5.5

and 5.0 (Table 5) respectively. So their high-affinity electrostatic interaction (Fig. 13) was unexpected since the previous identified FgγC peptide interaction was hydrophobic in nature. The C-terminus of α chain, located next to the FgD domain, may act as a potential binding site, as it is positively charged at pH 7.4.

Recently, it was found that in addition to its originally identified FgγC peptide, ClfA A domain binds to another distinct site in Fg.[91] The structure of a blocking monoclonal antibody in complex with the N2N3 domain of ClfA revealed that the epitope for the mAb is located on "top" of N3 but does not affect N2N3 cleft where FgγC peptide binding site is located. Molecular modeling identifies the partially overlapping N3 epitope for the mAb to be the second Fg-binding site.[91] Since ClfA and FnBPA are structurally and functionally related MSCRAMMs, it is likely that FnBPA binding to Fg also involves a two-site mechanism. Among *S. aureus* isotypes, FnBPA sequence diversity is found most divergent in N3 subdomain[24] (Fig. 1). It is reasonable to speculate that N3 is exposed to contact with the host ligand Fg and subjected to selective pressure to carry out functions. Overall, the mechanism of Fg binding to FnBPA is more complicated than originally proposed and more so than prototype Fg-ClfA interaction. The absence of "latching" event due to the potential overlap between residues in FnBPA-1 (or linker between N3 subdomain and FnBR, Fig. 1) affected by Fg and Fn binding. It seems that these two ligand-binding events are coupled and influence each other, making multifunctional FnBPA unique in response to host environment (salt, pH, and ligand concentration) change.

4.3. Function of N1 domain

Subdomain N1 of the A domain is highly conserved among different FnBPA isotypes (Fig. 1),[24] suggesting functional importance. Even though the structure and function of the N1 domain are unknown, it is reasonable to speculate that N1 serves as a regulatory domain through intramolecular interactions (e.g., with the distant FnBR region) within FnBPA. There are several lines of evidence that support the proposed N1 fold-back structure and function: first, specific residues (Q139 and Q141) in N1, far from the C-terminal FnBR, are involved in Fn cross-linking,[92] suggesting engagement with FnBR (Fig. 1). Second, a short sequence within N1 is required for surface expression of FnBPA, which contains the disordered FnBR region.[29] Third, data from this study suggest that proteolytic removal of N1 could regulate Fg-binding activity, suggesting a regulatory role of N1. Fourth, it is possible that serine proteinase cleavage of FnBPA on the cell surface occurs in vivo either via thrombin from the host or the *S. aureus* coagulase-prothrombin complex.[93] Fifth, the previous study identified Gln139 in the N1 subdomain of FnBPA as a major cross-linking site in the factor XIIIa-mediated reaction with α chains of Fg.[94] Therefore, the question of whether N1 could fold-back toward N2N3 subdomains to form an optimal conformation for Fg binding was investigated. Surprisingly, when comparing the N1 sequence with the Fg γ-chain, N1 contains a similar amino acid sequence to the 17-aa FgγC peptide (highlighted in blue in Fig. 30). The FgγC peptide binds to the cleft between the N2 and N3 subdomains of FnBPA, and it is likely that a similar sequence in N1 can fold back to occupy the hydrophobic cleft through intramolecular interactions. If this holds true, the interaction could also occur

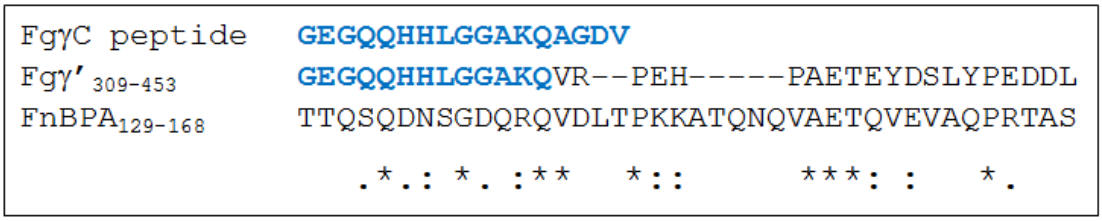

Figure 30. Sequence comparison of N1 and FgγC region
Sequence from N1 of FnBPA ($FnBPA_{120–168}$) compared to the C-terminal ends of two Fg γ-chain isoforms (Fgγ and elongated variant Fgγ'). The 17-aa FgγC peptide sequence is highlighted in blue.

between molecules to promote dimerization of surface FnBPA on neighboring cells, a possible mechanism for the protein-based biofilm[30] of *S. aureus*. An Experiment is underway to test this possible interaction using a synthetic N1 peptide.

4.4. Modeling FnBPA–Fg interaction

Fluorescence and CD spectroscopy analyses of the full-length FnBPA confirmed that the protein is composed of both compact and disordered regions. It is possible that a non-linear structure existed in full-length FnBPA, in which the N- and C-terminal disordered regions wrap around or closely associate with the structured A domain. These results also suggest that the original A domain assignment, which included N1 and FnBPA-1, is the most relevant functional ligand-binding domain. By correlating this solution structure with the ligand-binding activity of FnBPA proteins measured by SPR, the results imply that the N1 and FnBPA-1 regions may be involved in maintaining an appropriate FnBPA fold. This active FnBPA provides an optimal conformation for rapid ligand recognition and the formation of more stable complexes, resulting in tighter Fg binding. Based on this observation and the N1 function revealed in this study, as well as

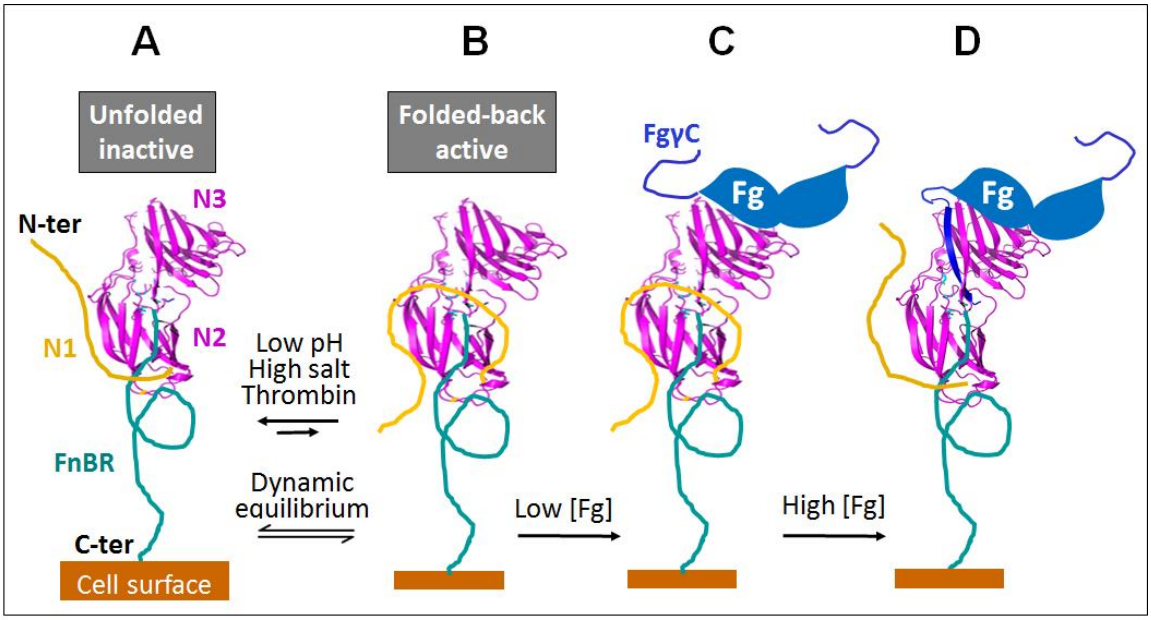

Figure 31. Selective binding model of FnBPA–Fg interaction
Surface-anchored FnBPA is in a dynamic equilibrium between (A) unfolded and (B) fold-back conformations because of intramolecular interactions between the N1 region and hydrophobic cleft between N2N3 subdomains. Fold-back form could be further stabilized by C-terminal FnBR region and represent the active conformation, with a preformed binding site ready for a strong interaction with soluble Fg. Low pH and high salt conditions or N1 removal by thrombin shift the equilibrium to the inactive conformation, making the Fg interaction unfavorable. On the host side, soluble Fg dimer exists in blood as an assemble of different conformers. Under high shear flow conditions, only a small portion of these conformers can rapidly recognize FnBPA (or low concentrations of active Fg for FnBPA binding), presumably through exposed N3 surface binding to structured Fg domain, but not through the disordered FgγC region (C). This initial strong recognition of N3 may cause rearrangement of N2N3 orientation and unfold N1 from the cleft. The unoccupied cleft is then ready to accommodate FgγC in the proximity (D). Alternatively, the high local concentration of FgγC, achieved through initial binding or high concentration of Fg in the blood, induces competition between FgγC and N1 to bind the cleft region of FnBPA. N2N3 domain structures (apo and in complex with FgγC) are from published data.[28]

the existing N2N3 structure, I propose a Fg-binding model for FnBPA (Fig. 31).

The surface-anchored FnBPA is not a rigid structure, but a dynamic equilibrium between unfolded and folded conformations. This is because the dynamics of the

intramolecular interaction allow N1 to fold-back and occupy the hydrophobic cleft between N2N3 subdomains. The fold-back form could also be further stabilized by the C-terminal FnBR region and represents the active conformation, with a preformed binding site, ready for a strong interaction with soluble Fg. The low pH or high salt conditions or N1 removal by thrombin will shift the equilibrium to the inactive conformation, making the Fg interaction unfavorable. On the host side, soluble Fg dimers exist in blood as an assembly of different conformers. Under high shear flow conditions, only a small portion of these conformers can rapidly recognize FnBPA (or a low concentration of active Fg for FnBPA binding), presumably through exposed N3 surface binding to structured Fg domain, but not through the disordered FgγC region. This initial strong recognition of N3 may cause rearrangement of N2N3 orientation and unfold N1 from the cleft. The unoccupied cleft is then ready to accommodate a proximal and available FgγC molecule. Alternatively, the high local concentration of FgγC, achieved with initial binding or high concentration of Fg in the blood, can compete with N1 for binding to the cleft region of FnBPA.

4.5. Modeling allosteric activation of Fn–integrin by FnBPA

Results from DLS (Table 7), CD (Fig. 22), and FRET (Fig. 23) measurements indicate a conformational rearrangement of Fn involving domains distant from the FnBPA binding site. SPR experiments demonstrate a significant enhancement of Fn-$\alpha_5\beta_1$ integrin affinity in the presence of FnBPA (Fig. 25). Detailed kinetic analyses of these interactions reveal that this change in affinity can be attributed solely to an increase in the initial Fn-$\alpha_5\beta_1$ on-rate (Fig. 26), and this rate enhancement depends on high-affinity

Fn-binding by FnBPA (Fig. 27). These data implicate MSCRAMM-induced perturbation of specific intramolecular contacts within the Fn heterodimer, resulting in activation by exposing previously cryptic $\alpha_5\beta_1$ interaction motifs. By manipulating the conformation of key Fn functional domains, FnBPA enables *S. aureus* to hijack normal host physiology. Enhanced Fn-$\alpha_5\beta_1$ interactions lead to the recruitment of focal contact-associated proteins, and subsequent integrin clustering at a bacterial attachment site initiates intracellular signaling through the focal adhesion kinase (FAK) and Src kinases.[60, 95-96]

Together, these experiments provide a detailed structure–activity relationship of FnBPA–host interactions and strongly suggest an allosteric mode of Fn-$\alpha_5\beta_1$ affinity enhancement for FnBPA (Fig. 32). I speculate that dimeric native Fn exists as an array of conformers in solution. At equilibrium, the predominate forms of Fn are compact and sterically occlude $\alpha_5\beta_1$ interaction domains ($^{9\text{-}10}$FnIII) by long-range intramolecular interactions, thereby impeding Fn-$\alpha_5\beta_1$ recognition. The equilibrium of Fn conformers shifts upon high-affinity binding of FnBPA, and native intramolecular contacts are disrupted, exposing previously cryptic $\alpha_5\beta_1$ binding sites and promoting Fn-$\alpha_5\beta_1$ binding. Domains involved in integrin binding by Fn are located at a site distant from the FnBPA binding site. Therefore, a critical feature of FnBPA-induced activation of Fn-$\alpha_5\beta_1$ is allosteric modes of host protein modulation, which have been previously reported for *S. aureus*.[97] By correlating structural changes in Fn (Fig. 23) to direct measurements of increased Fn-$\alpha_5\beta_1$ affinity (Table 8), this work significantly advances our understanding of the structural basis of modulation of integrin function by Fn-binding MSCRAMMs.

Interestingly, polymorphisms have been recently reported in high-affinity FnBPA

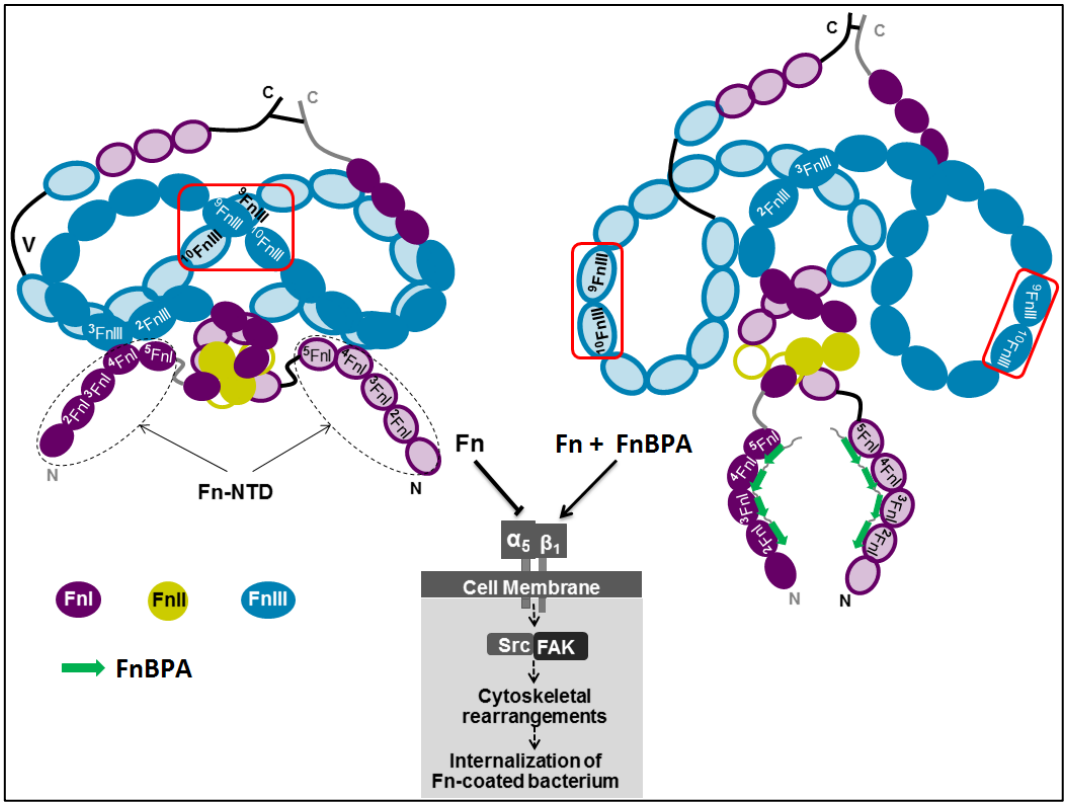

Figure 32. Model for allosteric enhancement of Fn-$\alpha_5\beta_1$ binding by FnBPA
Fn is represented in the native state (left) or bound by FnBPA (right). Model of native Fn, including intermolecular contacts, was adapted from a previously proposed model based on multiple independent studies. In a native state, major solution conformations of Fn occlude the canonical $\alpha_5\beta_1$ interaction motifs located in the $^{9-10}$FnIII domains. Upon binding to Fn, FnBPA disrupts specific intermolecular contacts in the N-terminal domain of Fn (FnNTD), resulting in global structural rearrangements at sites distant from the FnBPA binding site. Previously cryptic integrin interaction sites are exposed, promoting interaction of Fn with $\alpha_5\beta_1$. This initiates "outside-in" signaling events, leading to cytoskeletal rearrangement and eventual internalization of Fn-coated *S. aureus*.

repeats (Fig. 1), and *S. aureus* strains that harbor these mutations are highly correlated with infection of cardiovascular devices.[22, 25] How these FnBPA mutations impact bound Fn tertiary structure is currently unknown. However, I predict that sequence changes to

residues in FnBPA repeats could result in different global Fn structures and thus functions.

Some studies have shown that surface induced unfolding of Fg promotes integrin $\alpha_M\beta_2$ (Mac-1) receptor activation and inflammation.[98] A high-affinity Mac-1 binding site existed in the C-terminal tail region of the Fg γ chain, but it is buried and protected within the hydrophobic core of the protein.[99] One primary $\alpha_M\beta_2$ binding sites, P2 ($Fg\gamma_{377–395}$), is located next to FnBPA binding site.[100] Allosteric activation of the Fg-receptor interaction by FnBPA could also generate the strong Fg binding demonstrated in the study. It is very likely that Fg unfolds on FnBPA surface, and FnBPA-bound Fg interacts with $\alpha_M\beta_2$ receptors.

4.6. Modeling FnBPA-dependent *S. aureus* host interactions

From commensal to infectious states, the *S. aureus* host interaction involves a complex interplay of many different proteins and events. First, cells must recognize each other, adhere to one another, and create an interface through which a biological signal can be generated, ultimately producing a specific outcome that leads to the initiation of bacterial adhesion, host defense, bacterial invasion, or gene regulation. In light of the discoveries described in this dissertation and the possible functions in disease process[38], I propose a model (Fig. 33) to summarize multi-faceted FnBPA-dependent ligand binding, activation, and host cell signaling. (1) *S. aureus* utilizes the cell wall surface protein FnBPA to bind directly to the Fn and Fg in tissue, Fn/Fg-coated medical devices, or thrombus containing Fg/Fn. The high-affinity and avidity interactions between two

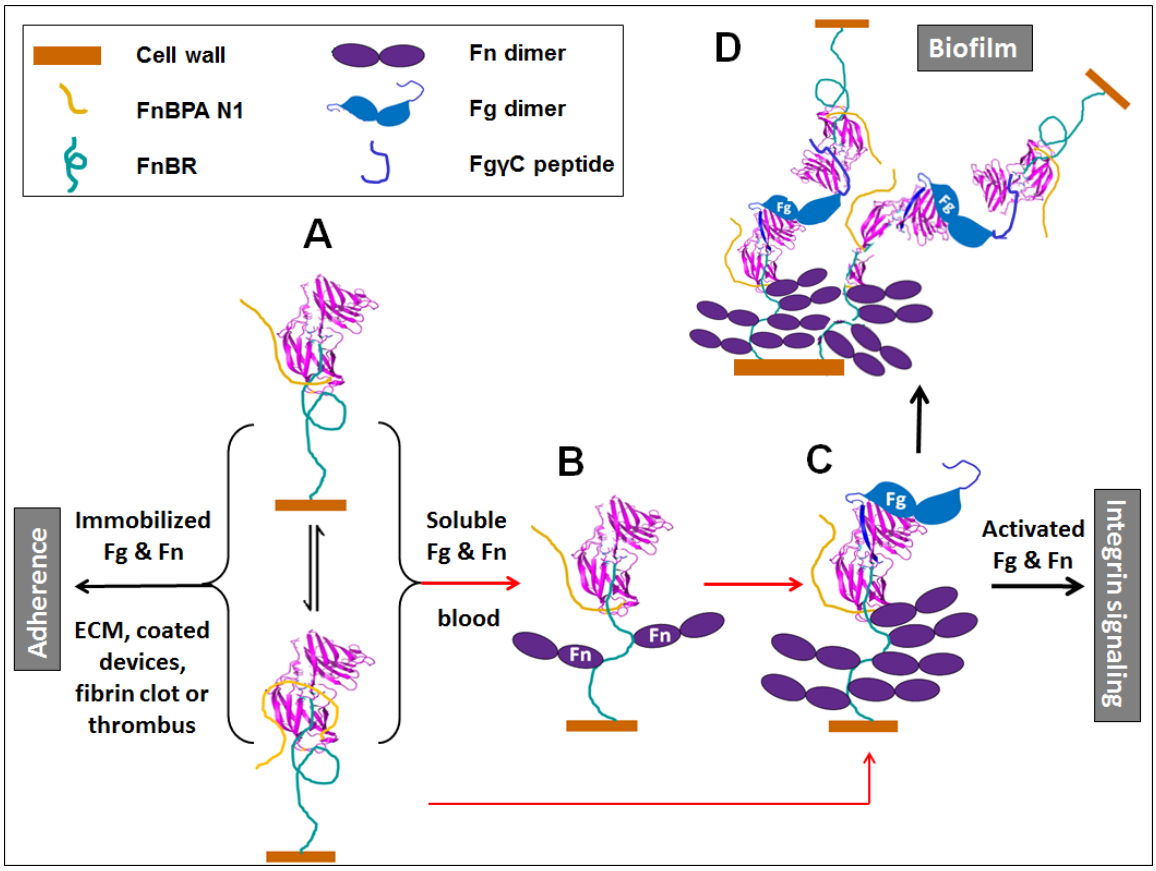

Figure 33. A Model for FnBPA-mediated *S. aureus* host interaction
(A) Surface-associated FnBPA (both unfolded and fold-back forms) can bind directly to Fn and Fg in tissue ECM, Fn/Fg-coated medical devices, or thrombus containing Fg/Fn . High-affinity and avidity interactions between two surfaces ensures the firm attachment of *S. aureus* to the host site. (B) Circulating plasma Fg and Fn can rapidly and firmly adsorb onto the bacterial surface via FnBPA. Fast binding and high-affinity ligand Fn is likely the first molecule adsorbed to FnBPA via one or more specific FnBR, allosterically activating A domain and exposing N2N3 cleft for Fg binding. (C) FnBPA-bound Fn and FnBPA-bound Fg are activated and exposed to integrin binding sites, triggering integrin signaling in endothelium and immune cells. Location of an array of high-affinity Fn-binding repeats close to the bacterial cell wall enables the establishment of intimate contact with the host cell. FnBPA-bound Fg and Fn can also engage different integrins for cross-talk, resulting in more robust activation of the signaling network. (D) Dimeric nature of Fn and Fg enables functionality as bridging molecules between surface FnBPA on *S. aureus* and cells, leading to the formation of extensive adhesive contacts for a protein-based biofilm community.

surfaces ensure the firm attachment of *S. aureus* to the host site. (2) Circulating plasma Fg and Fn can rapidly and firmly adsorb onto the bacterial surface via FnBPA. The fast binding and high-affinity ligand Fn is likely one of the first molecules to be adsorbed to FnBPA via one or more specific FnBR, allosterically activating the A domain and exposing the N2N3 cleft for Fg binding. (3) FnBPA-bound Fn and Fg are activated and exposed to integrin binding sites to trigger integrin signaling in endothelium and immune cells. The location of an array of high-affinity Fn-binding repeats close to the bacterial cell wall enables the establishment of intimate contact with the host cell. It is also possible that FnBPA-bound Fg and FnBPA-bound Fn can engage different integrins for cross-talk, resulting in more robust activation of the signaling network. This appears to confer an advantage to *S. aureus*, by facilitating immune evasion and serving as a bacterial reservoir in chronic infections.[54, 60] (4) The dimeric nature of Fn and Fg enables their function as bridging molecules between surface FnBPA on *S. aureus*, along with the A domain-mediated self-association of FnBPA, and between cells. Host factor XIIIa-catalyzed cross-linking reactions can further stabilize this network and contribute to biofilm development.

4.7. Future studies

To gain a true mechanistic understanding of FnBPA and host ligand interactions, the relevant complexes should be reconstituted and their three-dimensional structures determined, to reveal the molecular mechanisms of the interactions. The initial crystallization trials of the minimal domain ($FnBPA_{38–550}$) and the minimal domain in complex with FgD indicated that the unstructured region in N1 needs to be further

removed. Although thrombin-treated FnBPA ($FnBPA_{166–981}$) altered Fg binding, the partial interaction still remained. Recombinant $FnBPA_{166–550}$ and constructs with an extended N-terminus can be used for future crystallization studies.

The binding study of disease-related polymorphisms in FnBPA only focused on the Fn-binging region (FnBR) of FnBPA. Considering that the multifunctional role of FnBPA is important during the disease process, in which both Fg- and Fn-binding synergistically initiate attachment to endothelium, and multiple Fn-binding events can activate the integrin for host cell invasion. Variant sequences found in FnBRs are associated with variations elsewhere in the protein, for example, the Fg-binding A domain, which is known to have greater sequence diversity.[24] By measuring the ligand-binding characteristics (k_{on} and k_{off}, affinity, and stoichiometry) of recombinant full-length FnBPA from clinical isolates that carry disease-related variations and comparing them with wild-type FnBPA, a mechanistic explanation for the clinical outcomes observed can be generated.

The bioanalytical SPR and adhesin functionalized biosensor platform can be used as an assay system for screening and developing therapeutics and biologics, such as small molecules or antibodies from healthy or infected populations.

CHAPTER V

CONCLUSIONS

The *S. aureus* surface protein FnBPA is essential for *S. aureus* adhesion and invasion of host cells. In this study, I applied a set of biochemical and biophysical methods (CD, DLS, fluorescence spectroscopy, FRET, ITC, and SPR) to investigate FnBPA and probe structure–activity relationships of FnBPA-dependent host interactions. Based on the results presented in this dissertation, the following conclusions are made. First, circulating plasma Fn and Fg can bind simultaneously and tightly to surface-anchored full-length FnBPA. Second, several physiologically relevant factors, such as proteolytic processes, ionic strength, and pH, can affect the fold-back conformation of the N1 subdomain of FnBPA, resulting in altered Fg binding. Third, the strong interaction between FnBPA and Fn induces conformational changes in Fn at distant sites, resulting in exposed cryptic integrin binding sites and enhanced Fn−$\alpha_5\beta_1$ interaction. Fourth, disease-causing polymorphisms in FnBPA may impart conformational variability to the ligand complex, which affects adhesion reactions and attachment. Finally, this study demonstrates that SPR with a functionalized biosensor is an effective technique to study interactions between bacterial surface proteins and host ligands.

REFERENCES

1. Patti, J. M.; Allen, B. L.; McGavin, M. J.; Hook, M., MSCRAMM-mediated adherence of microorganisms to host tissues. *Annual review of microbiology* **1994,** *48*, 585-617.

2. Patti, J. M.; Hook, M., Microbial adhesins recognizing extracellular matrix macromolecules. *Current opinion in cell biology* **1994,** *6* (5), 752-8.

3. Foster, T. J.; Geoghegan, J. A.; Ganesh, V. K.; Hook, M., Adhesion, invasion and evasion: the many functions of the surface proteins of Staphylococcus aureus. *Nat Rev Microbiol* **2014,** *12* (1), 49-62.

4. Henderson, B.; Nair, S.; Pallas, J.; Williams, M. A., Fibronectin: a multidomain host adhesin targeted by bacterial fibronectin-binding proteins. *FEMS Microbiol Rev* **2011,** *35* (1), 147-200.

5. Flock, J. I.; Froman, G.; Jonsson, K.; Guss, B.; Signas, C.; Nilsson, B.; Raucci, G.; Hook, M.; Wadstrom, T.; Lindberg, M., Cloning and expression of the gene for a fibronectin-binding protein from Staphylococcus aureus. *The EMBO journal* **1987,** *6* (8), 2351-7.

6. Joh, D.; Wann, E. R.; Kreikemeyer, B.; Speziale, P.; Hook, M., Role of fibronectin-binding MSCRAMMs in bacterial adherence and entry into mammalian cells. *Matrix Biol* **1999,** *18* (3), 211-23.

7. Wann, E. R.; Gurusiddappa, S.; Hook, M., The fibronectin-binding MSCRAMM FnbpA of Staphylococcus aureus is a bifunctional protein that also binds to fibrinogen. *J Biol Chem* **2000,** *275* (18), 13863-71.

8. Roche, F. M.; Downer, R.; Keane, F.; Speziale, P.; Park, P. W.; Foster, T. J., The N-terminal A domain of fibronectin-binding proteins A and B promotes adhesion of Staphylococcus aureus to elastin. *J Biol Chem* **2004,** *279* (37), 38433-40.

9. Jenkins, A.; Diep, B. A.; Mai, T. T.; Vo, N. H.; Warrener, P.; Suzich, J.; Stover, C. K.; Sellman, B. R., Differential expression and roles of Staphylococcus aureus virulence determinants during colonization and disease. *MBio* **2015,** *6* (1), e02272-14.

10. Heying, R.; van de Gevel, J.; Que, Y. A.; Moreillon, P.; Beekhuizen, H., Fibronectin-binding proteins and clumping factor A in Staphylococcus aureus experimental endocarditis: FnBPA is sufficient to activate human endothelial cells. *Thromb Haemost* **2007,** *97* (4), 617-26.

11. Brouillette, E.; Talbot, B. G.; Malouin, F., The fibronectin-binding proteins of Staphylococcus aureus may promote mammary gland colonization in a lactating mouse model of mastitis. *Infect Immun* **2003,** *71* (4), 2292-5.

12. Que, Y. A.; Haefliger, J. A.; Piroth, L.; Francois, P.; Widmer, E.; Entenza, J. M.; Sinha, B.; Herrmann, M.; Francioli, P.; Vaudaux, P.; Moreillon, P., Fibrinogen and fibronectin binding cooperate for valve infection and invasion in Staphylococcus aureus experimental endocarditis. *J Exp Med* **2005,** *201* (10), 1627-35.

13. Piroth, L.; Que, Y. A.; Widmer, E.; Panchaud, A.; Piu, S.; Entenza, J. M.; Moreillon, P., The fibrinogen- and fibronectin-binding domains of Staphylococcus

aureus fibronectin-binding protein A synergistically promote endothelial invasion and experimental endocarditis. *Infect Immun* **2008,** *76* (8), 3824-31.

14. Fowler, T.; Wann, E. R.; Joh, D.; Johansson, S.; Foster, T. J.; Hook, M., Cellular invasion by Staphylococcus aureus involves a fibronectin bridge between the bacterial fibronectin-binding MSCRAMMs and host cell beta1 integrins. *Eur J Cell Biol* **2000,** *79* (10), 672-9.

15. Schroder, A.; Schroder, B.; Roppenser, B.; Linder, S.; Sinha, B.; Fassler, R.; Aepfelbacher, M., Staphylococcus aureus fibronectin binding protein-A induces motile attachment sites and complex actin remodeling in living endothelial cells. *Molecular biology of the cell* **2006,** *17* (12), 5198-210.

16. Hoffmann, C.; Ohlsen, K.; Hauck, C. R., Integrin-mediated uptake of fibronectin-binding bacteria. *Eur J Cell Biol* **2011,** *90* (11), 891-6.

17. Marjenberg, Z. R.; Ellis, I. R.; Hagan, R. M.; Prabhakaran, S.; Hook, M.; Talay, S. R.; Potts, J. R.; Staunton, D.; Schwarz-Linek, U., Cooperative binding and activation of fibronectin by a bacterial surface protein. *J Biol Chem* **2011,** *286* (3), 1884-94.

18. Edwards, A. M.; Potts, J. R.; Josefsson, E.; Massey, R. C., Staphylococcus aureus host cell invasion and virulence in sepsis is facilitated by the multiple repeats within FnBPA. *PLoS Pathog* **2010,** *6* (6), e1000964.

19. Edwards, A. M.; Potter, U.; Meenan, N. A.; Potts, J. R.; Massey, R. C., Staphylococcus aureus keratinocyte invasion is dependent upon multiple high-affinity fibronectin-binding repeats within FnBPA. *PLoS One* **2011,** *6* (4), e18899.

20. Massey, R. C.; Kantzanou, M. N.; Fowler, T.; Day, N. P.; Schofield, K.; Wann, E. R.; Berendt, A. R.; Hook, M.; Peacock, S. J., Fibronectin-binding protein A of Staphylococcus aureus has multiple, substituting, binding regions that mediate adherence to fibronectin and invasion of endothelial cells. *Cellular microbiology* **2001,** *3* (12), 839-51.

21. Holden, M. T.; Hsu, L. Y.; Kurt, K.; Weinert, L. A.; Mather, A. E.; Harris, S. R.; Strommenger, B.; Layer, F.; Witte, W.; de Lencastre, H.; Skov, R.; Westh, H.; Zemlickova, H.; Coombs, G.; Kearns, A. M.; Hill, R. L.; Edgeworth, J.; Gould, I.; Gant, V.; Cooke, J.; Edwards, G. F.; McAdam, P. R.; Templeton, K. E.; McCann, A.; Zhou, Z.; Castillo-Ramirez, S.; Feil, E. J.; Hudson, L. O.; Enright, M. C.; Balloux, F.; Aanensen, D. M.; Spratt, B. G.; Fitzgerald, J. R.; Parkhill, J.; Achtman, M.; Bentley, S. D.; Nubel, U., A genomic portrait of the emergence, evolution, and global spread of a methicillin-resistant Staphylococcus aureus pandemic. *Genome Res* **2013,** *23* (4), 653-64.

22. Lower, S. K.; Lamlertthon, S.; Casillas-Ituarte, N. N.; Lins, R. D.; Yongsunthon, R.; Taylor, E. S.; DiBartola, A. C.; Edmonson, C.; McIntyre, L. M.; Reller, L. B.; Que, Y. A.; Ros, R.; Lower, B. H.; Fowler, V. G., Jr., Polymorphisms in fibronectin binding protein A of Staphylococcus aureus are associated with infection of cardiovascular devices. *Proceedings of the National Academy of Sciences of the United States of America* **2011,** *108* (45), 18372-7.

23. Hos, N. J.; Rieg, S.; Kern, W. V.; Jonas, D.; Fowler, V. G.; Higgins, P. G.; Seifert, H.; Kaasch, A. J., Amino acid alterations in fibronectin binding protein A

(FnBPA) and bacterial genotype are associated with cardiac device related infection in Staphylococcus aureus bacteraemia. *J Infect* **2015,** *70* (2), 153-9.

24. Loughman, A.; Sweeney, T.; Keane, F. M.; Pietrocola, G.; Speziale, P.; Foster, T. J., Sequence diversity in the A domain of Staphylococcus aureus fibronectin-binding protein A. *BMC Microbiol* **2008,** *8*, 74.

25. Xiong, Y. Q.; Sharma-Kuinkel, B. K.; Casillas-Ituarte, N. N.; Fowler, V. G., Jr.; Rude, T.; DiBartola, A. C.; Lins, R. D.; Abdel-Hady, W.; Lower, S. K.; Bayer, A. S., Endovascular infections caused by methicillin-resistant Staphylococcus aureus are linked to clonal complex-specific alterations in binding and invasion domains of fibronectin-binding protein A as well as the occurrence of fnbB. *Infect Immun* **2015,** *83* (12), 4772-80.

26. McCarthy, A. J.; Lindsay, J. A., Genetic variation in Staphylococcus aureus surface and immune evasion genes is lineage associated: implications for vaccine design and host-pathogen interactions. *BMC Microbiol* **2010,** *10*, 173.

27. Keane, F. M.; Loughman, A.; Valtulina, V.; Brennan, M.; Speziale, P.; Foster, T. J., Fibrinogen and elastin bind to the same region within the A domain of fibronectin binding protein A, an MSCRAMM of Staphylococcus aureus. *Mol Microbiol* **2007,** *63* (3), 711-23.

28. Stemberk, V.; Jones, R. P.; Moroz, O.; Atkin, K. E.; Edwards, A. M.; Turkenburg, J. P.; Leech, A. P.; Massey, R. C.; Potts, J. R., Evidence for steric regulation of fibrinogen binding to Staphylococcus aureus fibronectin-binding protein A (FnBPA). *J Biol Chem* **2014,** *289* (18), 12842-51.

29. McCormack, N.; Foster, T. J.; Geoghegan, J. A., A short sequence within subdomain N1 of region A of the Staphylococcus aureus MSCRAMM clumping factor A is required for export and surface display. *Microbiology* **2014,** *160* (Pt 4), 659-70.

30. Geoghegan, J. A.; Monk, I. R.; O'Gara, J. P.; Foster, T. J., Subdomains N2N3 of fibronectin binding protein A mediate Staphylococcus aureus biofilm formation and adherence to fibrinogen using distinct mechanisms. *J Bacteriol* **2013,** *195* (11), 2675-83.

31. O'Neill, E.; Pozzi, C.; Houston, P.; Humphreys, H.; Robinson, D. A.; Loughman, A.; Foster, T. J.; O'Gara, J. P., A novel Staphylococcus aureus biofilm phenotype mediated by the fibronectin-binding proteins, FnBPA and FnBPB. *J Bacteriol* **2008,** *190* (11), 3835-50.

32. Herman-Bausier, P.; El-Kirat-Chatel, S.; Foster, T. J.; Geoghegan, J. A.; Dufrene, Y. F., Staphylococcus aureus Fibronectin-Binding Protein A Mediates Cell-Cell Adhesion through Low-Affinity Homophilic Bonds. *MBio* **2015,** *6* (3), e00413-15.

33. Kuusela, P., Fibronectin binds to Staphylococcus aureus. *Nature* **1978,** *276* (5689), 718-20.

34. Froman, G.; Switalski, L. M.; Speziale, P.; Hook, M., Isolation and characterization of a fibronectin receptor from Staphylococcus aureus. *J Biol Chem* **1987,** *262* (14), 6564-71.

35. Signas, C.; Raucci, G.; Jonsson, K.; Lindgren, P. E.; Anantharamaiah, G. M.; Hook, M.; Lindberg, M., Nucleotide sequence of the gene for a fibronectin-binding protein from Staphylococcus aureus: use of this peptide sequence in the synthesis of

biologically active peptides. *Proceedings of the National Academy of Sciences of the United States of America* **1989,** *86* (2), 699-703.

36. Jonsson, K.; Signas, C.; Muller, H. P.; Lindberg, M., Two different genes encode fibronectin binding proteins in Staphylococcus aureus. The complete nucleotide sequence and characterization of the second gene. *Eur J Biochem* **1991,** *202* (3), 1041-8.

37. Schwarz-Linek, U.; Werner, J. M.; Pickford, A. R.; Gurusiddappa, S.; Kim, J. H.; Pilka, E. S.; Briggs, J. A.; Gough, T. S.; Hook, M.; Campbell, I. D.; Potts, J. R., Pathogenic bacteria attach to human fibronectin through a tandem beta-zipper. *Nature* **2003,** *423* (6936), 177-81.

38. Foster, T. J., The remarkably multifunctional fibronectin binding proteins of Staphylococcus aureus. *Eur J Clin Microbiol Infect Dis* **2016,** *35* (12), 1923-1931.

39. Bingham, R. J.; Rudino-Pinera, E.; Meenan, N. A.; Schwarz-Linek, U.; Turkenburg, J. P.; Hook, M.; Garman, E. F.; Potts, J. R., Crystal structures of fibronectin-binding sites from Staphylococcus aureus FnBPA in complex with fibronectin domains. *Proceedings of the National Academy of Sciences of the United States of America* **2008,** *105* (34), 12254-8.

40. Meenan, N. A.; Visai, L.; Valtulina, V.; Schwarz-Linek, U.; Norris, N. C.; Gurusiddappa, S.; Hook, M.; Speziale, P.; Potts, J. R., The tandem beta-zipper model defines high affinity fibronectin-binding repeats within Staphylococcus aureus FnBPA. *J Biol Chem* **2007,** *282* (35), 25893-902.

41. To, W. S.; Midwood, K. S., Plasma and cellular fibronectin: distinct and independent functions during tissue repair. *Fibrogenesis & tissue repair* **2011,** *4*, 21.

42. Leiss, M.; Beckmann, K.; Giros, A.; Costell, M.; Fassler, R., The role of integrin binding sites in fibronectin matrix assembly in vivo. *Current opinion in cell biology* **2008,** *20* (5), 502-7.

43. Moretti, F. A.; Chauhan, A. K.; Iaconcig, A.; Porro, F.; Baralle, F. E.; Muro, A. F., A major fraction of fibronectin present in the extracellular matrix of tissues is plasma-derived. *J Biol Chem* **2007,** *282* (38), 28057-62.

44. Mao, Y.; Schwarzbauer, J. E., Fibronectin fibrillogenesis, a cell-mediated matrix assembly process. *Matrix Biol* **2005,** *24* (6), 389-99.

45. Deivanayagam, C. C.; Wann, E. R.; Chen, W.; Carson, M.; Rajashankar, K. R.; Hook, M.; Narayana, S. V., A novel variant of the immunoglobulin fold in surface adhesins of Staphylococcus aureus: crystal structure of the fibrinogen-binding MSCRAMM, clumping factor A. *The EMBO journal* **2002,** *21* (24), 6660-72.

46. Ganesh, V. K.; Rivera, J. J.; Smeds, E.; Ko, Y. P.; Bowden, M. G.; Wann, E. R.; Gurusiddappa, S.; Fitzgerald, J. R.; Hook, M., A structural model of the Staphylococcus aureus ClfA-fibrinogen interaction opens new avenues for the design of anti-staphylococcal therapeutics. *PLoS Pathog* **2008,** *4* (11), e1000226.

47. Mosesson, M. W., Fibrinogen and fibrin structure and functions. *Journal of thrombosis and haemostasis : JTH* **2005,** *3* (8), 1894-904.

48. Henschen-Edman, A. H., Fibrinogen non-inherited heterogeneity and its relationship to function in health and disease. *Ann N Y Acad Sci* **2001,** *936*, 580-93.

49. Bennett, J. S., Platelet-fibrinogen interactions. *Ann N Y Acad Sci* **2001,** *936*, 340-54.

50. Rostagno, A. A.; Schwarzbauer, J. E.; Gold, L. I., Comparison of the fibrin-binding activities in the N- and C-termini of fibronectin. *Biochem J* **1999,** *338 (Pt 2)*, 375-86.

51. Makogonenko, E.; Ingham, K. C.; Medved, L., Interaction of the fibronectin COOH-terminal Fib-2 regions with fibrin: further characterization and localization of the Fib-2-binding sites. *Biochemistry* **2007,** *46* (18), 5418-26.

52. Clement, S.; Vaudaux, P.; Francois, P.; Schrenzel, J.; Huggler, E.; Kampf, S.; Chaponnier, C.; Lew, D.; Lacroix, J. S., Evidence of an intracellular reservoir in the nasal mucosa of patients with recurrent Staphylococcus aureus rhinosinusitis. *J Infect Dis* **2005,** *192* (6), 1023-8.

53. Jarry, T. M.; Memmi, G.; Cheung, A. L., The expression of alpha-haemolysin is required for Staphylococcus aureus phagosomal escape after internalization in CFT-1 cells. *Cellular microbiology* **2008,** *10* (9), 1801-14.

54. Lehar, S. M.; Pillow, T.; Xu, M.; Staben, L.; Kajihara, K. K.; Vandlen, R.; DePalatis, L.; Raab, H.; Hazenbos, W. L.; Morisaki, J. H.; Kim, J.; Park, S.; Darwish, M.; Lee, B. C.; Hernandez, H.; Loyet, K. M.; Lupardus, P.; Fong, R.; Yan, D.; Chalouni, C.; Luis, E.; Khalfin, Y.; Plise, E.; Cheong, J.; Lyssikatos, J. P.; Strandh, M.; Koefoed, K.; Andersen, P. S.; Flygare, J. A.; Wah Tan, M.; Brown, E. J.; Mariathasan, S., Novel antibody-antibiotic conjugate eliminates intracellular S. aureus. *Nature* **2015,** *527* (7578), 323-8.

55. Hynes, R. O., Integrins: bidirectional, allosteric signaling machines. *Cell* **2002,** *110* (6), 673-87.

56. Hauck, C. R.; Borisova, M.; Muenzner, P., Exploitation of integrin function by pathogenic microbes. *Current opinion in cell biology* **2012,** *24* (5), 637-44.

57. Coburn, J.; Chege, W.; Magoun, L.; Bodary, S. C.; Leong, J. M., Characterization of a candidate Borrelia burgdorferi beta3-chain integrin ligand identified using a phage display library. *Mol Microbiol* **1999,** *34* (5), 926-40.

58. Kwok, T.; Zabler, D.; Urman, S.; Rohde, M.; Hartig, R.; Wessler, S.; Misselwitz, R.; Berger, J.; Sewald, N.; Konig, W.; Backert, S., Helicobacter exploits integrin for type IV secretion and kinase activation. *Nature* **2007,** *449* (7164), 862-6.

59. Isberg, R. R.; Leong, J. M., Multiple beta 1 chain integrins are receptors for invasin, a protein that promotes bacterial penetration into mammalian cells. *Cell* **1990,** *60* (5), 861-71.

60. Hauck, C. R.; Ohlsen, K., Sticky connections: extracellular matrix protein recognition and integrin-mediated cellular invasion by Staphylococcus aureus. *Current opinion in microbiology* **2006,** *9* (1), 5-11.

61. Sinha, B.; Herrmann, M., Mechanism and consequences of invasion of endothelial cells by Staphylococcus aureus. *Thromb Haemost* **2005,** *94* (2), 266-77.

62. Eichenberger, E. M.; Thaden, J. T.; Sharma-Kuinkel, B.; Park, L. P.; Rude, T. H.; Ruffin, F.; Hos, N. J.; Seifert, H.; Rieg, S.; Kern, W. V.; Lower, S. K.; Fowler, V. G., Jr.; Kaasch, A. J., Polymorphisms in Fibronectin Binding Proteins A and B among Staphylococcus aureus Bloodstream Isolates Are Not Associated with Arthroplasty Infection. *PLoS One* **2015,** *10* (11), e0141436.

63. BiacoreAB, BIACORE Technology Handbook. . **1994**.

64. Renaud, J. P.; Chung, C. W.; Danielson, U. H.; Egner, U.; Hennig, M.; Hubbard, R. E.; Nar, H., Biophysics in drug discovery: impact, challenges and opportunities. *Nature reviews. Drug discovery* **2016,** *15* (10), 679-98.

65. Laganowsky, A.; Reading, E.; Allison, T. M.; Ulmschneider, M. B.; Degiacomi, M. T.; Baldwin, A. J.; Robinson, C. V., Membrane proteins bind lipids selectively to modulate their structure and function. *Nature* **2014,** *510* (7503), 172-5.

66. Speziale, P.; Visai, L.; Rindi, S.; Di Poto, A., Purification of human plasma fibronectin using immobilized gelatin and Arg affinity chromatography. *Nature protocols* **2008,** *3* (3), 525-33.

67. Coe, A. P.; Askari, J. A.; Kline, A. D.; Robinson, M. K.; Kirby, H.; Stephens, P. E.; Humphries, M. J., Generation of a minimal alpha5beta1 integrin-Fc fragment. *J Biol Chem* **2001,** *276* (38), 35854-66.

68. Anthis, N. J.; Clore, G. M., Sequence-specific determination of protein and peptide concentrations by absorbance at 205 nm. *Protein Sci* **2013,** *22* (6), 851-8.

69. Baneyx, G.; Baugh, L.; Vogel, V., Coexisting conformations of fibronectin in cell culture imaged using fluorescence resonance energy transfer. *Proceedings of the National Academy of Sciences of the United States of America* **2001,** *98* (25), 14464-8.

70. Mohamed, N.; Teeters, M. A.; Patti, J. M.; Hook, M.; Ross, J. M., Inhibition of Staphylococcus aureus adherence to collagen under dynamic conditions. *Infect Immun* **1999,** *67* (2), 589-94.

71. Reddy, K.; Ross, J. M., Shear stress prevents fibronectin binding protein-mediated Staphylococcus aureus adhesion to resting endothelial cells. *Infect Immun* **2001,** *69* (5), 3472-5.

72. Kojima, N.; Shiota, M.; Sadahira, Y.; Handa, K.; Hakomori, S., Cell adhesion in a dynamic flow system as compared to static system. Glycosphingolipid-glycosphingolipid interaction in the dynamic system predominates over lectin- or integrin-based mechanisms in adhesion of B16 melanoma cells to non-activated endothelial cells. *J Biol Chem* **1992,** *267* (24), 17264-70.

73. Lakowicz, J., Principles of Fluorescence Spectroscopy, Springer, New York, 3rd edn, .

74. Eftink, M. R.; Ghiron, C. A., Fluorescence quenching studies with proteins. *Anal Biochem* **1981,** *114* (2), 199-227.

75. Provenza, G.; Provenzano, M.; Visai, L.; Burke, F. M.; Geoghegan, J. A.; Stravalaci, M.; Gobbi, M.; Mazzini, G.; Arciola, C. R.; Foster, T. J.; Speziale, P., Functional analysis of a murine monoclonal antibody against the repetitive region of the fibronectin-binding adhesins fibronectin-binding protein A and fibronectin-binding protein B from Staphylococcus aureus. *The FEBS journal* **2010,** *277* (21), 4490-505.

76. Alexander, S. S., Jr.; Colonna, G.; Edelhoch, H., The structure and stability of human plasma cold-insoluble globulin. *J Biol Chem* **1979,** *254* (5), 1501-5.

77. Osterlund, E.; Eronen, I.; Osterlund, K.; Vuento, M., Secondary structure of human plasma fibronectin: conformational change induced by calf alveolar heparan sulfates. *Biochemistry* **1985,** *24* (11), 2661-7.

78. Khan, M. Y.; Medow, M. S.; Newman, S. A., Unfolding transitions of fibronectin and its domains. Stabilization and structural alteration of the N-terminal domain by heparin. *Biochem J* **1990,** *270* (1), 33-8.

79. Wolff, C. E.; Lai, C. S., Inter-sulfhydryl distances in plasma fibronectin determined by fluorescence energy transfer: effect of environmental factors. *Biochemistry* **1990,** *29* (13), 3354-61.

80. Takagi, J.; Strokovich, K.; Springer, T. A.; Walz, T., Structure of integrin alpha5beta1 in complex with fibronectin. *The EMBO journal* **2003,** *22* (18), 4607-15.

81. Campbell, I. D.; Humphries, M. J., Integrin structure, activation, and interactions. *Cold Spring Harbor perspectives in biology* **2011,** *3* (3).

82. Akiyama, S. K.; Hasegawa, E.; Hasegawa, T.; Yamada, K. M., The interaction of fibronectin fragments with fibroblastic cells. *J Biol Chem* **1985,** *260* (24), 13256-60.

83. Vakonakis, I.; Staunton, D.; Ellis, I. R.; Sarkies, P.; Flanagan, A.; Schor, A. M.; Schor, S. L.; Campbell, I. D., Motogenic sites in human fibronectin are masked by long range interactions. *J Biol Chem* **2009,** *284* (23), 15668-75.

84. Bultmann, H.; Santas, A. J.; Peters, D. M., Fibronectin fibrillogenesis involves the heparin II binding domain of fibronectin. *J Biol Chem* **1998,** *273* (5), 2601-9.

85. Homandberg, G. A.; Erickson, J. W., Model of fibronectin tertiary structure based on studies of interactions between fragments. *Biochemistry* **1986,** *25* (22), 6917-25.

86. Miskei, M.; Antal, C.; Fuxreiter, M., FuzDB: database of fuzzy complexes, a tool to develop stochastic structure-function relationships for protein complexes and higher-order assemblies. *Nucleic Acids Res* **2017,** *45* (D1), D228-D235.

87. Liang, X.; Garcia, B. L.; Visai, L.; Prabhakaran, S.; Meenan, N. A.; Potts, J. R.; Humphries, M. J.; Hook, M., Allosteric Regulation of Fibronectin/alpha5beta1 Interaction by Fibronectin-Binding MSCRAMMs. *PLoS One* **2016,** *11* (7), e0159118.

88. Peacock, S. J.; Foster, T. J.; Cameron, B. J.; Berendt, A. R., Bacterial fibronectin-binding proteins and endothelial cell surface fibronectin mediate adherence of Staphylococcus aureus to resting human endothelial cells. *Microbiology* **1999,** *145 (Pt 12)*, 3477-86.

89. Sinha, B.; Francois, P. P.; Nusse, O.; Foti, M.; Hartford, O. M.; Vaudaux, P.; Foster, T. J.; Lew, D. P.; Herrmann, M.; Krause, K. H., Fibronectin-binding protein acts as Staphylococcus aureus invasin via fibronectin bridging to integrin alpha5beta1. *Cellular microbiology* **1999,** *1* (2), 101-17.

90. Kerdudou, S.; Laschke, M. W.; Sinha, B.; Preissner, K. T.; Menger, M. D.; Herrmann, M., Fibronectin binding proteins contribute to the adherence of Staphylococcus aureus to intact endothelium in vivo. *Thromb Haemost* **2006,** *96* (2), 183-9.

91. Ganesh, V. K.; Liang, X.; Geoghegan, J. A.; Cohen, A. L.; Venugopalan, N.; Foster, T. J.; Hook, M., Lessons from the Crystal Structure of the S. aureus Surface Protein Clumping Factor A in Complex With Tefibazumab, an Inhibiting Monoclonal Antibody. *EBioMedicine* **2016,** *13*, 328-338.

92. Anderson, E. T.; Fletcher, L.; Severin, A.; Murphy, E.; Baker, S. M.; Matsuka, Y. V., Identification of factor XIIIA-reactive glutamine acceptor and lysine donor sites

within fibronectin-binding protein (FnbA) from Staphylococcus aureus. *Biochemistry* **2004,** *43* (37), 11842-52.

93. Panizzi, P.; Friedrich, R.; Fuentes-Prior, P.; Richter, K.; Bock, P. E.; Bode, W., Fibrinogen substrate recognition by staphylocoagulase.(pro)thrombin complexes. *J Biol Chem* **2006,** *281* (2), 1179-87.

94. Severina, E.; Nunez, L.; Baker, S.; Matsuka, Y. V., Factor XIIIa mediated attachment of S. aureus fibronectin-binding protein A (FnbA) to fibrin: identification of Gln103 as a major cross-linking site. *Biochemistry* **2006,** *45* (6), 1870-80.

95. Agerer, F.; Lux, S.; Michel, A.; Rohde, M.; Ohlsen, K.; Hauck, C. R., Cellular invasion by Staphylococcus aureus reveals a functional link between focal adhesion kinase and cortactin in integrin-mediated internalisation. *Journal of cell science* **2005,** *118* (Pt 10), 2189-200.

96. Fraunholz, M.; Sinha, B., Intracellular Staphylococcus aureus: live-in and let die. *Frontiers in cellular and infection microbiology* **2012,** *2*, 43.

97. Chen, H.; Ricklin, D.; Hammel, M.; Garcia, B. L.; McWhorter, W. J.; Sfyroera, G.; Wu, Y. Q.; Tzekou, A.; Li, S.; Geisbrecht, B. V.; Woods, V. L., Jr.; Lambris, J. D., Allosteric inhibition of complement function by a staphylococcal immune evasion protein. *Proceedings of the National Academy of Sciences of the United States of America* **2010,** *107* (41), 17621-6.

98. Deng, Z. J.; Liang, M.; Monteiro, M.; Toth, I.; Minchin, R. F., Nanoparticle-induced unfolding of fibrinogen promotes Mac-1 receptor activation and inflammation. *Nat Nanotechnol* **2011,** *6* (1), 39-44.

99. Lishko, V. K.; Podolnikova, N. P.; Yakubenko, V. P.; Yakovlev, S.; Medved, L.; Yadav, S. P.; Ugarova, T. P., Multiple binding sites in fibrinogen for integrin alphaMbeta2 (Mac-1). *J Biol Chem* **2004,** *279* (43), 44897-906.

100. Ugarova, T. P.; Solovjov, D. A.; Zhang, L.; Loukinov, D. I.; Yee, V. C.; Medved, L. V.; Plow, E. F., Identification of a novel recognition sequence for integrin alphaM beta2 within the gamma-chain of fibrinogen. *J Biol Chem* **1998,** *273* (35), 22519-27.